# STUDIES IN THE VISUAL SYSTEM OF THE CAT.

# I. THE RETINOTHALAMIC PATHWAY IN NORMAL AND SIAMESE CATS.

# II. THE VERTICAL HOROPTER

Thesis by

Michael Lee Cooper

In Partial Fulfillment of the Requirements

for the Degree of

Doctor of Philosophy

California Institute of Technology

Pasadena, California

1979

(Submitted August 21, 1978)

ACKNOWLEDGMENTS

Detailed acknowledgments appear at the end of each chapter. However I would like to take the opportunity here to express my deep gratitude to my thesis advisor, Jack Pettigrew, for the help and counsel which he has provided during my time in his lab and for the lively example of personal flair which he has set for me and the other members of his group. I am also grateful to the other members of my thesis committee, John Allman, Jeremy Brockes, Mark Konishi, and David Van Essen, for their comments on my various manuscripts. My special thanks are due to Drs. Allman and Konishi, who have given me great support and encouragement throughout my stay here at Caltech.

I list here some of the people who have given me technical or other assistance during the course of my work: Gary Blasdel, Betty Hanson, Bill Lease, Sarah Kennedy, Phyllis Knudsen, and the women of the Biology Department typing pool. I am most appreciative of their help in easing the effort required to complete this thesis.

ABSTRACT

The naso-temporal division of the retinothalamic pathway was studied in normal and Siamese cats. One lateral geniculate nucleus (LGN) of each animal was filled with horseradish peroxidase (HRP) in order to visualize the retinothalamic ganglion cells over a wide area of retina. Whole-mounted retinae of normal animals showed clear vertical decussation lines between areas projecting ipsilaterally or contralaterally. The ipsilateral decussation was sharp and passed through the center of the area centralis; the contralateral decussation was somewhat less sharp, with scattered cells extending up to a few degrees into the temporal retina. However, in contrast to the findings in Stone's ('66) tract section material, no significant numbers of HRP-filled cells were found beyond a few degrees into the contralateral temporal retina.

In the Siamese cat retina there was no sharp vertical decussation line between areas sending axons ipsilaterally or contralaterally; rather there was overlap in the temporal retina between cell populations projecting to the two hemispheres. Thus there is no region of exclusive contralateral misprojection extending 20° temporally from the zero azimuthal meridian; in fact, there is a smooth, gradient-like decrease in the percentage of retinothalamic cells misprojecting contralaterally as one proceeds into the temporal retina. Cell-size measurements indicated that the large (presumably Y-type) ganglion cells are more affected by the Siamese defect than the rest of the retinothalamic population. Use of the anterograde transport of tritiated amino acids confirmed the existence of bilateral projection to the LGN from the central temporal retina of Siamese cats.

The second part of this thesis was an attempt to determine the form of the vertical horopter in the cat and burrowing owl by electrophysiologically mapping the receptive field positions of binocular cortical neurons at various elevations along the zero azimuthal meridian. Our recordings indicated that, in the alert, unparalyzed cat and owl, midline binocular units in the lower visual field have crossed receptive fields compared to the fixation point, while upper field cells have uncrossed receptive fields. It follows from our data that the vertical horopter is a straight line tilted away from the animal in both species, with the lower field horopter closer to the animal and the upper field horopter farther away.

# TABLE OF CONTENTS


| | |
|---|---|
| Acknowledgments | ii |
| Abstract | iii |
| Introduction | 1 |
| Chapter 1 | 2 |
| Chapter 2 | 57 |
| Chapter 3 | 129 |

# INTRODUCTION

The following thesis reports the results of my work in the laboratory of J. D. Pettigrew. The first two chapters are anatomical studies of the decussation pattern of the retinothalamic pathway in normal and Siamese cats, while the third chapter (rather unrelated to the first two) details our study of the vertical horopter in the cat and burrowing owl. Each of these chapters has been submitted separately for publication in the Journal of Comparative Neurology.

A brief introduction to each topic appears at the beginning of the appropriate chapter; the relevant figures and acknowledgements are also separated by chapter.

# CHAPTER 1

## The Decussation of the Retinothalamic Pathway in the Normal Cat

INTRODUCTION

Knowledge of the retinal distributions of ganglion cells with crossed and uncrossed axons is of considerable importance for the understanding of binocular interactions in the mammalian visual system. Ganser (1882) was the first to show in cat that the cells in the nasal retina project contralaterally, while those in the temporal retina send axons to the ipsilateral hemisphere. However, no quantitative study of the naso-temporal division of the cat's retina was made until Stone ('66) used optic tract section to demonstrate the projection pattern of the entire retinal output. The development in recent years of simple and general classification schemes for the various types of retinal ganglion cell (Enroth-Cugell and Robson, '66; Boycott and Wässle, '74; Stone and Fukuda, '74a, b; Cleland and Levick, '74a, b) has led to interest in determining the decussation patterns of the different cell groupings; and indeed, it has been shown that each of the major ganglion cell classes has its own particular pattern of naso-temporal division (Stone and Fukuda, '74b; Kirk et al., '76a, b).

To date, the only anatomical demonstrations of the crossed/uncrossed distributions of cat retinal ganglion cells have relied on tract section (Stone, '66; Stone and Fukuda, '74) and have thus included the output to both the midbrain and the thalamus. From this total decussation pattern we have attempted to extract the organization of just the retinothalamic component. To this end we have made use of the retrograde transport of horseradish peroxidase (HRP) (Krisstenson et al., '71; LaVail and LaVail, '74), which has already been shown to be of value in the study of retinal projections (Bunt et al., '74' Kelly and Gilbert,

'75; Magalhaes-Castro et al., '76; Bunt and Minckler, '77). We have made large injections of HRP into one lateral geniculate of the cat, hoping thereby to reveal over a large area of retina the pattern of crossed and uncrossed projection to the thalamus. The results presented here confirm and extend the previous descriptions of the naso-temporal division in the normal cat (Stone, '66; Stone and Fukuda, '74b; Kirk et al., '76a, b) and provide a background for the following study of the retinal projections in the Siamese cat (Cooper and Pettigrew, '78a). Abstracts of this work have been presented elsewhere (Cooper and Pettigrew, '77a, b).

## METHODS

### HRP Injections and Histochemical Procedures

Ten normal cats were used in this study. In order to visualize the entire distribution of retinothalamic ganglion cells in the retina, we attempted to fill the whole extent of one lateral geniculate nucleus (LGN) in each animal with horseradish peroxidase (HRP, Sigma Type VI). To this end we made three or four large injections of HRP in each animal. These injections were made through a Hamilton syringe at stereotaxic coordinates indicated in the atlas of Snider and Niemer ('61) and in the study of Sanderson ('71). We usually injected 1.5 µl of 10% HRP in saline at each of three sites located between Sanderson's coronal planes 5 and 8 at L9, V14 to 14.5. A fourth injection of 0.5 µl was sometimes placed at coronal 4. Each injection was made over a period of one-half to one hour; we allowed the needle to rest in place for 10 min after the completion of the injection. Four to

six hours usually elapsed between the beginning of the first injection and the completion of the last one. We used ketamine hydrochloride as the anesthetic during both the preparatory surgery and the actual injections; the initial dose of 20 mg/kg was supplemented as needed during the course of the injection session. Dexamethasone, penicillin, and streptomycin were administered for prophylaxis at the end of the session.

We allowed the cats to survive for 40 to 50 hours after the beginning of the first HRP injection in order to provide sufficient time for the retrograde transport of peroxidase to the retina. After this time the animals were perfused transcardially with warm saline followed by 20% formal-saline. We usually injected 2000 units of heparin into the heart before beginning the saline flush; the addition of 3000 units of heparin per liter of saline also helped ensure adequate removal of the blood. The high formalin concentration employed here produced very rapid fixation of the brain and retinae, allowing their removal within a few hours of the perfusion. We used this formalin concentration in order to give quick fixation of the retinae without the need for use of glutaraldehyde, which seems to hinder the removal of the retinae from the underlying choroid.

After removal of the eyes, the anterior portion of each eyeball was separated by cutting just in front of the ora terminalis (terminology of Hughes, '76); the vitreous was stripped away from the retina at the same time. We then made a number of relieving cuts around the entire perimeter of the fundus in order to facilitate flattening of the hemispherical retina on a slide. Next, each fundus was left in

cold distilled water overnight; this procedure provided a good rinse and allowed the retinae to float free from the underlying choroid. On the following day it was usually easy to complete the removal of the retina by sliding a blunt forceps along the ora terminalis and by undercutting the optic disk with a scalpel blade.

After removal from the choroid, the retinae were reacted with benzidine (Strauss, '64; Lynch et al., '73) in order to visualize the HRP-containing ganglion cells. The tissue was rinsed briefly in room temperature 25% ethanol and then incubated from 5 to 10 min in a room temperature solution containing 10 ml of 0.2% benzidine-dihydrochloride in 30% ethanol, 10 ml distilled water and 20 µl 30% $H_2O_2$. Next the retinae were washed twice in cold 30% ethanol and transferred for at least one-half hour to cold 6% sodium nitroprusside in 50% ethanol. We mounted the retinae fiber layer uppermost on glass slides which had been subbed twice with Gatenby's solution. After air-drying overnight, the tissue was dehydrated, cleared, and cover-slipped without counterstaining.

The high formalin concentration used in the perfusion made it necessary to examine the brain as soon as possible for the spread of HRP from the injection site. After the brain had been blocked coronally and removed from the skull, we placed it overnight in cold 30% sucrose without fixative. On the next day the LGN, superior colliculus, and visual cortex were cut at 30 or 80 µm, and the sections were reacted with benzidine for one minute. Counterstaining the sections lightly with neutral red facilitated the determination of the extent

of diffusion of HRP through the brain. Layers V and VI of the ipsilateral visual cortex were examined for evidence of retrograde transport from the superior colliculus or LGN to the cortex (Gilbert and Kelly, '75).

Photography

Macrophotography was performed on the freshly-prepared whole mounts before dehydration. Direct and indirect illumination, alone and in combination, were used to obtain clear definition of both blood vessel patterns and stained ganglion cells. Color slides (35 mm, magnification 4X - 10X) were obtained with a reversed 50 mm macro lens attached to the front of either a 100 mm or 200 mm lens (Blaker, '76). This method allowed briefer exposure times and better resolution than the use of the macro lens in combination with a bellows.

Ganglion Cell Density Maps

The extensive labeling of retinal ganglion cells after our injections of HRP into the thalamus enabled us to construct maps of labeled ganglion cell density using the uncounterstained whole-mounted retinae (Stone, '65, '78; Hughes, '75; Wässle et al., '75). The first step in the construction of these maps was to draw the retinae at 37X magnification; various landmarks on the drawing enlargements could then be related to the coordinates on the micrometer stage of a compound microscope. In this way it was possible to establish the relationship between a grid coordinate system on the drawing and the various points on the actual histological specimen. We counted cell densities across the temporal retina and the nasal retina as far as the optic disk.

The initial cell counts were made at the intersections of a 1 mm lattice. Extra counts were made at more closely spaced intervals

in regions of central retina where the ganglion cell densities changed rapidly with eccentricity. We counted the ganglion cells through a 10X eyepiece fitted with a square graticule; the magnification was chosen so as to maintain 50 to 150 cells within the graticule field. In the areas of low cell density we used a 16X objective (field = 0.372 $mm^2$). A 100X oil objective (field = 0.0096 $mm^2$) served to count the region of highest cell density in the area centralis itself. After calculating the labeled cell density for each point of the retina, we then constructed the isodensity lines by linear interpolation between adjacent data points.

Shrinkage

Shrinkage of the retinae was estimated by comparing the distance from the area centralis to the optic disk with the average distance of 3.42 mm given by Bishop et al. ('62), and also by comparing the distance from the optic disk to the temporal margin of the retina before and after dehydration. For the later animals in this series, LGN-35 and -36, we photographed the retinae before and after dehydration in order to obtain even more accurate estimates of shrinkage. The retinae presented in this study did not show significant shrinkage (1% for the ipsilateral retinae of LGN-35 and -36, 2-3% for the contralateral retina of LGN-35) and therefore were not corrected for length or cell density.

The position of the area centralis on the drawings of the uncounterstained retinae was estimated by inspection and confirmed by counting under the microscope. Since there was not a distinct region of high labeled cell density in the ipsilateral retinae of the Siamese cats

used in the following study (Cooper and Pettigrew, '78a), these retinae were decoverslipped and counterstained with cresyl violet after the necessary quantitation had been performed. The estimate of the position of the area centralis on each counterstained retina was corrected for any shrinkage occurring during the staining with cresyl violet.

Cell Size Measurements

In order to determine the diameters of HRP-filled ganglion cells, we drew fields of cells under a 40X lens with a camera lucida attachment. The drawings were made at a magnification of 800X and covered an area large enough to include 150-200 labeled ganglion cells. Since we found that counterstaining with cresyl violet or neutral red often obscured the blue color of the benzidine reaction product, we first drew each field from the uncounterstained retinae. After decoverslipping and counterstaining, a drawing was made of all the cells, labeled and unlabeled, in the same area as the initial drawing. Comparison of the two drawings ensured that no lightly labeled cells were missed in the final counterstained drawing. We measured the area of each cell on a digitizing tablet kindly lent by J.-P. Revel; the diameters were then calculated from the area data by assuming a circular profile for the ganglion cells. There was sometimes considerable shrinkage of the cell diameters during the staining and dehydration procedures (e.g., in LGNS-25 and -26 of the following study). We made no attempt to correct for this shrinkage.

RESULTS

As seen in figures 1 and 2, the large injections used here gave very good filling of the retinal ganglion cells. The large cells were usually especially well labeled and one could often determine their dendritic morphology in considerable detail, even under light field optics. Due to the heavy labeling of the ganglion cells and to the thickness of the retinal whole-mounts, we found it more convenient to study the retinae under light-field optics, rather than to use the conventional dark-field. All of the quantitative work in this study was done using the light field condenser.

Extent of Diffusion of HRP

As might be expected from the large amounts of HRP injected into the LGN (see Methods), there was considerable diffusion of the HRP away from the injection sites. We have divided the region of HRP spread into two regions, as shown for a typical injection in figure 3. In the central region, represented by vertical stripes, the benzidine reaction product was diffusely spread throughout the extracellular space; the degree of extracellular labeling varied from most intense in the immediate vicinity of the injection site in the LGN to rather lighter at the edges of this central region. This region of diffuse extracellular reaction product usually covered the entire extent of the thalamic nuclei known to receive retinal input, viz., the dorsal lateral geniculate nucleus (LGNd, or simply, LGN), ventral lateral geniculate nucleus (LGNv), and medial interlaminar nucleus (MIN). In figure 3 heavy label extends throughout the rostro-caudal extent

of the LGNd, except for the most caudal tip of this nucleus (although often the entire LGN was filled with moderately heavy label). The region of diffuse labeling usually spread part-way across the pulvinar, medial geniculate nucleus, optic tract, and optic radiation. Surrounding this central area of diffuse reaction product was a band in which the benzidine reaction product was confined mainly or entirely to the walls of blood vessels. This region is represented in solid grey in figure 3 and probably represents the maximum extent of HRP diffusion away from the injection site (Hedreen and McGrath, '77; Vanegas et al., '78). This area of light labeling usually extended across the pulvinar and medial geniculate nuclei, about half-way across the lateral posterior nucleus, up the optic radiation into part of the suprasylvian gyrus, and across the ventricles into the hippocampus. It is important to note that in the animals presented in this study (as well as in the following one, for which this discussion of diffusion also holds), even the region of lightest label never extended into the mesencephalic areas known to receive retinal input, i.e., the superior colliculus (SC), nucleus of the optic tract (NOT), posterior pretectal nucleus (NPP), or pretectal olivary nucleus (Kanaseki and Sprague, '74). The one exception to this was LGNS-20 (following study), in which some heavier label did extend into the lateral SC and NOT.

Other workers have noticed that the region of effective uptake of HRP is usually smaller than the apparent maximum diffusion of extracellular marker (Nauta et al., '74; Bunt et al., '75; Jones, '75; Vanegas et al., '78). Our data outlined below support these findings and suggest that effective retrograde transport of HRP to the retina

took place from a rather smaller area than that indicated by the maximum spread of HRP. In particular, the data below make it unlikely that there was significant uptake due to diffusion of HRP to the midbrain centers of retinal termination.

We examined layers V and VI of areas 17, 18, and 19 ipsilateral to the injected LGN for evidence of retrograde transport from the LGN or SC (Gilbert and Kelly, '75). We did not find strong cortical labeling in all of our animals, possibly on account of the high formalin concentration used during fixation. However, in those animals where there was good transport of HRP from the LGN to layer VI, we did not find significant labeling of layer V. This indicated that there probably was not significant contamination of our results by transport from the SC. The only exception to this was the Siamese cat LGNS-20, in which the heavy labeling of layer VI was accompanied by light but significant staining of layer V, indicating that there may have been some transport of HRP from the midbrain to the retina of this animal. LGNS-20 will be discussed in more detail in the following paper.

The fact that the mesencephalic primary visual areas did not contain reaction product, coupled with the data on transport to the retina presented below, indicates that our experiments deal with the projection of the retina to the thalamus and are not contaminated significantly by uptake due to spread of HRP to the midbrain. The reasons for discounting the possibility of transport through cut retinomesencephalic axons will also be discussed below.

It has been pointed out to us (Peter Stirling, personal communication) that the possibility exists of spurious staining of ganglion cells due to perikaryal uptake of HRP leaking from adjacent heavily labeled cells. Other investigators studying the retrograde transport of HRP to the retina have not noticed significant amounts of HRP in the extracellular space of the ganglion cell layer, even under the EM (Bunt et al., '74; LaVail and LaVail, '74). Nor has labeling of retinal glial cells been noted in these studies or in the present study. We have not observed lightly stained profiles surrounding more heavily labeled cells, as might be expected if leakage were a problem. The exception to this was seen in the central areas of some retinae (e.g., LGN-36, ipsi); in the regions of highest ganglion cell density we could sometimes observe faint, diffusely stained profiles which did not contain obvious grains. In such cases, only definitely filled profiles with distinct grains were counted as retinothalamic neurons. This problem was only encountered in a restricted region of LGN-35 contra and LGN-36 ipsi.

The remaining sections of these Results will be devoted to a quantitative description of the naso-temporal division of the retinothalamic pathway in normal cats. The following paper will present the results of similar studies in the Siamese cat (Cooper and Pettigrew, '78a).

Appearance of the Naso-Temporal Division

Quantitative data from two cats (LGN-35 and LGN-36) will be presented here; the other cats gave results which were qualitatively very similar to those presented here, but which were not quantitated extensively either because of some apparent spread of HRP to the

midbrain or because the benzidine reaction product faded before the cell counting could be accomplished. (Fading of the blue benzidine color was a considerable problem, especially from the heat of the projection lamp used to draw the retinae.)

Low power photographs of the whole-mounts for LGN-35 are presented in figures 4 and 5. These photographs demonstrate a number of features of the naso-temporal division of the retinothalamic pathway in normal cats. In the ipsilateral retina a rather sharp vertical line separates the ipsilaterally projecting temporal retina from the unstained contralaterally projecting nasal retina (see also Stone, '66). The darker region near the center of the photograph represents the area centralis, which is divided approximately down its center by the vertical decussation line. The contralateral retina also shows a vertical division between the stained nasal retina and the unstained temporal retina. The area centralis appears somewhat more heavily stained than its ipsilateral counterpart, corresponding to a higher density of cells in the nasal half-centralis (see below). It is clear, however, that the vertical decussation in the contralateral retina is not as sharp as that for its ipsilateral partner; many cells spill across the decussation line into the temporal retina. The large ganglion cells (Boycott and Wässle, '74; Wässle et al., '75) stand out clearly in these HRP-stained whole-mounts, and it is evident that most of the cells spreading into the temporal contralateral retina are actually large cells. In fact, beyond a few degrees temporally, there are no small cells labeled in the contralateral temporal retina.

Figure 6 is a camera lucida drawing of the filled cells in the ipsilateral and contralateral areae centrales. This figure reinforces the impressions obtained from the macrophotographs. The ipsilateral decussation line is sharp, while the contralateral line is much more diffuse. The "median edges" of the nasal and temporal retina, as named by Stone ('66), have been fixed by inspection on these drawings. (We have determined the ipsilateral median edge as the line of most-nasal ipsilateral cells.) Although some small cells do spread across the median edge of the nasal retina into the contralateral temporal retina, figure 6 makes it clear that more than a few hundred micra beyond the median edge most of the contralateral cells are large cells. In addition, the most temporally situated contralateral cells are all large cells. It is interesting to note that in the drawing of the ipsilateral area centralis there appears to be an absence of large cells near the median edge of the temporal retina; this presumably is due to the fact that most of the large cells in the first few degrees of temporal retina project contralaterally (see below).

Overlap of Median Edges

The camera lucida drawings of figure 6 were ruled off in squares 100 μm on a side; the number of cells in each square was counted and is displayed in figure 7. The reader will notice that the peak density in the contralateral retina is higher (8538 cells/$mm^2$) than that in the ipsilateral retina (5518 cells/$mm^2$). This was also the case in the other pair of areae centrales which was counted (LGN-15);

the peak contralateral density was 6247 cells/mm$^2$, while the maximum ipsilateral density was 4790 cells/mm$^2$. In addition it is apparent in this figure that the peak density in each retina is displaced slightly from the median edge of the retina. This can be explained by assuming that there is overlap between the median edges of the nasal and temporal retinae overlap, so that there is a strip of bilateral projection running down the center of the area centralis. Such an explanation was first proposed by Stone ('66), who showed that by overlapping the median edges of tract-sectioned retinae by 200 µm (with one retina reversed left to right), an appropriately shaped isodensity map of the complete area centralis could be obtained. Stone coined the term "median strip of overlap" for this region of intermingling of contralateral and ipsilateral cells. We have verified that an overlap of approximately 200 µm (1°; Bishop et al., '62; Hughes, '76) yields an appropriately shaped area centralis; overlap of less than 200 µm results in a depression between two peaks of cell density when the two retinae are superimposed.

Using the data in figure 7 the reader can verify the amount of overlap for himself, if he wishes.

If one assumes symmetry between the two eyes, one should be able to superimpose the contralateral and ipsilateral density counts (fig. 7) and, after overlapping the median edges by 200 µm, calculate the relative proportion of the retinothalamic population projecting ipsilaterally or contralaterally from any given point in the retina.

This was done for the area centralis by summing the ipsilateral and contralateral densities (from fig. 7) in adjacent 100 µm-wide vertically-oriented strips running from 500 µm above to 500 µm below the horizontal meridian; the ipsilateral density was taken as a percentage of the total retinothalamic cell density in each strip. The resulting "%-ipsilateral" curve (fig. 8) shows how the proportion of ipsilaterally projecting cells increases as one proceeds temporally. Nasal to the median strip of overlap all the ganglion cells send their axons contralaterally. Within the median strip, on the other hand, there is an intermingling of ipsilateral and contralateral cells, with the 50%-ipsilateral projection line falling near the center of the median strip (and therefore near the center of the area centralis). Temporal to the region of overlap defined by Stone ('66), increasing percentages of the retinothalamic cells project homolaterally, until by about 800 µm (about 3.5°) temporally, no contralateral cells remain. It is important to emphasize here that the 75%-ipsilateral/25%-contralateral line is reached at a point only about 200 µm (1°) into the temporal retina and that all the retinothalamic cells project ipsilaterally only slightly beyond that point. In other words, there is no population of cells which maintains contralateral projection across the entire extent of temporal retina and which might thus correspond to the 25% contralateral projection found by Stone ('66).

A similar %-ipsilateral curve is shown for the large cells in figure 8. Only a small fraction (about 6%) of the large cells sends axons ipsilaterally in the median strip, whereas approximately 50% of the total population does so. The 50% line for large cells is not reached until about 700 µm (3°) into the temporal retina. Thus

the naso-temporal decussation line for the "giant" cells is shifted temporally relative to that of the total retinothalamic population. (This was noted previously by Stone and Fukuda ['74] and by Kirk et al. ['76a, b].)

In figure 9, a %-ipsilateral curve similar to that in figure 8 is shown for points on a horizontal line 2 mm above the area centralis. This curve is calculated from the cell densities along the line of maximum contralateral spread into the temporal retina of LGN-35 (see below, fig. 10). Even here, the 75%-ipsilateral line is reached only 500 μm (2.5°) temporally and the 99% line is reached only 1 mm beyond that, again indicating that there is no significant population of contralaterally projecting cells extending across most of the temporal retina.

As indicated in figure 6, the contralaterally projecting cells in the temporal retina tend to be large cells. This is verified by a plot showing how the proportion of large cells in the total contralateral retinothalamic population varies with horizontal eccentricity (fig. 8). In the central nasal retina large cells make up about 3% of the total labeled-cell population. However, as one moves temporally to the median strip, the large cells come to form an increasing percentage of the total contralateral population, until by 600-700 μm temporally, all of the contralateral cells are large.

Density Maps

Maps of the density of HRP-filled cells were constructed for both retinae of LGN-35 (fig. 10) and for the ipsilateral retina of LGN-36 (fig. 11). (The contralateral retina of LGN-36 faded before it could be counted.) Care was taken to plot the positions of the

nasal-most filled cells in the ipsilateral retinae and the temporal-most cells in the contralateral retina. (These lines are denoted "1" on the density maps.) The median edge of the temporal retina is marked by arrows in the ipsilateral density map of LGN-35 (fig. 10) and falls at an angle of about 68° to the line between the center of the blind spot and the area centralis.

In the density map for contralateral retina of LGN-35 (fig. 10) the median edge of the nasal retina (arrows) falls at 62° with respect to the area centralis-blind spot line. (The reason for this asymmetry between the ipsilateral and contralateral retina in LGN-35 is unclear, but it probably just represents individual variation. See Stone, '66.) The contralateral isodensity lines spill across the median edge into the temporal retina. The line of most temporal contralateral cells is rather ragged and extends farthest temporally along a horizontal line about 2 mm above the area centralis. However, this greater spread into the temporal retina is rather deceptive, since the contralateral density falls off rapidly beyond the nasal median edge (see above and fig. 10), so that even along this horizontal line of farthest excursion, only 1-2% of the retinothalamic cells project contralaterally 1.6 mm (about 8°) temporal to the median edge (see above and fig. 9).

An interesting pattern in the ipsilateral density maps of LGN-35 and -36 is revealed in figure 12, in which we have shaded the region between the most nasal ipsilateral cell ("1"-line) and the point of maximum ipsilateral density at each elevation above the area centralis. It is evident that the distance from the nasal edge

of the ipsilateral retina to the point of maximum ipsilateral density increases as one moves above the area centralis. As shown in figure 12 (see also fig. 7), the distance from the most nasal cell to the peak density is about 200 μm in the area centralis itself, but in both retinae this value increases to about 1.3 mm along a line 3 mm above the horizontal meridian. This increase is much more than would be expected (on the order of 100 μm) from the distortion of a straight line due to flattening of the hemispherical retina. Since the lower densities within the shaded region presumably result because the corresponding cells are projecting contralaterally, figure 12 may indicate that the region of intermingling of contralaterally and ipsilaterally projecting cells is consistently greater above than along the horizontal meridian.

Cell Size Measurements

We have determined the diameters of the cells labeled with HRP at a point located near the horizontal meridian approximately 4.7 mm into the contralateral nasal retina of LGN-35. Our data confirm the findings of Kelly and Gilbert ('75) that all of the large cells are filled after injections into the thalamus and that there is a population of medium-sized cells (mean diameter = 14.7 μm, range = 11 to 20 μm) which is also filled (fig. 13). It is noteworthy that the smallest ganglion cells (8 μm to 11 μm diameter) in the retina are not significantly labeled after our thalamic injections. This stands in contrast to the results of an injection into the superior colliculus (fig. 13). At a point located 6 mm into the nasal contralateral retina, only about one-half of the large cells are labeled.

The medium-sized population is not heavily labeled, but the smallest ganglion cells (8 μm to 11 μm) do contain HRP. The mean diameter of the retinomesencephalic cells labeled here is 11.5 μm (range = 8 to 18 μm).

## DISCUSSION

### Relation to Previous Work

The present study is the first anatomical investigation to examine the naso-temporal division of the retinothalamic pathway in the cat, although a more restricted study has been reported in the monkey (Bunt and Minckler, '77). Previous anatomical work by Stone ('66) has used tract-sectioned material to study the decussation pattern of the entire retinofugal output. The present findings confirm and extend those of previous workers who have applied both physiological and anatomical techniques to these questions (Stone, '66; Stone and Fukuda, '74b; Kirk et al., '76a, b). In particular, the finding of a 200 μm overlap between the median edges of the two retinae and the displacement of the decussation line for the large, presumably Y-type cells have been reported previously and are confirmed here.

However, there are certain differences between our results and those published elsewhere. Stone ('66) has shown that approximately 25% of the cells in the ipsilateral temporal retina survive tract section and must therefore project contralaterally. A small percentage of these cells are large cells. In our contralateral retinae we have found that the large cells spill up to several millimeters into the temporal retina and that they have a decussation line lying several degrees temporal to that for all the retinothalamic cells. This

confirms the histological finding of Stone ('66), as well as the anatomical and physiological results of Stone and Fukuda ('74) and Kirk et al. ('76a, b) (since the large cells are presumably Y-cells (Boycott and Wässle, '74). It is likely that the temporal large cells project to the medial interlaminar nucleus (MIN), inasmuch as the amount of naso-temporal overlap of these cells fits well with that reported by Sanderson ('71) and Sanderson and Sherman ('71) for this structure. In addition, it is known that the major input to the MIN is from Y-cells (Mason, '75). However, some of the temporal large cells could also send axons to the lamina C of the LGN, since Sanderson and Sherman ('71) found similar amounts of overlap in lamina "B" (old terminology for C-laminae) as in the MIN and since recent work has shown lamina C to contain Y-cells (Wilson et al., '76).

In spite of the extensive naso-temporal overlap of the large Y-cells, Stone ('66) found that the great majority of the contralaterally projecting cells in the temporal retina are small in size. (This is evident by comparing Stone's finding that about 5% of the temporal Y-cells project contralaterally with the fact that Y-cells make up only about 5% of the total retinal population [Stone, '66, '78; Wässle et al., '75].) The smallest ganglion cells of the retina have come to be identified with W-cells (Boycott and Wässle, '74; Stone and Fukuda, '74a; Cleland and Levick, '74b; Kelly and Gilbert, '75) and physiological studies have confirmed that there is substantial contralateral projection of W-cells from virtually the entire temporal retina (Fukuda and Stone, '74; Kirk et al., '76a, b). However, as shown in figure 6, we found no small cells more than a few hundred micra beyond the median edge of the contralateral nasal retina; most

of the more temporally located cells were large, and in fact the very most temporal cells were invariably large. along the horizontal meridian the 25% contralateral/ 75% ipsilateral line was found to lie only about 200 μm 91°) temporal to the median strip, while contralateral projection fell to less than 1% only 600 μm) about 2.5°, fig. 8) more temporally. In other words, our study of the retinothalamic pathway does not reveal the presence of a substantial population of contralaterally projecting small cells in the temporal retina. Thus, the large population of contralaterally projecting W-cells in the temporal retina probably does not project to the thalamus. Temporal W-cells have been stimulated antidromically from the contralateral superior colliculus, however (Fukuda and Stone, '74). In addition, up to 40° of ipsilateral visual field (i.e., virtually the entire extent of temporal retina) has been mapped in the rostral pole of the superior colliculus (Feldon et al., '70; Berman and Cynader, '72; Lane et al., '74). That this ipsilateral field projection is probably due to the small W-cells is shown by the fact that lesions in even the most temporal edge of the retina produce fine-grained degeneration in the rostral pole of the contralateral superior colliculus (Harting and Guillery, '75). The fineness of the degeneration indicates that it corresponds to small caliber axons, which are most likely those of W-cells (Cleland and Levick, '74a; Stone and Fukuda, '74a).

Of course, it is not possible for us to rule out absolutely the possibility that the temporal W-cells do project to the thalamus but could not transport HRP, since there are axonal systems which

apparently cannot be labeled with HRP (Nauta et al., '74). Given the fact that the smallest ganglion cells in the retina can be filled from the superior colliculus (fig. 13 and Kelly and Gilbert, '75), and given the size of the injections employed here, if this lack of filling of the temporal small cells is due to lack of uptake and/or transport, then the contralateral projection from the temporal W-cells to the thalamus would differ considerably from that to the midbrain. Such a difference could be due to a difference in extent of arborization, for instance. The smaller cells which do spill a short distance into the contralateral temporal retina in our material may be W-cells, however (see fig. 6), since the decussation line for the X-cells (the only other candidates at present for these smaller cells) is known to pass sharply through the area centralis (Stone and Fukuda, '74b; Kirk et al., '76a).

It is interesting that not only are the small cells in the contralateral temporal retina unlabeled in our material, but in general the smallest ganglion cells of the retina remain unfilled. This is in spite of the fact that, as just mentioned, these cells are capable of transporting HRP from the superior colliculus. However, we do find that the larger end of the retinocollicular size distribution overlaps considerably with the cell population filled by injection of HRP into the thalamus. Kelly and Gilbert ('75) noticed this also and speculated that these larger retinocollicular ganglion cells could be either large $\gamma$-cells (presumably W-cells) or a small number of $\beta$-cells projecting to the superior colliculus. Although Fukuda and Stone ('74) have shown that X-cells, which have come to be identified

with β-cells (Boycott and Wässle, '74), do project to the midbrain in small numbers, they do not seem to send axons to the colliculus. In this regard it should be noted that Kelly and Gilbert's injections were large enough (0.5 µl) to fill the entire LGN, and they often found translaminar spread and uptake of HRP. Thus it is conceivable that their results contained some uptake from W-cells in the C-laminae. However, their study was completed before it was known that W-cells project to these laminae of the LGN (Wilson and Stone, '75; Cleland et al., '76). It is thus tempting to speculate that the tail of retinocollicular ganglion cells which overlaps with the LGN size distribution represents larger W-cells which project to the LGN as well as to the superior colliculus. It may then be that the smallest W-cells do not in fact send axons to the lateral geniculate. It should be noted here that differences in mean cell size have already been suggested in other contexts for different classes of W-cells (Stone and Fukuda, '74b).

Evidence Against Uptake by Ganglion Cells Projecting to Midbrain

Whatever the reason for the lack of filling of smallest cells in general, and of those in the contralateral temporal retina in particular, such findings make it unlikely that uptake from the mesencephalon (due to diffusion of HRP to the midbrain or to transport through damaged retinomesencephalic axons) contributed significantly to our results. Our reasons for believing this have been suggested above, and are outlined here. First, the entire LGN was always filled with HRP after our injections; in spite of this, uptake was confined mainly to the upper retina, corresponding to the anterior portion

of the LGN where the injections were made. This absence of significant transport to the lower retina indicates that the region of effective uptake was smaller than the apparent spread of extracellular HRP (see also Bunt et al., '75; Jones, '75). Since we did not find significant amounts of extracellular HRP in the midbrain nuclei receiving retinal input, and since there was little or no uptake from the posterior LGN (which was filled with HRP), it is unlikely that there was uptake from the mesencephalic visual nuclei. This is confirmed by the lack of filling of the small cells in the contralateral temporal retina. Stone ('66) has shown that approximately 25% of the ganglion cells in the temporal retina project contralaterally and that most of these are small cells. Data of Harting and Guillery ('75) as well as of Lane et al. ('74), and Feldon et al. ('70), make it clear that many or most of these cells must project to the rostral tip of the superior colliculus (see above). If there were direct spread of HRP to the midbrain, one would expect uptake to occur first in the rostral tip of the colliculus, which is closest to the LGN. Since the smallest ganglion cells are capable of transporting HRP after injections directly into the superior colliculus (fig. 13, and Kelly and Gilbert, '75), the absence of labeling of these small neurons in the temporal contralateral retina thus indicates that there was no significant uptake due to direct spread of HRP to the midbrain. The fact that, in general, there is no extensive labeling of the smallest cells of the contralateral retina (figs. 4, 5, 6, 8) also indicates the absence of transport from spread of HRP to the mesencephalon. These reasons for excluding the contribution of uptake directly from the midbrain also

can be applied against the possibility of transport of HRP through cut or damaged retinomesencephalic axons. This evidence against contamination of our results by ganglion cells sending axons to the midbrain is an important control for the following study of the retinothalamic pathway in Siamese cats.

In a way it seems odd that cut axons should not be an important factor in this study, since the injection needle did sometimes pass through the LGN and penetrate the underlying optic tract. However, Halperin and LaVail ('75) have shown that the cell bodies with cut axons accumulate HRP at a different rate from those with intact axons. These authors found that by 24 hours after the injection of the enzyme marker, perikarya with cut axons began to show significantly lower amounts of HRP activity compared to intact cells. It is possible that with the longer survival times used here (about two days), most of the HRP had disappeared from the cells with cut axons, leaving significant staining only in those cells taking in HRP through their terminals. Consistent with this suggestion is the observation that in some retinae there were several circular zones of non-stained or very lightly stained ganglion cells; these zones were centered at eccentricities corresponding approximately to the positions of the injection needle tracks in the LGN.

Is the Width of the Median Strip of Overlap Constant?

The fact that the distance from the most nasal ipsilateral cell to the point of maximum ipsilateral density increases considerably above the horizontal meridian (fig. 12) suggests that the amount of naso-temporal overlap also increases with eccentricity above the

area centralis. The implication here is that the displacement of the density maximum away from the median edge is due to a proportion of the cells close to the median edge projecting contralaterally instead of ipsilaterally. We attempted to determine whether there was in fact more overlap of the median edges about 3 mm above than in the area centralis, and it appeared that an overlap of the contralateral and ipsilateral median edges by 400 µm or more gave the most satisfactory isodensity lines. However, the results of this attempt were not clear-cut, because in this region 3 mm above the horizontal meridian the cell densities change much more slowly with eccentricity than they do within the area centralis itself. This made it somewhat arbitrary to decide just how much overlap was appropriate, since a number of different amounts of overlap seemed to give rather similar isodensity profiles. In addition, because of the low densities (relative to the area centralis) at this more periperhal eccentricity, the cells at the median edges of the nasal and temporal retinae become quite scattered, so that it was difficult to place each median edge accurately. (This was especially true of the contralateral retina, where some difficulty was encountered even in the area centralis, cf. fig. 6.) Thus the amount of overlap could not be determined with confidence at this eccentricity 3 mm above the area centralis.

The center of the median strip of overlap has been assumed to correspond to the zero meridian of the retina (Stone, '66). Since it also has been assumed that the median strip maintains a constant width above and below the area centralis, the median edge has been presumed to lie parallel to the zero meridian. But if, in fact,

there is more overlap of the median edges above the area centralis, then it may be that the zero meridian is actually skewed away from the median edge, so that the angle which the line between the area centralis and blind spot makes with the zero meridian (Bishop et al., '62; Stone, '66) may be different from that which it makes with the median edge.

The median edge of the retina has also been described physiologically in terms of the decussation pattern of X-cells, which is sharper than that for the other classes of ganglion cells (Stone and Fukuda, '74b; Kirk et al., '76a, b). It is still possible that the X-cell decussation line remains distinct at eccentricities above the area centralis and that the "fuzziness" in the contralateral median edge reflects the decussation pattern of other cell types. It thus may be that physiological recordings would show the median edges to be sharp even at these eccentricities. In this case the width of the median strip of overlap could still be a constant 200 μm at all elevations. This point cannot be resolved using our material, since we have not found it possible to distinguish absolutely between X- and W-cells on the basis of soma size.

Conclusion

The use of the retrograde transport of HRP has provided a clear and, we feel, aesthetic demonstration of the decussation pattern of the retinothalamic pathway in normal cats. It has also allowed the construction of density maps describing just the population of ganglion cells projecting to the thalamus. Such maps may be useful in comparisons of cortical and retinal magnification. These comparisons have been attempted previously using ganglion cell densities obtained

from Nissl-stained material (Hughes, '75; Tusa et al., '78) and have suffered from the obvious disadvantage of including cells projecting to the midbrain. The proper comparison would be one made between the cortex and the population of ganglion cells which projects to it via the thalamus. An attempt at this type of comparison is currently under way (Myerson and Cooper, unpublished observations).

The results of this study also provide an important control for the work reported in the following paper, in which the horseradish peroxidase technique is used to examine the retinothalamic pathway in Siamese cats (Cooper and Pettigrew, '78).

ACKNOWLEDGEMENTS

We would like to thank Gary Blasdel, Carol Shotwell, and Monica Wengrowicz de Cooper for their technical assistance. John Allman and Richard Russell kindly lent photographic and optical equipment. This manuscript was typed by Betty Hanson. The work reported here was supported by the Spencer Foundation and by grants from U.S.P.H.S., Nos. MH 25852 and EY 01909 to J.D.P. M.L.C. held a National Science Foundation Predoctoral Fellowship during most of this study.

LITERATURE CITED

Berman, N., and M. Cynader 1972 Comparison of receptive field organization of the superior colliculus in Siamese and normal cats. J. Physiol. (London), 224: 363-389.

Bishop, P. O., W. Kozak, and G. J. Vakkur 1962 Some quantitative aspects of the cat's eye: axis and plane of reference, visual field coordinates and optics. J. Physiol. (London), 163: 466-502.

Blaker, A. A. 1976 Field Photography: Beginning and Advanced Techniques. W. H. Freeman and Company, San Francisco.

Boycott, B. B., and H. Wässle 1974 The morphological types of ganglion cells of the domestic cat's retina. J. Physiol. (London), 240: 397-419.

Bunt, A. H., A. E. Hendrickson, J. S. Lund, R. D. Lund, and A. F. Fuchs 1975 Monkey retinal ganglion cells: Morphometric analysis and tracing of axonal projections, with a consideration of the peroxidase technique. J. Comp. Neur., 164: 265-286.

Bunt, A. H., R. D. Lund and J. S. Lund 1974 Retrograde axonal transport of horseradish peroxidase by ganglion cells of the albino rat retina. Brain Res., 73: 215-228.

Bunt, A. H., and D. S. Minckler 1977 Bilateral projection of the central retina of the monkey. Abstracts of Annual Meeting of Association for Research in Vision and Ophthalmology, Sarasota, Florida, p. 86 (Abst.)

Cleland, B. G., and W. R. Levick 1974a Brisk and sluggish concentrically organized ganglion cells in the cat's retina. J. Physiol., 240: 421-456.

———— 1974b Properties of rarely encountered types of ganglion cells in the cat's retina and an overall classification. J. Physiol., 240: 457-492.

Cleland, B. G., W. R. Levick, R. Morstyn, and H. G. Wagner 1976 Lateral geniculate relay of slowly conducting retinal afferents to cat visual cortex. J. Physiol., 225: 299-320.

Cooper, M. L., and J. D. Pettigrew 1977a The retinothalamic pathway in Siamese cats studied with horseradish peroxidase. Abstracts of Annual Meeting of Association for Research in Vision and Ophthalmology, Sarasota, Florida, p. 86 (Abst.)

———— 1977b Naso-temporal division of retinothalamic pathway in normal and Siamese cats. Neuroscience Absts. III, p. 556.

———— 1978a The retino-thalamic pathway in Siamese cats. J. Comp. Neur., submitted for publication.

———— 1978b A neurophysiological study of the vertical horopter in the cat and owl. J. Comp. Neur., submitted for publication.

Enroth-Cugell, C., and J. G. Robson 1966 The contrast sensitivity of retinal ganglion cells of the cat. J. Physiol., 187: 517-552.

Feldon, S., P. Feldon, and L. Kruger 1970 Topography of the retinal projection upon the superior colliculus of the cat. Vision Res., 10: 135-143.

Fukuda, Y., and J. Stone 1974 Retinal distribution and central projections of Y-, X- and W-cells of the cat's retina. J. Neurophysiol., 37: 749-772.

Ganser, S. 1882 Über die periphere und zentrale Anordnung der Sehnervenfasern and über das Corpus bigeminum anterius. Arch. Psychiat. Nervenkr., Bd. 13: 341-381.

Gilbert, C. D., and J. P. Kelly 1975 The projections of cells in different layers of the cat's visual cortex. J. Comp. Neur., 163: 81-106.

Halperin, J. J., and J. H. LaVail 1975 A study of the dynamics of retrograde transport and accumulation of horseradish peroxidase in injured neurons. Brain Res., 100: 253-269.

Harting, J. K., and R. W. Guillery 1975 Organization of retinocollicular pathways in the cat. J. Comp. Neur., 166: 133-134.

Hedreen, J. C., and S. McGrath 1977 Observations on labeling of neuronal cell bodies, axons, and terminals after injection of horseradish peroxidase into cat brain. J. Comp. Neur., 176: 225-246.

Hughes, A. 1975 A quantitative analysis of the cat retinal ganglion cell topography. J. Comp. Neur., 163: 107-128.

———— 1976 A supplement to the cat schematic eye. Vision Res., 16: 149-154.

Jones, E. G. 1975 Possible determinants of the degree of retrograde neuronal labeling with horseradish peroxidase. Brain Res., 85: 249-253.

Kanaseki, T., and J. M. Sprague 1974 Anatomical organization of pretectal nuclei and tectal laminae in the cat. J. Comp. Neur., 158: 319-338.

Kelly, J. P., and C. D. Gilbert 1975 The projections of different morphological types of ganglion cells in the cat retina. J. Comp. Neur., 163: 65-81.

Kirk, D. L., W. R. Levick, B. G. Cleland, and H. Wässle 1976a Crossed and uncrossed representation of the visual field by brisk-sustained and brisk-transient cat retinal ganglion cells. Vision Res., 16: 225-232.

———— 1976b The crossed or uncrossed destination of axons of sluggish-concentric and non-concentric ganglion cells, with an overall synthesis of visual field representation. Vision Res., 16: 233-236.

Kristensson, K., Y. Olssen, and J. Sjöstrand 1971 Axonal uptake and retrograde transport of exogenous proteins in the hypoglossal nerve. Brain Res., 32: 399-406.

Lane, R. H., J. H. Kaas, and J. M. Allman 1974 Visuotopic organization of the superior colliculus in normal and Siamese cats. Brain Res., 70: 413-430.

LaVail, J. H., and M. M. LaVail 1974 The retrograde intraaxonal transport of horseradish peroxidase in the chick visual system: A light and electron microscopic study. J. Comp. Neur., 157: 303-357.

Lynch, G. S., R. L. Smith, P. Mensah, and C. W. Cotman 1973 Tracing the dentate gyrus mossy fiber system with horseradish peroxidase histochemistry. Exp. Neur., 40: 516-524.

Magalhaes-Castro, H. H., L. A. Murata, and D. Magalhaes-Castro 1976 Cat retinal ganglion cell projections to the superior colliculus as shown by the horseradish peroxidase method. Exp. Brain Res., 25: 541-549.

Mason, R. 1975 Cell properties in the medial interlaminar nucleus of the cat's lateral geniculate complex in relation to the transient/sustained classification. Exp. Brain Res., 22: 327-329.

Nauta, J. H. W., M. B. Pritz, and R. J. Lasek 1974 Afferents to the rat caudoputamen studied with horseradish peroxidase. An evaluation of a retrograde neuroanatomical research method. Brain Res., 67: 219-238.

Sanderson, K. J. 1971 The projection of the visual field to the lateral geniculate and medial interlaminar nuclei in the cat. J. Comp. Neur., 143: 101-118.

Sanderson, K. J., and S. M. Sherman 1971 Naso-temporal overlap in visual field projected to lateral geniculate nucleus in the cat. J. Neurophysiol., 34: 453-466.

Snider, R. S., and W. T. Niemer 1961 A Stereotaxic Atlas of the Cat Brain. Univ. of Chicago Press, Chicago.

Stone, J. 1965 A quantitative analysis of the distribution of ganglion cells in the cat's retina. J. Comp. Neur., 124: 337-352.

———— 1966 The naso-temporal division of the cat's retina. J. Comp. Neur., 126: 585-600.

———— 1978 The number and distribution of ganglion cells in the cat's retina. J. Comp. Neur., 180: 753-772.

Stone, J., and Y. Fukuda 1974a Properties of cat retinal ganglion cells. A comparison of W-cells with X- and Y-cells. J. Neurophysiol., 37: 722-748.

———— 1974b The naso-temporal division of the cat's retina re-examined in terms of W-, X- and Y-cells. J. Comp. Neur., 155: 377-394.

Strauss, W. 1964 Factors affecting the cytochemical reaction of peroxidase with benzidine and the stability of the blue reaction produced. J. Histochem. Cytochem., 12: 462-469.

Tusa, R. J., L. A. Palmer, and A. C. Rosenquist 1978 The retinotopic organization of area 17 (striate cortex) in the cat. J. Comp. Neur., 177: 213-236.

Vanegas, H., H. Hollländer, and H. Distel 1978 Early stages of uptake and transport of horseradish peroxidase by cortical structures, and its use for the study of local neurons and their processes. J. Comp. Neur., 177: 193-212.

Wässle, H., W. R. Levick, and B. G. Cleland 1975 The distribution of the alpha type of ganglion cells in the cat's retina. J. Comp. Neur., 159: 419-438.

Wilson, P. D., M. H. Rowe, and J. Stone 1976 Properties of relay cells in the cat's lateral geniculate nucleus. A comparison of W-cells with X- and Y-cells. J. Neurophysiol., 39: 1193-1209.

Wilson, P. D., and J. Stone 1975 Evidence of W-cell input to the cat's visual cortex via the C-laminae of the lateral geniculate nucleus. Brain Res., 92: 472-478.

FIGURE LEGENDS

Fig.1 Bright-field photograph of HRP-filled ganglion cells in far periphery of uncounterstained retinal whole mounts. These profiles were obtained after large injections into one LGN of a normal cat (see Methods). The dendritic filling in the large,alpha-type cells is quite extensive; while the dendrites of the surrounding smaller cells are much less heavily labeled. Scale:50 μm.

Fig. 2 See Fig. 1.

Fig. 3 Spread of HRP from the injection sites in a typical experiment. The vertical stripes represent the region of high density of benzidine reaction product. The light stippling corresponds to the region in which reaction product was confined mainly or entirely to the walls of blood vessel ( and probably represents the maximum extent of HRP spread. See Results.). The thalamic nuclei receiving retinal input ( LGNd, LGNv, MIN) were all filled with HRP, while even the lightest label was not found extending into the midbrain nuclei which contain retinal terminals ( NOT, NPP, SC ). BCI, brachium of the inferior colliculus; BSC, brachium of the superior colliculus; CP, cerebral peduncle; CSC, commissure of the superior colliculus; HAB, habenula; IN, interpeduncular nucleus; LD, lateral dorsal nucleus; LGNd, dorsal lateral geniculate nucleus; LGNv, ventral lateral geniculate nucleus; LP, lateral posterior nucleus; MB, mammillary body; MGN, medial geniculate nucleus; MIN, medial interlaminar nucleus; NOT, nucleus of the optic tract; NPA, anterior pretectal nucleus; NPM, medial pretectal

nucleus; N III, oculomotor nucleus; OR, optic radiation; OT, optic tract; PC, posterior commissure; PN, pontine nuclei; PUL, pulvinar; RN, red nucleus; SC, superior colliculus; SN, substantia nigra; ST, subthalamic nucleus; THI, habenulo -interpeduncular tract; ZI, zona incerta.

Fig. 4 Low power photographs of naso-temporal division of the retinothalamic pathway in the normal cat LGN-35. The uncounterstained whole-mounts were obtained after the injection of HRP into one LGN. In the contralateral retina ( left ), the nasal hemiretina is filled with HRP-stained ganglion cells; a few large cells spill into the temporal retina. In the ipsilateral retina ( right ) the vertical decussation line is sharp and separates the labeled temporal hemiretina from the unlabeled nasal hemiretina. The optic disk is visible as a pale disk in the lower left of the contralateral retina and the lower right in the ipsilateral retina. The large, alpha-cells stand out particularly well in these whole-mounts. N, nasal; T, temporal. Scale: 2 mm.

Fig. 5 Higher power photographs of the same retinae as in Figure 4. Note the higher density of HRP-filled cells in the contralateral ( left ) than in the ipsilateral ( right ) area centralis. Also note how much sharper is the ipsilateral than the contralateral decussation line. N, nasal; T, temporal.

Fig. 6 Camera lucida drawings of areae centrales of the ipsilateral ( top ) and contralateral ( bottom ) retinae of LGN-35. The median edges of the temporal ( top ) and nasal ( bottom ) retinae are

indicated by the vertical arrows; the oblique arrows point to the optic disk in each case. ( Temporal is to the left in the top figure and to the right in the bottom drawing ). Note that the most temporal contralateral cells tend to be large. No attempt has been made here to represent precisely the diameters of the HRP-filled cells; however, the cell sizes are roughly correct. Scale:200 μm.

Fig. 7 Counts of HRP-filled cells in the region of the ipsilateral ( top ) and contralateral ( bottom ) retinae of LGN-35. The camera lucida drawings of figure 6 were ruled off into squares 100 μm on a side; the number of labeled cells in each square is shown here at the appropriate location. Arrows are the same as in figure 6. Scale: 200 μm.

Fig. 8 Plots of the changing proportion of ipsilaterally and contralaterally projecting retinothalamic cells along the horizontal meridian of LGN-35. The cell counts in figure 6 ( and similar counts for the large cells alone ) were used to construct these curves. The number of cells in adjacent 1100 μm high X 100 μm wide strips ( centered on the horizontal meridian ) were calculated in the ipsilateral and contralateral retinae. The ipsilateral retina was next inverted left-to-right and the median edges of the two retinae overlapped by 200 μm. The number of cells projecting ipsilaterally in each strip was then expressed as a percentage of the summed ipsilateral and contralateral densities in corresponding strips of the two retinae (i.e., as a percentage of the total retinothalamic cell number ) ( filled circles ). A similar calculation was performed for just the large cells themselves ( open circles ). In addition, the number of retinothalamic large cells in each strip of the

contralateral retina was taken as a percentage of the total number of HRP-filled cells in that strip ( filled triangles ). The "median strip of overlap" ( see text ) would lie between 100 μm nasal and 100 μm temporal and would include the 50% decussation point for the total retino thalamic population. The 50 % point for the large cells is shifted considerably temporally to that for all the cells projecting to the thalamus. The filled triangles make it clear that beyond a few hundred micra temporally, virtually all of the contralaterally projecting cells are large.

Fig. 9 The percentage of the retinothalamic cells in LGN-35 which project ipsilaterally at various points along a horizontal line 2 mm above the horizontal meridian. The greatest excursion of contralateral cells into the temporal retina takes place along this line ( see fig.10). This curve was calculated from the density maps in figure 10; the ipsilateral map was inverted left-to-right and the median edges overlapped by 200 μm. The densities at corresponding points in the ipsilateral and contralateral retinae were summed and the ipsilateral counts were expressed as percentage of the total retinothalamic densities at the various points. Note that even along this line of greatest contralateral extent, the contralateral projection falls to less than 25% ( 75% ipsilateral ) about 600 μm into the temporal retina. Thus, the data here and in figure 8 do not indicate the presence of a substantial contralaterally projecting retinothalamic population across the temporal retina (cf. Stone, '66).

Fig. 10 Maps of HRP-filled ganglion cell density in the uncounterstained contralateral ( top ) and ipsilateral retinae of LGN-35.( See Methods for details of the preparation of these maps. ). Temporal is to the left in the upper figure and to the right in the lower figure. Labeled cell densities are expressed in cells/$mm^2$. The line of most-temporal contralateral cells ( top ) or most-nasal ipsilateral cells ( bottom ) is marked "1". The stippled circles represent the optic disks and the black dots the points of maximum retinothalamic density in the areae centrales. Note the rapid fall-off of contralateral density beyond the median edge of the nasal retina ( broken arrows in top figure. The median edge of the temporal retina is shown by broken arrows in the bottom figure.) Densities in the inferior retinae could not be obtained due to lack of filling of the ganglion cells. Scale: 1 mm.

Fig 11 Map of ipsilateral retinothalamic densities in the normal cat LGN-36. Orientation and symbols are the same as in figure 10 (bottom). ( The densities in the area centralis could not be counted because of a tear in the retina.) There is considerable similarity in the size and shape of isodensity lines in the ipsilateral retinae of LGN-35 and 36.

Fig. 12 Ipsilateral retinae of LGN-35 and 36. We have shaded the region between the line of most nasal ipsilateral retinothalamic cells (solid line) and the points (at each elevation) of maximum ipsilateral density (black dots). The point of maximum density in the area centralis

is shown as a cross; the other symbols are the same as in figures 10 and 11. It is clear that the distance to the peak ipsilateral density increases with distance above the horizontal meridian. The dotted horizontal line is drawn through the tips of the isodensity contour lines in figures 10 and 11.

Fig. 13 Cell-size histograms after large injections of HRP into the thalamus ( top ) and midbrain ( bottom ). The thalamic injection was made in the usual manner described in the Methods; the field of cells counted was centered near the horizontal meridian about 4.7 mm into the contralateral nasal retina. All the large cells (mean diameter = 27.5 μm) were filled with HRP. There was also a population of labeled medium-sized cells (mean diameter= 14.7 μm; range = 11 - 19 μm).However, the population of smallest ganglion cells was unlabeled (mean diameter= 10.9 μm, range= 8-18 μm); note particularly the lack of filling of the ganglion cells in the 8 - 11 μm range. The bottom histogram was constructed from measurements made after a large injection into the superior colliculus ( with probable involvement of the pretectum as well). The region of data collection was centered 6 mm along the horizontal meridian into the contralateral nasal retina, and 0.9 mm above this meridian. Only about one-half the large cells were filled with HRP (mean diameter= 28.8 μm). The medium-sized population was, on the whole, unlabeled (mean diameter= 14.5 μm; range= 8-19 μm). However, the smallest ganglion cells did contain HRP ( mean = 11.5 μm; range = 8-18 μm). Note that there is some overlap between the upper end of the midbrain size distribution and the thalamic distribution. These data thus confirm Kelly and Gilbert ('75).

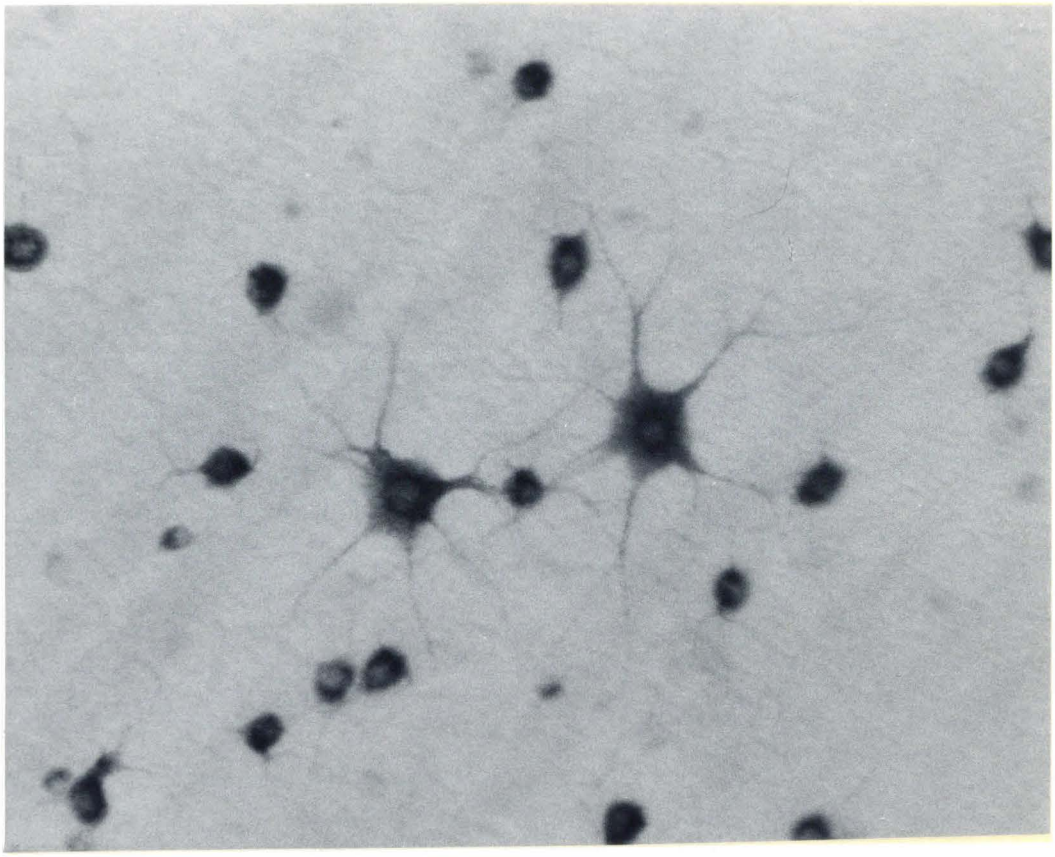

Figure 1

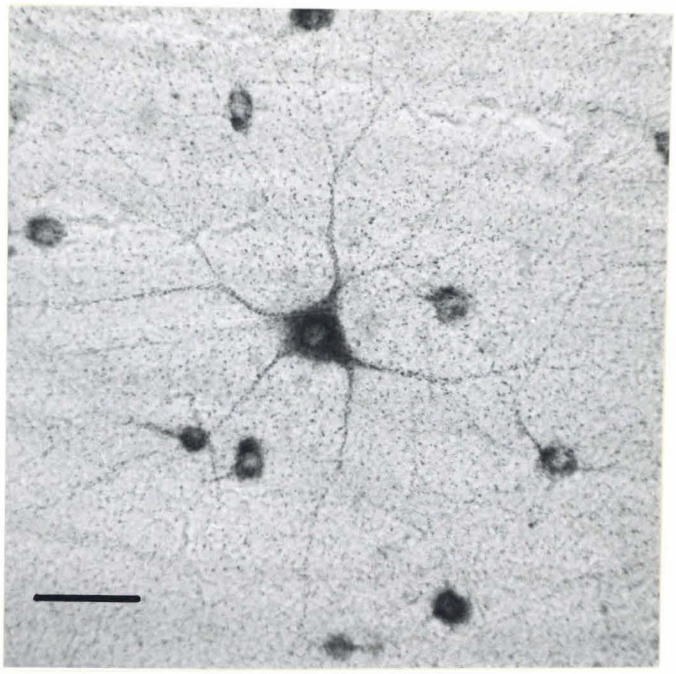

Figure 2


LGN$_s$–26
2 mm
LD
PUL
LP
HAB
LGN$_d$
ZI
ST
CP
MB
OT
THI
SN
OR
LGN$_v$
MIN
NOT
NPM
NPA
PC
MGN
RN
CSC
NPP
BSC
SC
NIII
IN
PN
BCI
NR

Figure 3


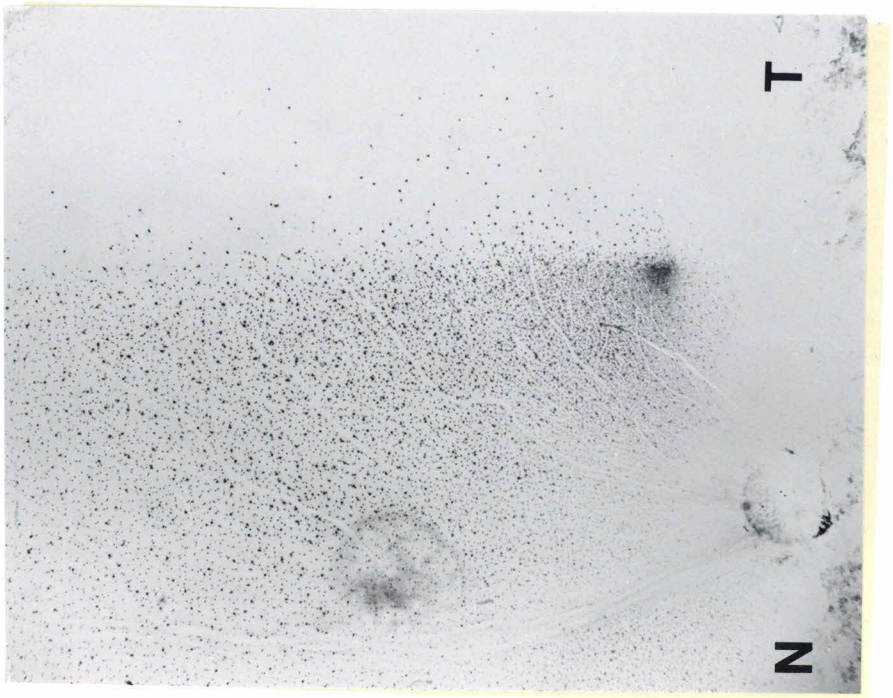


Figure 4

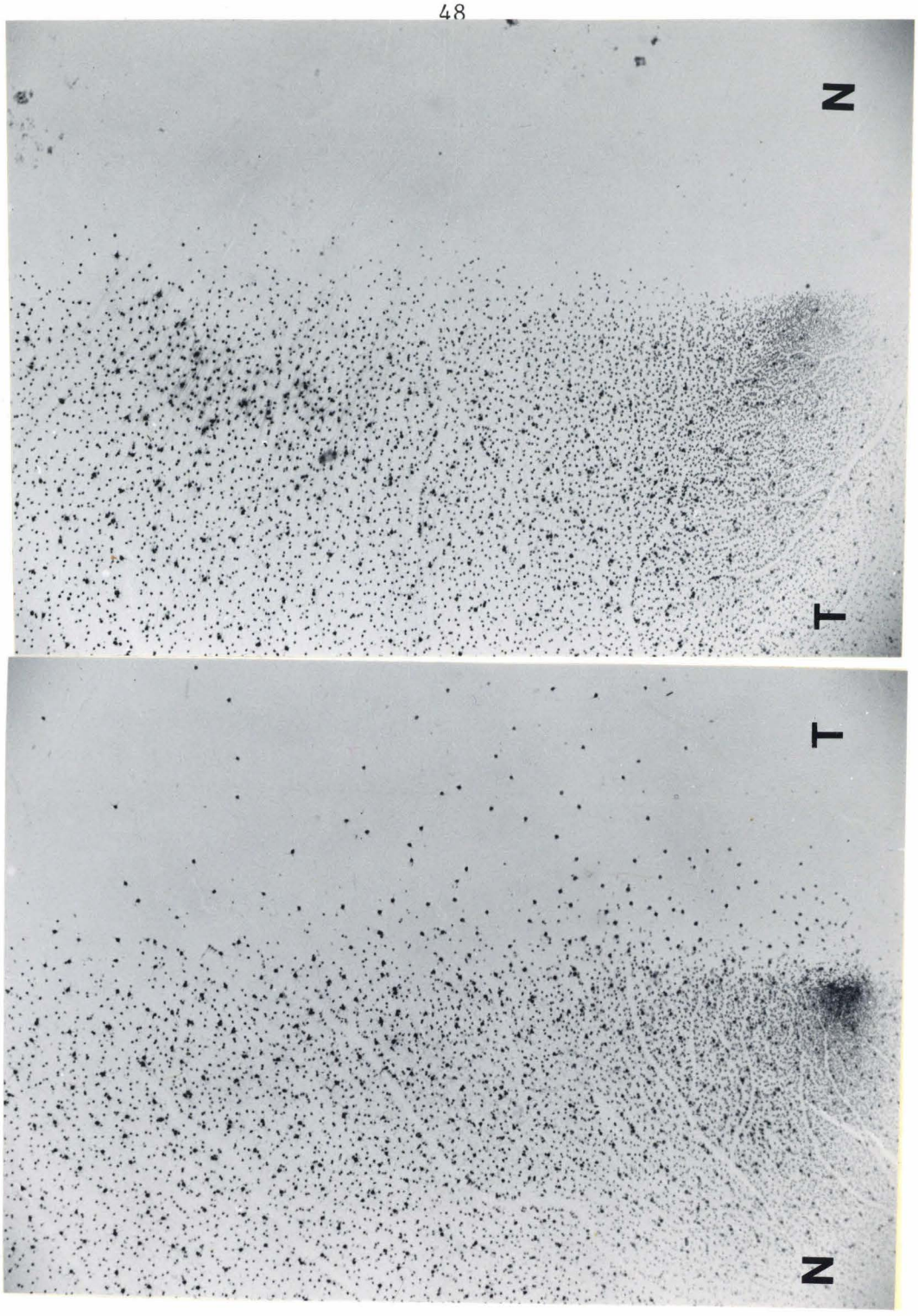


Figure 5

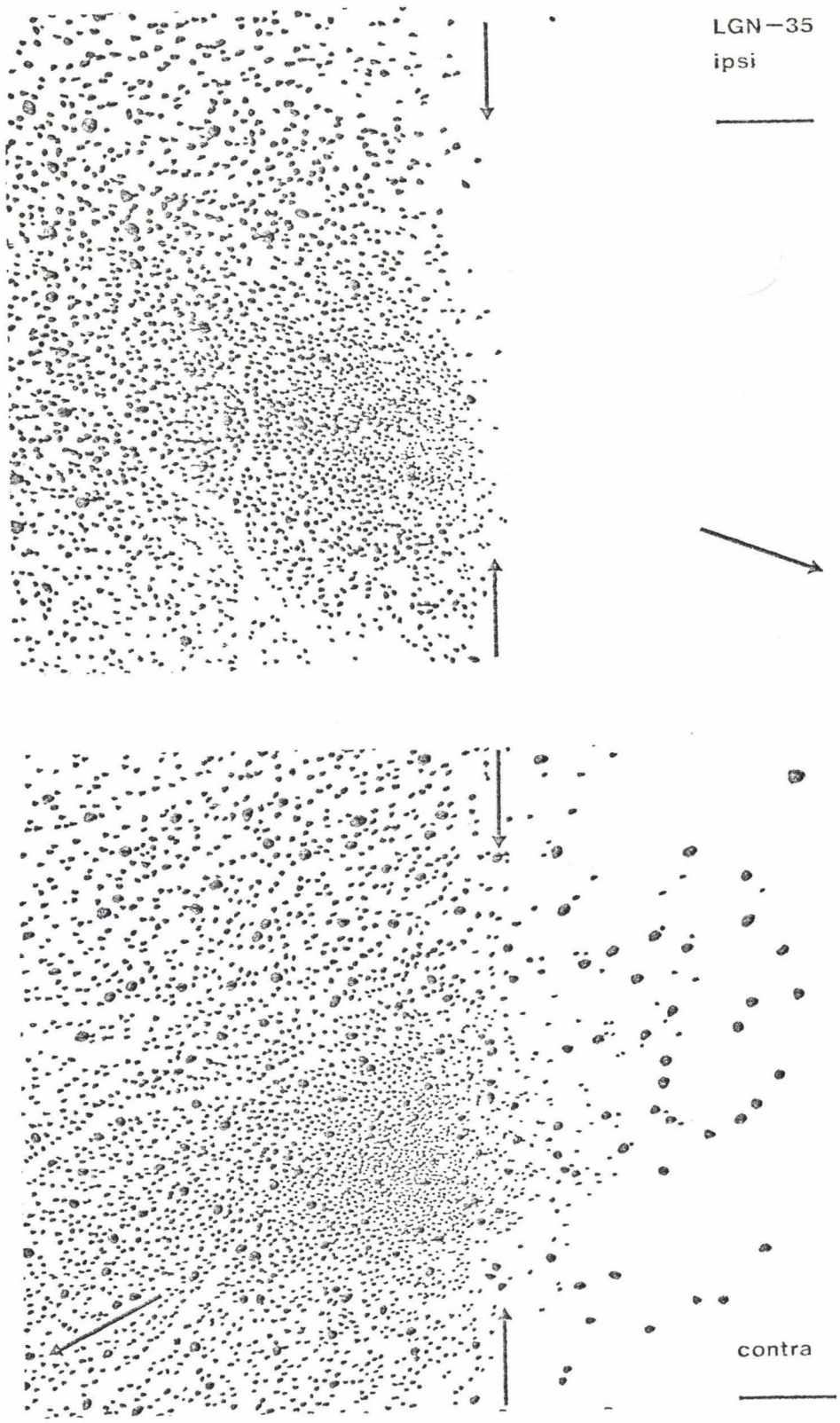


Figure 6

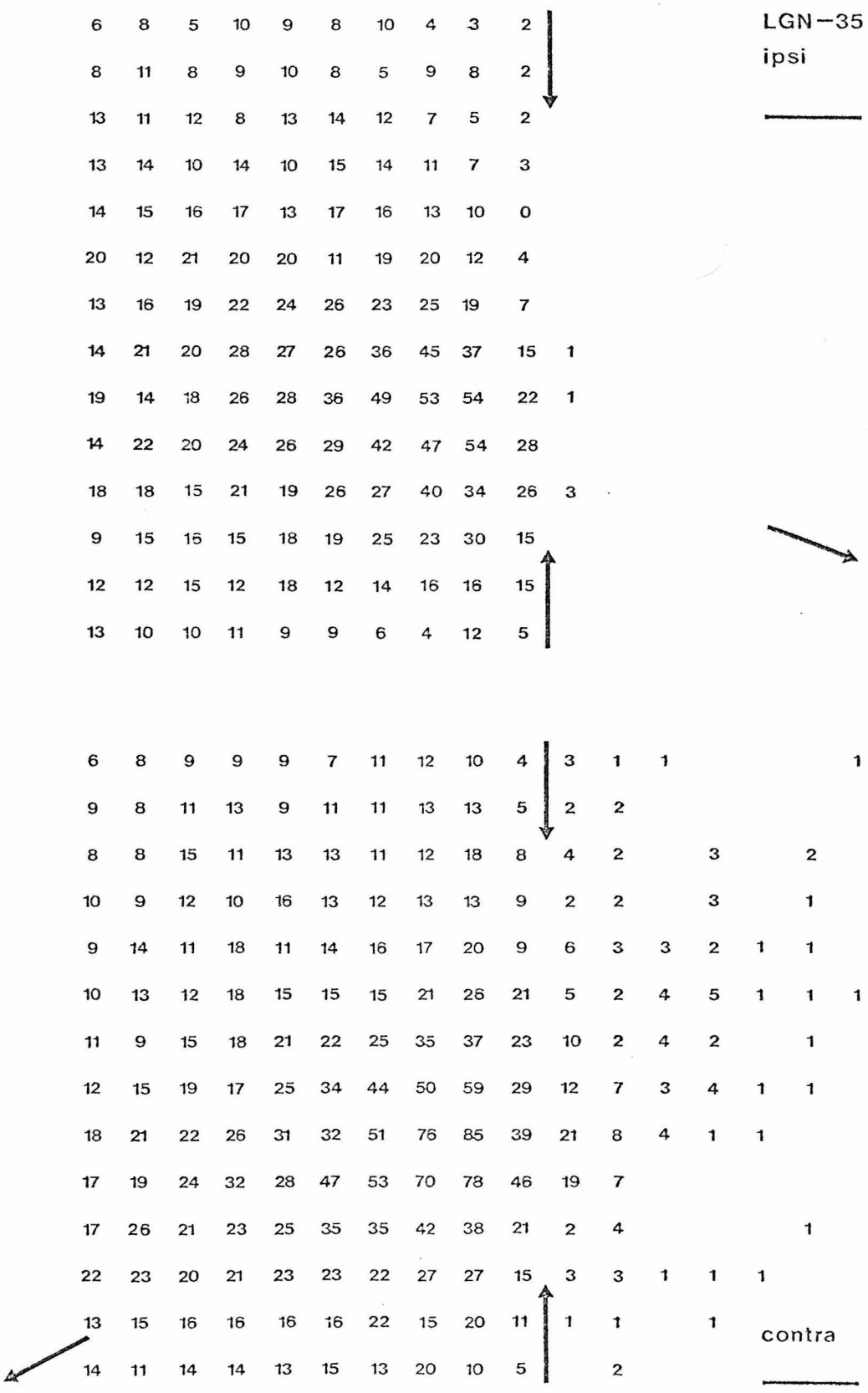


Figure 7

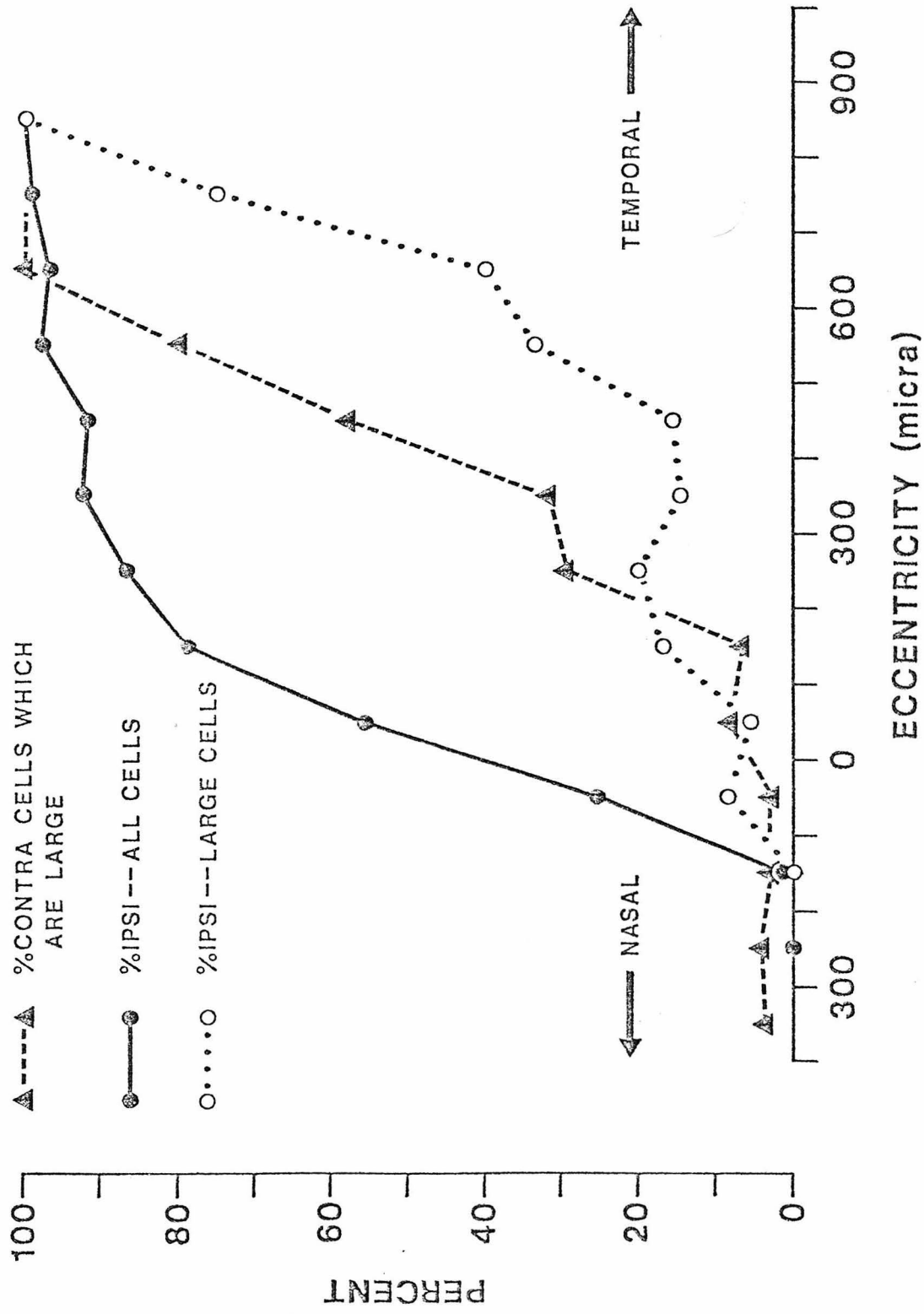
%CONTRA CELLS WHICH ARE LARGE
%IPSI--ALL CELLS
%IPSI--LARGE CELLS
NASAL
TEMPORAL
PERCENT
100
80
60
40
20
0
300
0
300
600
900
ECCENTRICITY (micra)

Figure 8

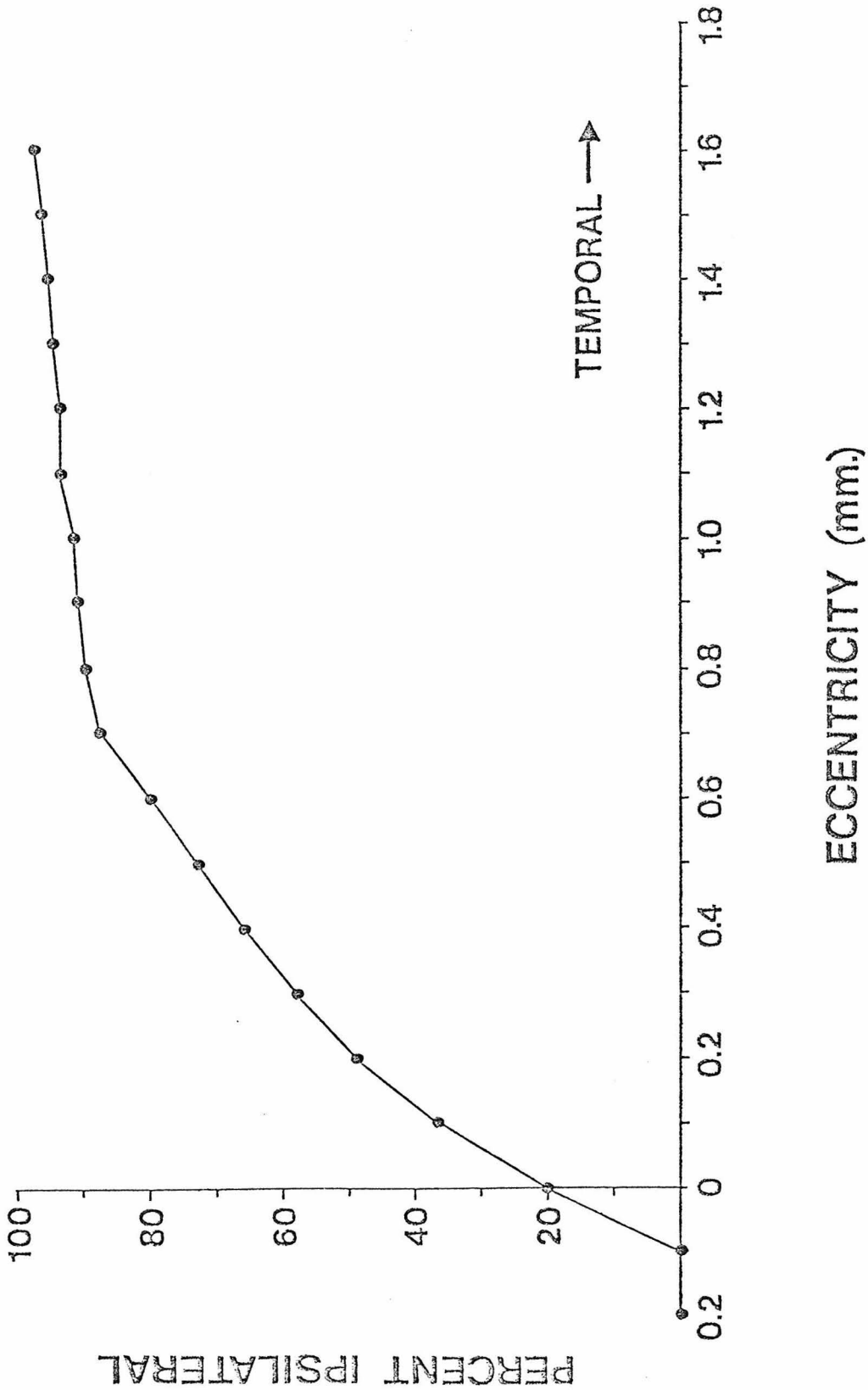
PERCENT IPSILATERAL
100
80
60
40
20
0
0.2
0.4
0.6
0.8
1.0
1.2
1.4
1.6
1.8
TEMPORAL
ECCENTRICITY (mm.)

Figure 9

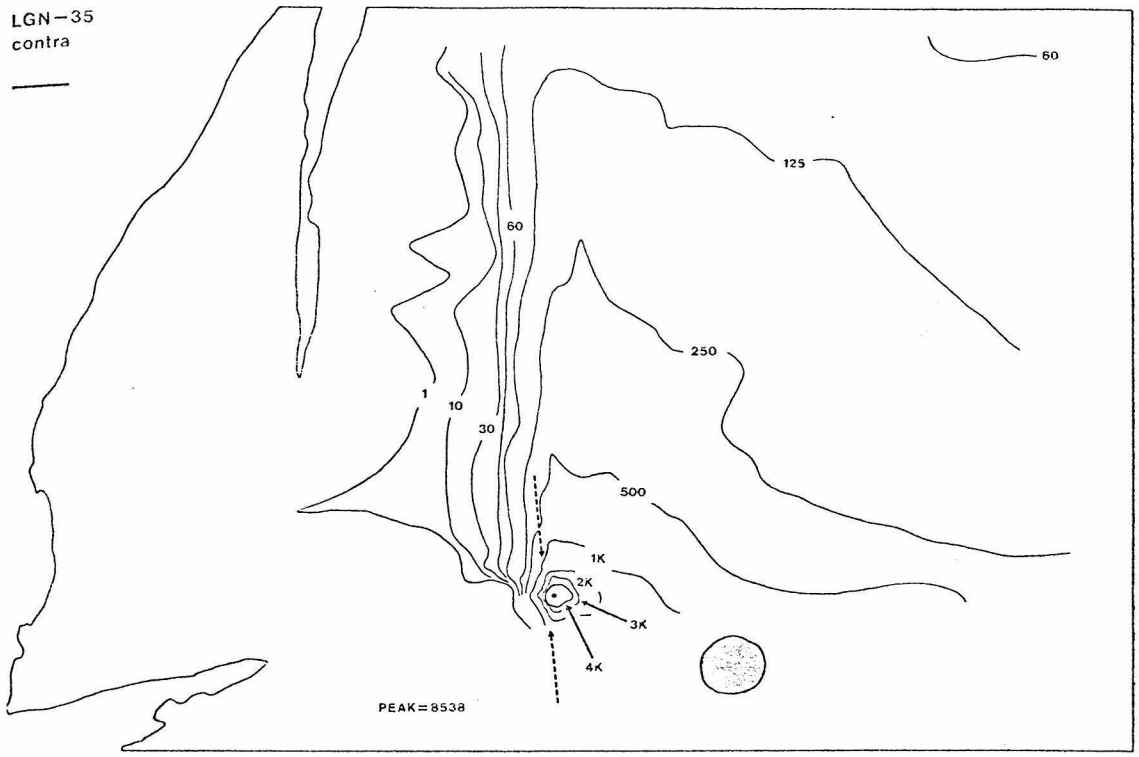
LGN–35
contra
60
125
60
250
1
10
30
500
1K
2K
3K
4K
PEAK=8538

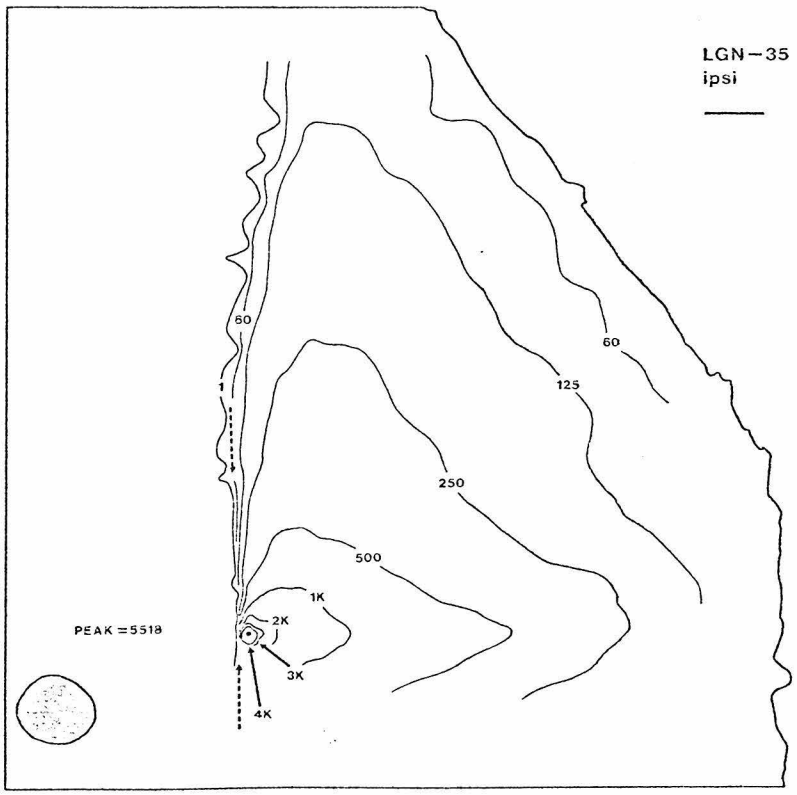
LGN–35
ipsi
60
60
125
250
500
1K
2K
3K
4K
PEAK=5518

Figure 10

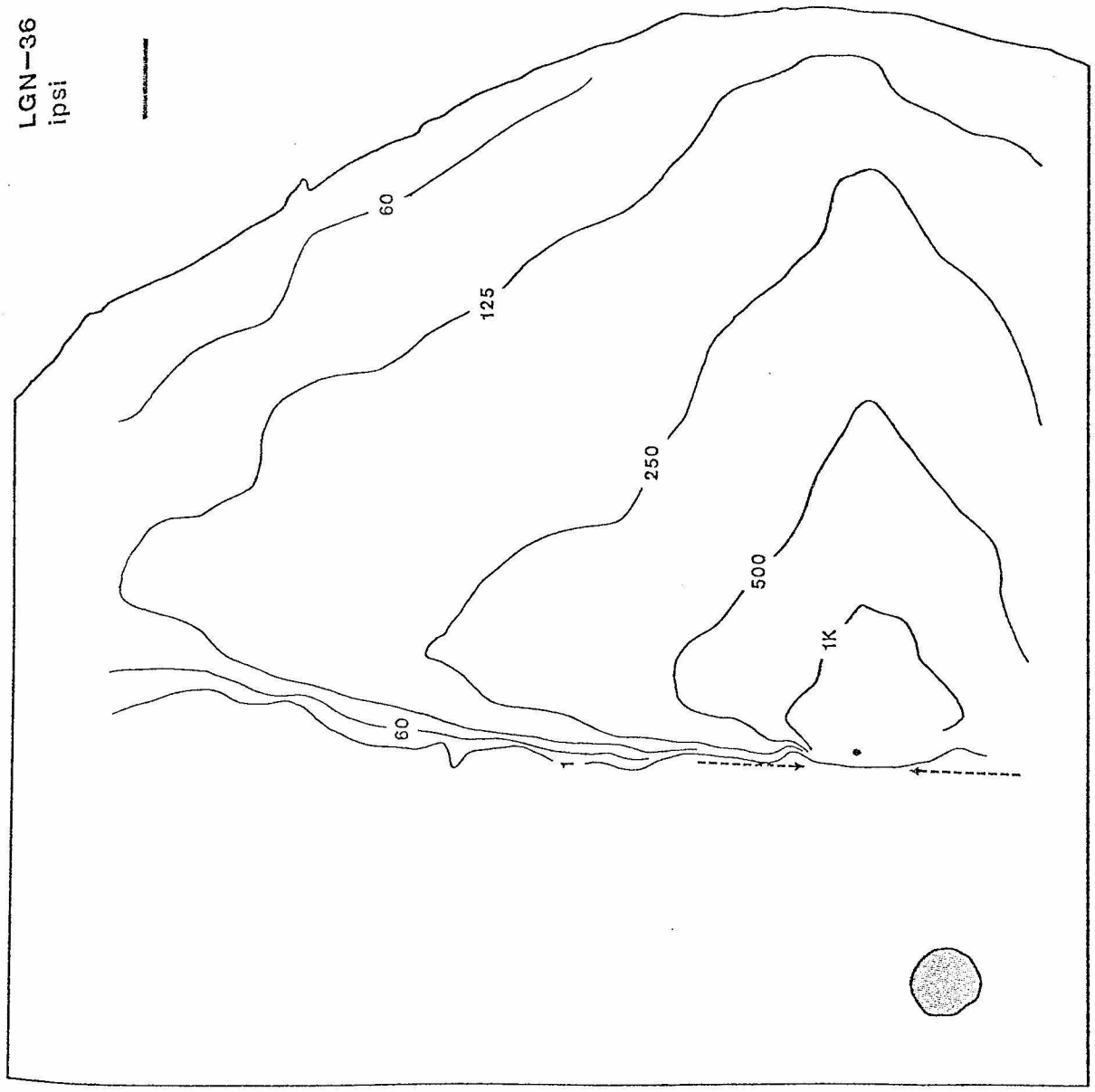


Figure 11

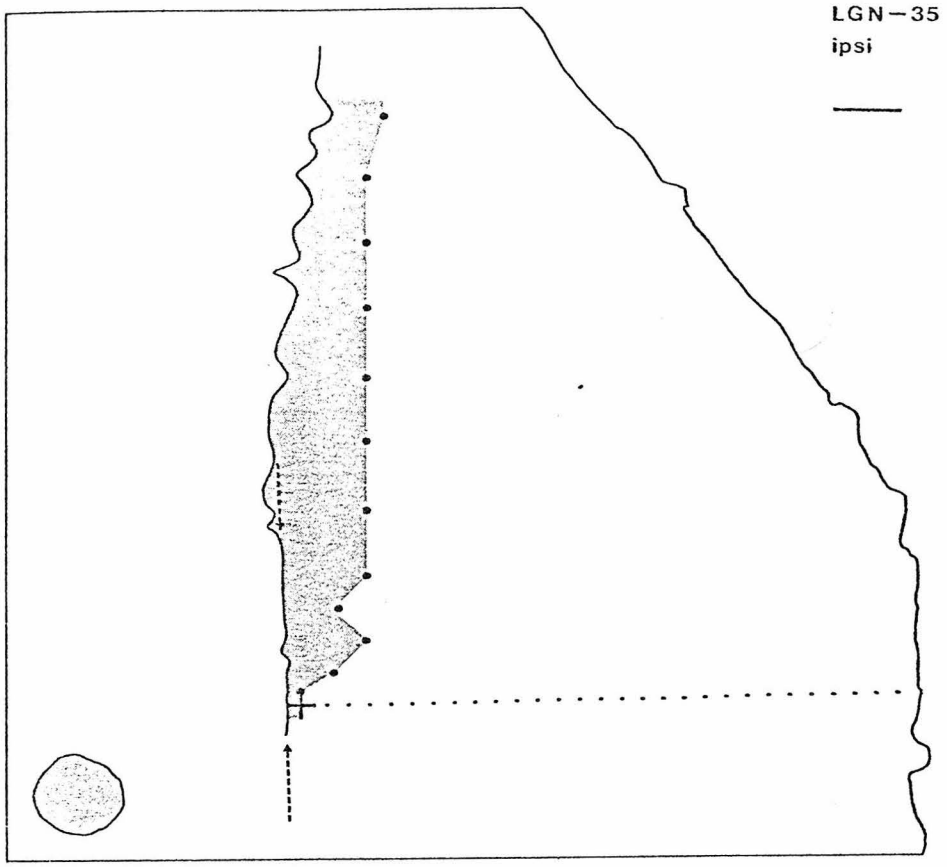


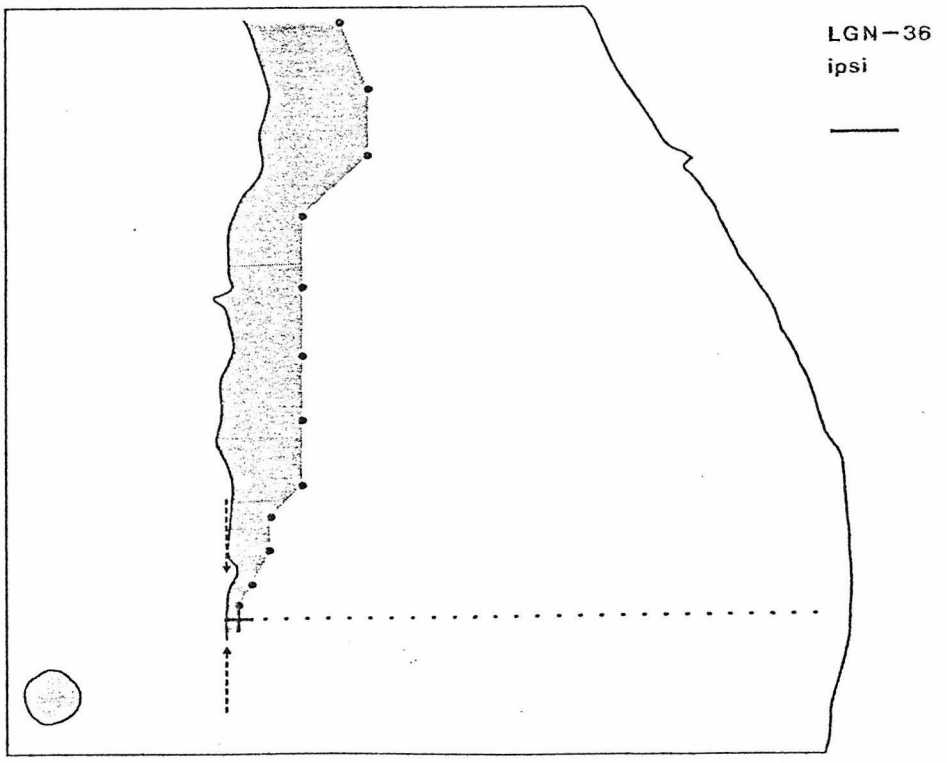


Figure 12

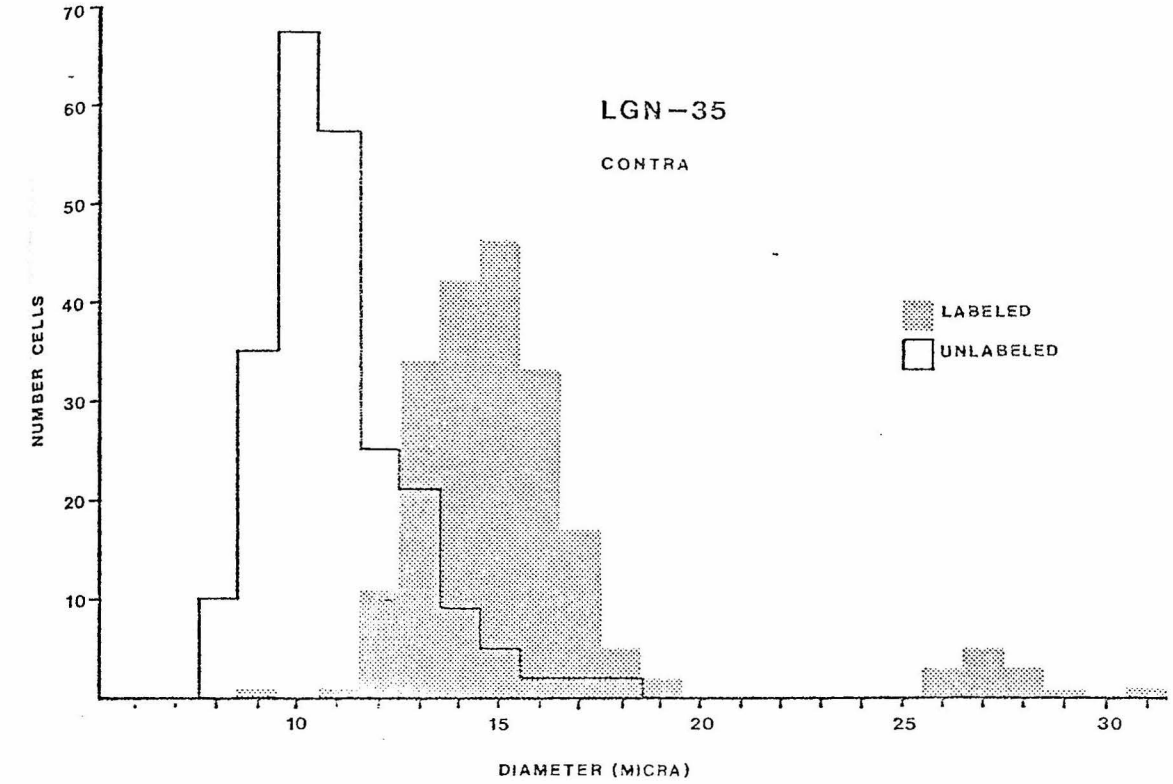
LGN–35
CONTRA
LABELED
UNLABELED
NUMBER CELLS
DIAMETER (MICRA)
70
60
50
40
30
20
10
10
15
20
25
30

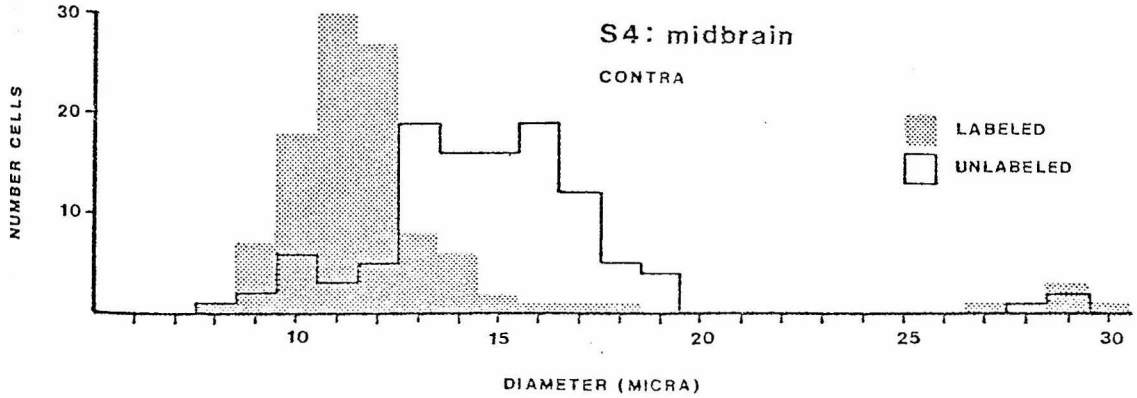
S4: midbrain
CONTRA
LABELED
UNLABELED
NUMBER CELLS
DIAMETER (MICRA)
30
20
10
10
15
20
25
30

Figure 13

# CHAPTER 2

## The Retinothalamic Pathway in the Siamese Cat

# INTRODUCTION

The developmental processes determining the laterality of retinal projections are but little understood (see Lund '75 and '78 for reviews). Mechanisms whereby the optic axons are directed to one or the other hemisphere are of interest not only for their importance in understanding binocular visual function, but also because they may relate to the general phenomenon of the decussation of fiber tracts (e.g., pyramidal tract, decussation of the brachium conjunctivum). One system which seems to hold promise for shedding light on these questions is the retinogeniculate pathway of albino animals. In these animals, a genetic mutation results in the misrouting of optic fibers which are normally directed ipsilaterally, so that these fibers instead project to the contralateral hemisphere (see Lund, '75 for references). The most extensively studied albino animal is the Siamese cat. Guillery ('69) and Guillery and Kaas ('71) were the first to describe and interpret the abnormal projection pattern of the Siamese retinogeniculate system, basing their description of this pathway on degeneration studies and electrophysiological recordings (see also Kalil et al., '71). More recently, Shatz ('77) has used the transport of tritiated amino acids to support the original conclusions of Guillery and Kaas concerning the input from the eye to the dorsal lateral geniculate nucleus (LGNd, or simply, LGN) in Siamese cats.

According to these previous studies, there is a vertical strip of Siamese retina, extending approximately 20° temporally from the zero meridian, in which all of the ganglion cells misproject contralaterally. The pattern of misprojection proposed in these studies is outlined in figure 1. The axons of the misrouted cells are held to terminate in the "abnormal segment of lamina A1" (abA1), while the ganglion cells lying temporal to the 20° meridian supposedly project correctly

and exclusively to the ipsilateral hemisphere and terminate there in the "lateral normal segment of A1" (LNS). Thus, in effect, this formulation proposes that the Siamese defect is a simple shift of the naso-temporal decussation line to a meridian lying 20° into the temporal retina. In addition, the descriptions of Guillery and Kaas and of Shatz indicate that there is a small region of temporal retina immediately adjacent to the zero meridian which is spared the contralateral misprojection and instead sends fibers to the "medial normal segment" (MNS) of ipsilateral A1. This MNS is supposed to subtend the first 2-3° of temporal retina. Since there may also be a small "medial abnormal segment" in the LGN in addition to the MNS, the possibility is raised that this most medial region of the temporal retina projects bilaterally.

The main purpose of our experiments was to attempt to visualize directly the topography of the misprojecting segments in whole mounts of the Siamese retina, since the previous studies had only inferred the pattern of retinal output from examination of the LGN. Our use of the horseradish peroxidase (HRP) labeling technique in normal cats has enabled us to obtain a clear picture of the naso-temporal division of thalamopetal ganglion cells over a wide area of retina (Cooper and Pettigrew, '78b); it was our hope that the same approach would reveal precise details concerning the manner in which the Siamese cat departed from the normal pattern. We thought that information about the shape of the misprojecting retinal segments would be of value in assessing the various developmental models proposed for the albino defect (cf. Guillery and Kaas, '71; Sanderson et al., '74; Lund, '75). In addition, we wished to use the retrograde transport of HRP to test the previous formulations of a 20° strip of misprojection, the predictions of which are schematized in figure 1. In the ipsilateral temporal retina, one would expect labeling in a narrow

sector near the zero meridian; this sector would correspond to those cells projecting to the MNS. One would also anticipate finding a wider vertical strip of temporal retina extending from 20° to the retinal margin due to retrograde transport from the LNS. On the other hand, in the contralateral retina the expectation would be to find labeling of a vertical strip covering the first 20° of temporal retina.

The data we have obtained from our HRP injections are not in exact accord with the expected results which we have just outlined. Our findings indicate that in fact there is bilateral projection to the thalamus from almost the whole of the Siamese temporal retina. In addition, we have observed differential effects of the Siamese defect on the different classes of retinal ganglion cells.

While this study was in progress, we learned of the investigations carried out independently by Kirk ('76) and Stone et al. ('78a). These two studies were aimed at describing the decussation of the total retinofugal pathway in Siamese cats and yielded results consistent with those presented here.

Abstracts of this work have been presented elsewhere (Cooper and Pettigrew, '77a,b).

# METHODS

All of the cats used here had blue eyes and typical Siamese coat markings. The alignment of the eyes under paralysis was estimated in each cat. In cats LGNS-25, LGNS-26, and BCC-3, the visual axes diverged by 5-10°, while in BCC-6 they diverged by about 15°. In contrast, the axes were crossed by 2-4° in LGNS-20 and -21, by about 10° in LGNS-19, and by 20° in LGNS-24. In the normal cat, the visual axes are divergent by about 5° under paralysis (Bishop et al., '62).

In general, the methods of tissue preparation and data collection and reduction were the same as those employed in the preceding study (Cooper and Pettigrew, '78b). We describe here just those aspects of our methods which were unique to the present investigation.

## Preparation of the retinae

We used a method for making relieving cuts in the fundus which was slightly different from that of the previous study. In the first animals of the present series (LGNS-19 through LGNS-21), two horizontal cuts were made along the length of the retinae in order to separate them into three strips (Stone, '65). The middle strip was centered on the horizontal meridian and contained the area centralis and optic disk. For LGNS-25 and -26, a quadrant was removed from the fundus, as shown by the dotted lines in figure 1; a vertical cut placed nasal to the disk and a horizontal cut placed inferior to the tapetal margin ensured that the quadrant contained the optic disk and area centralis as well as the dorsal part of the zero meridian separating nasal from temporal retina.

## Estimation of shrinkage

Our methods for determining the shrinkage of the retinae are described in the preceding report. In LGNS-25, both retinae showed about 15% uniform shrinkage across the retina; these retinae were corrected accordingly. The ipsilateral retina LGNS-21 shrank uniformly by about 11% and was corrected to the dimensions of the contralateral retina of the same animal. The shrinkage of the other retinae was estimated to be less than 5%, and these retinae therefore were not corrected for length or cell density.

It should be noted that the contralateral retina of LGNS-26 and ipsilateral retina of LGNS-25 did not shrink more than their partner retinae, as may appear to be the case in figures 5 and 7. The smaller overall length in these two cases is due to the loss of part of the temporal edge of these retinae during their removal from the fundus.

## Contour maps

As was done for the animals in the preceding investigation, we produced maps of ipsilateral and contralateral ganglion cell density for most of the Siamese cats mentioned below. In order to demonstrate the overlap between ipsilaterally and contralaterally projecting populations in the temporal retina of Siamese cats, we prepared a further map for each cat. In this map, we calculated the percentage, for any given point in the retina, of the total retinothalamic population which sent axons ipsilaterally. Such "%-ipsilateral" maps were constructed by summing the cell densities at corresponding points of the ipsilateral and contralateral temporal retinae. The number of ganglion cells which projected ipsilaterally at each point was then expressed as a percentage of the total number of ganglion cells projecting to the thalamus from that point.

These "%-ipsilateral" maps were prepared on the assumption that there is no significant branching of ganglion cell axons to both optic tracts. Such bifurcation has been found in the normal rat (Cunningham and Freeman, '77) and Kolliker described three bilaterally branching axons in Golgi preparations of the chiasma of 13 kittens (Kolliker, 1899). However, Stone ('66) has presented evidence against there being significant numbers of branching fibers in the adult cat. This question will be addressed further below.

## Electrophysiological methods

We made single unit recordings in the visual cortex of all of our Siamese cats in order to determine whether they conformed to the "Boston" or "Midwestern" cortical patterns (Hubel and Wiesel, '71; Kaas and Guillery, '73; Shatz, '77). These recording sessions started on the morning after the injection of the HRP. The ketamine used during the injections had worn off by this time.

Our recording procedure was similar to that described previously (Pettigrew, '74; Cooper and Pettigrew, '78a). After insertion of venous and tracheal cannulae under fluothane anesthesia, we transferred the cats to a stereotaxic headholder and started continuous infusion of a paralytic mixture containing Flaxedil and d-tubocurarine (Rodieck et al., '67). This paralytic necessitated force-hyperventilation of the animals with a $N_2O$:$O_2$:$CO_2$ (75%:22.5%:2.5%) mixture. The pupils were dilated with atropine and the corneas protected with contact lenses of zero power. Temperature was maintained at 37-38°C.

The cats faced a tangent screen placed 57 cm away. The positions of the optic disks and, where possible, the areae centrales, were projected on the tangent screen with a reversible ophthalmoscope. In those cases where the areae

centrales were not clearly defined (Hubel and Wiesel, '71; Shatz, '77; Stone et al., '78b), the zero meridians were taken to lie 15.8° nasal to the projections of the optic disks (Nikara et al.,'68).

We used tungsten-in-glass microelectrodes (Levick, '72) in order to record the activity of single units in the visual cortex contralateral to the injected LGN. The penetrations were made between HC A1 and A4; in each penetration we attempted to determine whether there was a systematic representation of the ipsilateral hemifield in the region of the 17/18 border. Electrolytic lesions were made in each track in order to facilitate subsequent reconstruction. At the end of the recording sessions, the cats were perfused as outlined in the preceding report (Cooper and Pettigrew, '78b). Blocks of the visual cortex were cut on the freezing microtome at 40 μm, and the sections were stained with cresyl violet.

## Autoradiographic procedures

In four of the Siamese cats which received HRP injections (LGNS-21, -25, -26, and BCC-5), we injected the vitreous of the contralateral eye with 100-500 μCi of $^{3}$H-proline in 30 μl of saline. The cats were perfused 12-20 hours later, at the end of the recording sessions. In these cats, the brains were cut coronally at 30 μm, and every third section through the LGN was processed for autoradiography (Cowan et al., '72). (The other two sections served for the determination of the spread of HRP and for cresyl violet staining.) We mounted the autoradiographic sections on subbed slides, coated them with Kodak NTB-2 emulsion, and exposed them at 4°C in the dark for 4-10 weeks. After this time, the slides were developed in Kodak D-19 and lightly counterstained with cresyl violet.

# RESULTS

## 1. HRP injections

### A. Individual Siamese cats

LGNS-20: Most extreme displacement of the decussation. We began these HRP injection experiments with the hope of demonstrating directly the shape and extent of the two large strips of exclusive unilateral projection which had been proposed to comprise the Siamese cat temporal retina (see Introduction). Figure 2 shows photographs of the retinae from Siamese cat LGNS-20 after the filling of one thalamus with HRP. Here, as in figure 1 and all subsequent figures, the ipsilateral retina has been reversed left-to-right so as to allow it to be superimposed with its contralateral mate. The contralateral retina in figure 2 shows features common to all the Siamese cats studied here. The area centralis (which appears as a darker oval region near the center of the retina) is complete, in contrast to its appearance in the normal cat, where the vertical decussation line divides the area centralis in half (see figs. 4 and 5 of the previous report, Cooper and Pettigrew, '78b; and also Stone, '66). Large numbers of contralaterally projecting cells spill into the temporal retina across what would normally be the vertical decussation line. (Compare fig. 2 with the corresponding fig. 4 for the normal.) The contralaterally projecting ganglion cells continue uninterrupted from the nasal into the temporal retina; indeed, some HRP-labeled cells are found at the very temporal edge of the contralateral retina. Thus, there is no sharp cutoff of contralaterally projecting cells at a vertical line about 20° into the temporal retina (arrow in figure). As in the normal (Cooper and Pettigrew, '78b), the large $\alpha$-type cells stand out quite well in this whole-mount preparation. It

is noteworthy that the most temporally situated contralateral cells are in the main large cells; certainly the proportion of labeled cells which are large increases toward the temporal margin of the contralateral retina. It is evident, then, that in the contralateral retina of LGNS-20, HRP-filled ganglion cells extend across the entire extent of temporal retina.

Figure 2 shows the ipsilateral retina for the same cat, LGNS-20. The dashed line represents the line of nasal-most ipsilateral cells. (Dots more nasal than this line are small pieces of pigment epithelium which unfortunately adhered to the retina during its removal from the fundus.) In spite of the nearby tear, it can be seen that the ipsilateral area centralis is devoid of HRP-filled ganglion cells; the most nasal ipsilaterally projecting ganglion cells are located about 3.5 mm (15-20°) into the temporal retina (except for a small tongue of a few cells found about 2 mm temporally). Thus, in LGNS-20, there is a strip of exclusive contralateral projection from the first 20° of temporal retina, just as proposed by Guillery and Kaas ('71).

Since the large HRP injections employed here gave such good filling of the ganglion cells, it has been possible to construct contour maps for the densities of HRP-labeled ganglion cells projecting to the ipsilateral or contralateral thalamus. Figure 3 shows the density maps for the retinae of LGNS-20. In the contralateral retina, the ganglion cell contour lines continue uninterrupted from the nasal retina across the normal vertical decussation line (vertical dotted line in the figure) into the temporal retina. The most temporally located contralateral cells are at the very edge of the retina. This density map as a whole is very reminiscent of the maps constructed for total ganglion cell density on the basis of Nissl-stained whole mounts (Stone, '65, '78; Hughes, '75). The peak density of ganglion cells in the contralateral area centralis is 4581 cells/mm$^2$.

Special care was taken to determine the line of most nasal cells in the ipsilateral retina of LGNS-20 and in all of the other homolateral retinae. (This line is marked "1" on the ipsilateral density maps. The most temporal contralateral cells were also mapped with care in all of the contralateral retinae.) In LGNS-20, as mentioned above, no ipsilateral cells are found central to an approximately vertical line located about 3.5 mm temporal to the area centralis. The densities of labeled ganglion cells in this ipsilateral Siamese retina are low compared to those in the normal as a result of the large numbers of ganglion cells misprojecting to the contralateral hemisphere.

The line of the most nasal ipsilateral large cells is even more temporally displaced (by about 2 mm) than the line for all of the cells. Such a finding is consistent with the already-mentioned observations that the most temporal contralateral cells tend to be large, thus leaving fewer large cells to project ipsilaterally. This is evidence that the large cells are more affected by the Siamese defect than the rest of the population of retinothalamic cells; this point will be documented more fully a number of times below.

Thus, in some aspects LGNS-20 conforms to the results expected on the basis of the descriptions of Guillery and Kaas ('71) and Shatz ('77). In particular, there is a region of temporal retina from 0-20° which projects exclusively contralaterally. The labeling pattern in this cat differs from the expected result, however, in that there is no large region of unilateral ipsilateral projection. In addition, no filled cells were found near the homolateral zero meridian, as would be expected on the basis of the usual idea of a medial normal segment.

The HRP injection procedures and analyses used in LGNS-20 were also employed for the other Siamese cats; and while the contralateral retinae are

qualitatively similar in all of the cats, the rest of the cats do differ significantly from LGNS-20 in the organization of the ipsilateral projection to the thalamus. In addition, none of the other Siamese cats studied shows such an extreme displacement of the decussation, since they all lack the wide strip of exclusive contralateral projection found in the temporal retina of LGNS-20.

LGNS-26: Less severe displacement of the decussation. This cat was identified as a "Boston" cat on the basis of its cortical physiology. Figure 4 shows an electrode penetration made in the left visual cortex of LGNS-26. The electrode entered the cortex in area 18, and the first unit encountered had its receptive field located about 10° into the left (ipsilateral) hemifield. As the electrode was advanced towards the 17/18 border, the fields moved progressively more ipsilaterally, until at the border itself (arrow) unit 8 was found approximately 21° into the ipsilateral visual field. As the track continued medially into area 17, the fields moved back towards the midline; the last unit in the track (unit 15) was located near the vertical meridian, only 3° into the left hemifield. Thus, LGNS-26 had a well-ordered representation of the first 20° of homolateral visual field, thereby conforming to Hubel and Wiesel's ('71) description of the cortical topography in the "Boston" cat. In fact, all of the cats in our study (with the exception of LGNS-19, see below) were identified as "Boston".

The ganglion cell density map for the retina contralateral to the HRP injection in LGNS-26 is shown in figure 5 and is similar in most respects to that of LGNS-20. The peak density in the area centralis is slightly higher, being 6976 cells/mm$^2$, and the line of temporal-most contralateral cells does not quite reach the edge of the retina. However, here again, as in all of the other contralateral retinae, the isodensity lines continue uninterrupted across the normal zero meridian

through the area centralis. Thus, in LGNS-26, as in LGNS-20, there is contralateral output from virtually all of the temporal retina.

In the contralateral temporal retina of LGNS-26, the number of labeled large cells was expressed as a fraction of the total number of HRP-filled cells in several vertically-oriented strips lying various distances from the zero azimuthal meridian. (These 4 mm-high strips were located between the horizontal meridian and a line lying 4 mm above this meridian.) In the 600 μm-wide band centered 2 mm from the zero meridian, only 7.5% of the contralaterally-projecting cells were large. Further temporally, in the band of the same width centered 4 mm from the zero meridian, large cells made up 11% of the total contralateral population. However, in the 4 mm-high strip lying between the temporal edge of the retina and a vertical line 5 mm from the zero meridian, fully 28% of the contralateral cells counted were large. These data show that the large cells make up an increasing proportion of the contralaterally misprojecting cells as one proceeds into the temporal periphery of LGNS-26.

In contrast to the contralateral retina, the map of the ipsilateral retina from LGNS-26 (fig. 5) shows a major difference with that of the previous animal. Unlike in LGNS-20, it is evident that in LGNS-26 virtually all of the temporal retina projected ipsilaterally (as well as contralaterally). However, there do seem to be two peaks of ipsilateral density in the map of LGNS-26, one near the zero meridian and the other far into the temporal periphery. The point of highest density in the central retina (250 labeled cells/$mm^2$) lies on the horizontal meridian about 0.6 mm (2-5°) from the zero vertical meridian, and thus is displaced from the peak of total ganglion cell density in the area centralis (as revealed by Nissl counterstaining). The other point of high ipsilateral density (242 labeled cells/$mm^2$) lies

near the horizontal meridian approximately 6.1 mm (about 30°) temporal to the area centralis. The central and peripheral density maxima may have given rise to the terminals in the MNS and LNS, respectively. However, even at the point of the lowest labeled cell count on the horizontal meridian, situated about midway between the two maxima, the density is still 81 cells/mm$^2$. Thus, in contrast to expectations based on the proposal of Guillery and Kaas ('71), we find in LGNS-26 no 20°-wide vertical strip of temporal retina which projected exclusively contralaterally.

LGNS-21, LGNS-25 and LGNS-19: Least extreme displacement of the decussation. LGNS-21 and -25 were derived from our Siamese cat colony; their genetic relationships will be shown in a subsequent report.

The density map of the contralateral retina of LGNS-21 shows contralateral projection from the entire expanse of temporal retina, with a peak density in the area centralis of 4685 cells/mm$^2$ (fig. 6). The ipsilateral density map is similar qualitatively to that of the previously-described cat, LGNS-26; there are some quantitative differences, however. The isodensity lines are more elongated along the horizontal meridian in LGNS-21 (fig. 6), and although there are again two peaks of ipsilateral density, the central peak (218 cells/mm$^2$) is shifted temporally by 1.7 mm (8°) from the area centralis. Also, the point of low density (142 cells/mm$^2$) between the two peaks is relatively higher than that for LGNS-26, the ratios being 250:81:242 (3.1:1:3.0) for LGNS-26 versus 218:142:172 (1.5:1:1.2) for LGNS-21 (see figs. 5 and 6). This point may be of significance later in the interpretation of the autoradiographs from these two cats. However, the main point here is that in LGNS-21 virtually all parts of the temporal retina projected ipsilaterally, as well as contralaterally, to the thalamus.

The maximum density in the contralateral area centralis is somewhat lower in LGNS-25 (fig. 7) than in the other Siamese cats, being 3798 cells/mm$^2$. As in the other Siamese, there is considerable extension of contralateral cells across the temporal retina; in this case, the most temporal contralateral cells are found about 7 mm (approximately 35°) from the zero meridian. The isodensity lines in the ipsilateral retina show pronounced horizontal elongation and less development of two peaks than in LGNS-21. Again there is ipsilateral labeling throughout virtually the whole of the temporal retina.

As in the normals, LGN-35 and -36 (Cooper and Pettigrew, '78b), the density maps for LGNS-21 and -26 do not show good filling of ganglion cells more than a few degrees inferior to the horizontal meridian. This indicates, as mentioned in the preceding report (Cooper and Pettigrew, '78b), that the region of effective uptake of HRP was confined to the anterior portion of the LGN and was therefore smaller than the apparent maximum extent of HRP diffusion from the injection site. This makes it unlikely that there was direct uptake from the mesencephalic visual nuclei, where no label was seen. LGNS-25 showed more extensive filling of the lower retina. However, even in this cat, the labeling extended only about half as far into the inferior retina as into the superior retina. Here again, there was no obvious spread of HRP to the midbrain.

The density maps for LGNS-19 are shown in figure 8 and are similar to those just described. This cat could not be positively identified as "Boston" or "Midwestern" because the cortical electrode track passed through the white matter near the 17/18 border. A sixth Siamese cat, LGNS-24, also yielded ganglion cell density maps qualitatively very similar to those of the other cats (besides LGNS-20); in particular, both ipsilateral and contralateral cells extended across

almost the entire temporal retina. The isodensity maps are not presented for this cat because faint staining of some parts of the peripheral retina precluded obtaining reliable density estimates in these areas. The density maps for BCC-5 will be presented and discussed elsewhere (Cooper and Blasdel, manuscript in preparation).

B. Bilaterally projecting retinal regions

The preceding section has shown that contralaterally projecting cells spread across the major part of the temporal retina in all of our Siamese cats. This observation indicates that there is intermingling of the ganglion cells which project to the two hemispheres. This intermingling can be quantitatively expressed by preparing a density map in which the number of cells projecting ipsilaterally at any given point is expressed as a percentage of the total number of retinothalamic ganglion cells at that point (see Methods).

The resulting "%-ipsilateral" density map for LGNS-20 is shown in figure 9. It is evident that there is a smooth gradient-like increase in the percentage of cells projecting ipsilaterally as one proceeds temporally from the 20° line marking the nasal limit of such cells ("<0" in the figure). The 50% line for the total retinothalamic population, at which half of the cells send axons ipsilaterally and half contralaterally, is an approximately vertical line located about 7.4 mm (35°) from the usual zero meridian through the area centralis; the other "%-ipsilateral" lines are also vertically oriented.

The 50% line for the large cells alone is shifted temporally from that for the total HRP-labeled population. In fact, there were so few large cells remaining in the ipsilateral retina of LGNS-20 that the 50% isodensity line is not continuous, but is broken into islands, the regions in between showing less than

50% homolateral projection of large cells. This indicates that at most points in the temporal retinas of LGNS-20, the percentage of the large cells misprojecting contralaterally is greater than that of the total retinothalamic population.

The "%-ipsilateral" map for LGNS-26 (fig. 9) again shows a smooth increase in the percentages of retinothalamic cells sending fibers ipsilaterally as one proceeds into the temporal retina. At the region of peak total ganglion cell density in the area centralis, only 0.4% of the retinothalamic cells projected to the homolateral thalamus. The %-ipsilateral isodensity lines again run approximately vertically, and the 50% line intersects the horizontal meridian about 4.7 mm (23°) temporally. There is some indication that the lowest density lines (0-20%) are not straight, but tend to bulge nasally along the horizontal meridian.

The small crosshairs in figure 9 represent the point on the retina which corresponds approximately to the farthest excursion into the ipsilateral visual field found in the cortical recordings in LGNS-26 (fig. 4). This visual field reversal point lies on the 40% ipsilateral line. This may indicate that the area around the 50% line can be considered a region of decussation in the same manner as that through the center of the area centralis in the normal animal. This possibility will be discussed further in a subsequent report (Cooper and Blasdel, manuscript in preparation).

The "%-ipsilateral" isodensity map for LGNS-21 (fig. 10) exhibits vertically-oriented lines with the 50% line located about 4.3 mm (21°) peripherally; the lower density lines again evidence a slight nasal bulge near the horizontal meridian. Only 0.6% of the retinothalamic cells sent their axons ipsilaterally from the center of the area centralis, and the map shows a gradual increase of ipsilateral projection moving peripherally from the centralis.

The isodensity lines for the %-ipsilateral map of LGN-25 (fig. 11), although still running more or less vertically, show more of a nasal bulge near the horizontal meridian than they do in the other cats. This is particularly pronounced in the 20% line, the difference in azimuth between a point 0.4 mm above the horizontal meridian and a point 0.6 mm below the meridian being 2.2 mm (about 10°). The 50% ipsilateral line crosses the horizontal meridian about 4.2 mm (21°) temporally to the zero meridian; the corresponding 50% line for the large cells alone is shifted up to 2.2 mm even more temporally and in some places almost coincides with the 100%-ipsilateral line (which represents the line temporal to which all cells project ipsilaterally).

The "%-ipsilateral" map for LGNS-19 is shown in figure 10 and is similar to those already described. The 50% ipsilateral line crosses the horizontal meridian about 3.4 mm (approximately 17°) temporal to the area centralis.

C. Ipsilaterally projecting cells in the nasal retina

Stone et al. ('78a) have demonstrated that in some Siamese cats there appear to be significant numbers of ipsilaterally projecting cells in the nasal retina. Montero and Guillery (quoted in Guillery and Casagrande, '77) report a similar result. We have looked for such cells but have found no evidence of any significant amount of ipsilateral projection from the nasal retinae of our animals. The fact that the ipsilaterally projecting nasal cells in Stone's tract-sectioned material are mainly small and medium in size, coupled with our negative result, suggests that these aberrant nasal cells send their axons to the midbrain.

D. Comparison of total retinothalamic densities in Siamese and normal cats

As a check for the possible existence of significant numbers of bilaterally

branching axons in the Siamese cat, we compared the total retinothalamic ganglion cell density at various points in the temporal retinae of normal and Siamese cats. This comparison was performed by summing the ipsilateral and contralateral densities at points 3, 4, and 5 mm along the horizontal meridian, and at a point 1 mm above the 4 mm point. Due to the fact that there are virtually no contralateral retinothalamic cells at these locations in normals, we averaged the ipsilateral densities from LGN-35 and -36 (see preceding study) in order to obtain the normal data. Using at each point the mean of the densities from all five of our Siamese (LGNS-19, -20, -21, -25, and -26), we found that the mean densities in the Siamese cat are lower than those in the normal, varying from 70-80% of the normal value at each point.

The cause of this reduction in the retinothalamic density in the Siamese cat is unclear, especially since in all but one of their cats, Stone et al. ('78b) did not notice any great difference in total ganglion cell numbers in Nissl-stained material. It is possible that the difference in retinothalmic densities between Siamese and normal could have been masked in the data of Stone et al. by their including the cells projecting to the midbrain. The density difference noted here between Siamese and normals could result from some defect in the transport of HRP in the Siamese. Alternatively, it could be indicative of some more fundamental difference in the Siamese cat, such as a decrease in the numbers of cells generated (possibly X-cells, see Stone et al., '78b) or cell death due to, for instance, competition between the two eyes for terminal space in the LGN (e.g., Landmesser and Pilar, '74, see Discussion).

The fact that the total retinothalamic densities in the Siamese seem to be somewhat lower than in the normal prevents our using such data to examine the question of bilateral branching of axons. However, it is worth noting here

that if bifurcation were an important mechanism in Siamese cats, then one would expect significant labeling of the ipsilateral area centralis; in fact, no such labeling is found in the Siamese retinae.

E. Cell-size measurements

The results for LGNS-20 and -25 indicate that the large cells are more affected by the Siamese defect than the retinothalamic population as a whole. This observation is based on the fact that the 50% ipsilateral isodensity lines for the large cells are displaced temporally to the 50% lines for all the cells. This finding has been verified by making cell-size measurements at equivalent points in the ipsilateral and contralateral retinae of three Siamese cats. (The regions in which the HRP-labeled and unlabeled ganglion cells were drawn and measured are represented as stippled rectangles on the appropriate "%-ipsilateral" maps.) The cell-size histograms (figs. 12 and 13) show that the large cells stand out as a clearly distinct cell population. In LGNS-26 (fig. 12), the cell-size counts were made in a region centered 3.9 mm (about 19°) temporally and about 0.8 mm above the horizontal meridian. In this region, centered on a point where about 30% of the total retinothalamic population projected ipsilaterally, only one out of 52 large cells (2%) was filled with HRP. On the other hand, in the corresponding region of the contralateral retina, where 70% of the cells sent axons contralaterally, 25 out of 26 large cells (96%) were labeled with HRP. Figure 13 shows a similar histogram for the ipsilateral retina of LGNS-25. The region of cell size measurements was centered 3.6 mm (18°) temporally and about 0.7 mm above the horizontal meridian, at which point 53% of the retinothalamic cells sent axons homolaterally. In the ipsilateral retina, four out of 25 large cells (16%) were labeled, while in

the contralateral retina (not shown), 21 out of 25 large cells (84) were found marked with HRP. (The slight difference between the values for the large cells presented here and those in fig. 14 below is due to the fact that the data for fig. 14 are taken only along the horizontal meridian, where there happened to be no large cells at this eccentricity. Because of the small number of ipsilateral large cells at any given point, small variations in the actual number of labeled large cells will produce some difference in the calculated "%-ipsi" values.) It can be seen from the histograms of figs. 12 and 13 that there was considerable shrinkage of cell diameters in LGNS-25 and -26. For instance, the mean diameter of the large cells is 22 μm, compared with 28 μm in fig. 13 of the previous report (Cooper and Pettigrew, '78b) or 36 μm found by Kelly and Gilbert ('75). In spite of this shrinkage, the large cells still comprise a distinct group in the Siamese cat histograms. The amount of shrinkage evident in these histograms makes it difficult to make any detailed statements about the distribution of the smaller X- and W-cells in the retina. However, it is apparent that the very smallest cells (8-11 μm in diameter) are not significantly labeled after these large injections into the Siamese LGN, as they are after tectal injections (see fig. 13 of previous report). This is further evidence against midbrain contamination from HRP diffusion or transport through cut retinomesencephalic axons. (See previous report for more detailed discussion of this point.)

Figure 13 also contains a cell-size histogram for LGNS-19; this shows the ipsilateral size distributions for a Siamese cat in which there was not such significant shrinkage. Approximately 57% of the total retinothalamic population projected ipsilaterally at the center point of the sampling region (located 4.2 mm temporally and 1.3 mm above the horizontal meridian). However, in this histogram from the ipsilateral retina, only 3 out of 15 (20%) of the large cells were labeled with HRP.

F. Summary of HRP data: Siamese vs. normal

The principal results of our HRP study are summarized in the graph of figure 14, which compares the naso-temporal overlap in normal and Siamese cats (using LGN-35 and LGNS-25 as examples). The graph presents the percentage of retinothalamic ganglion cells projecting ipsilaterally at each eccentricity along the horizontal meridian. As mentioned in the preceding study, the total retinothalamic population in the normal (solid circles) has a rather sharp decussation line passing through the center of the area centralis. At the approximate center of the area centralis (0 mm eccentricity), 40% of the retinothalamic ganglion cells project ipsilaterally, and by about 0.8 mm (approximately 3.5°) into the temporal retina, all of the cells send axons to the homolateral side. The decussation line for the large cells in the normal (open circles) is shifted slightly temporally to that for the entire retinothalamic population, so that the point at which 50% of the large cells project ipsilaterally is found at about 0.7 mm (3°) eccentricity. In other words, the large cells tend to project contralaterally for the first few degrees of temporal retina. In addition, as mentioned in the preceding report, the large cells tend to form an increasingly large percentage of the total contralateral population as one proceeds temporally, so that the most temporal contralateral cells are almost entirely large cells (cf. figs. 6 and 8 of Cooper and Pettigrew, '78b).

The curve for the total retinothalamic population in the Siamese cat (filled triangles) is radically different from that of the normal. Not only is the 50% point shifted 4.2 mm (about 21°) into the temporal retina, but the entire curve is stretched out so that the transition from total contralateral projection to total ipsilateral projection takes place over a 7 mm extent of temporal retina (as compared

to the 0.8 mm extent in the normal LGN-35). As in the normal, the curve for the large cells in the Siamese (open triangles) is displaced temporally from that for all the HRP-filled cells, but the large-cell curve is also elongated compared to its normal counterpart. Figure 14 clearly shows that the Siamese defect is not merely a displacement of the decussation line; it also represents a smearing out of the naso-temporal decussation over a large extent of temporal retina.

## 2. Autoradiographic results

### A. Manner of presentation of autoradiographic data

We were puzzled by the presence in our whole mounts of contralateral cells temporal to 20° and by the relatively large numbers of ipsilateral cells central to the 20° meridian, since, according to the descriptions of Guillery and Kaas ('71) and of Shatz ('77), such cells should not have been found. In order to study the termination patterns of these unexpected cells, we administered an intraocular injection of tritiated proline to some of the cats which had also received thalamic injections of HRP. The autoradiographic results of some of these intraocular injections are shown in figures 15-20, which contains darkfield photographs of coronal sections through the midportion of the LGN of four animals. In these photographs, the autoradiographic silver grains (representing accumulations of radioactive tracer in the retinal terminals) appear as light spots against the dark background.

Due to the manner in which the visual field is mapped onto the LGN, the C-laminae at most coronal levels correspond to somewhat different elevations than the A-laminae. There is only one coronal level in the LGN, about 4.5/10 of the total length of the LGN from the caudal pole, in which the A- and C-laminae correspond to the same elevation (Sanderson, '71). We have taken care to ensure

that all of the photographs presented here are from this particular coronal level, which contains the representation of the horizontal meridian.

In most of these autoradiographs, we have included the approximate azimuth values at various points along the medio-lateral extent of each Siamese LGN. These values are based on Sanderson's ('71) map for coronal level 5 and are included simply to give an idea of how the visual field magnification changes across the LGN. Guillery and Kaas ('71) have shown that the representation of azimuth in the Siamese cat LGN is approximately normal, so we feel justified in using the data from Sanderson's map. Of course, the exact value of visual field azimuth for any given point will vary from cat to cat; thus, the eccentricity values in figure 15 should be considered only as rough guides to the representation of horizontal eccentricity.

We confirmed the approximate correctness of our placement of the azimuth marks by comparing them to the position of the optic disk discontinuity in nearby sections (Guillery and Kaas, '71). The center of the optic disk is known to lie at an eccentricity of about 15° (see for example, Bishop et al., '62; Nikara et al., '68; Hughes, '76); in our sections, it always fell somewhere between the 10° and 20° azimuth marks (although often rather closer to the 10° line).

The approximate laminar boundaries in each LGN have been determined by camera lucida tracing of cresyl violet counterstained sections and are included in each photograph.

B. Normal LGN

All of the sections in figures 15-20 come from the LGN ipsilateral to the injected eye. The ipsilateral LGN of a normal cat (fig. 15) shows the expected labeling across the entire medio-lateral extent of lamina A1, as well as the

usual somewhat patchy labeling of C1 (Hickey and Guillery, '74; Shatz, '77). Autoradiograph grains are also present in the MIN.

C. Confirmation of ipsilateral projection from central retina in Siamese cat

The Siamese cat lateral geniculates are noticeably different from the normal. In the section from cat LGNS-26 (fig. 16), ipsilateral labeling is very much reduced compared to the normal. Lamina A1 is broken into a number of islands, with most of ipsilateral A1 devoid of terminals (which instead have been routed contralaterally to the abnormal segment (abA1) of A1). The label in the ipsilateral A1-lamina appears as two separate islands which can be identified as the "medial normal segment" (MNS) and "lateral normal segment" (LNS) (see Introduction and fig. 1). As expected from the previous reports (Guillery and Kaas, '71; Shatz, '77), the ipsilateral label in the LNS is confined to eccentricities peripheral to about 20°. However, the pattern of retinal termination in the C1-lamina of LGNS-26 is strikingly different from that in the A1-lamina; ipsilateral retinal terminals spread across a much greater extent of C1 than of A1 and correspond to eccentricities well within the central 20° of temporal retina. Thus, in cat LGNS-26, many of the HRP-filled cells found within the central 20° of the ipsilateral temporal retina probably sent their axons to lamina C1. It is likely that these central ipsilateral cells were W-cells, since it appears that the exclusive input to lamina C1 is from the W-cells of the temporal retina (Wilson et al., '76; Cleland et al., '76).

The Siamese cat BCC-6 was used for the cortical recordings in another study and was not injected with HRP. A section from the ipsilateral LGN of this cat is shown in figure 17 in order to present another example of a labeling pattern

similar to that found in LGNS-26. In BCC-6, the ipsilateral labeling in C1 is again much more extensive than that in A1 and includes eccentricities well within the central 20° of temporal retina. In this cat, as in LGNS-26, the pattern of retinal terminals indicates that the ganglion cells projecting to lamina C1 (probably W-cells) maintained their proper ipsilateral projection in regions of temporal retina where cells sending fibers to lamina A1 misprojected contralaterally. This more extensive labeling of C1 persists throughout most of the rostro-caudal extent of the LGN in both LGNS-26 and BCC-6.

In LGNS-21 (fig. 18), the ganglion cell terminals in the ipsilateral LGN again extend throughout most of the medio-lateral extent of lamina C1, once more indicating projections from W-cells lying within the central 20° of ipsilateral temporal retina. However, the labeling pattern in LGNS-21 is different from that in LGNS-26 or BCC-6 in that abA1 is smaller and the LNS is correspondingly much larger. In fact, the LNS of LGNS-21 reaches across virtually the whole of lamina A1. This result indicates that, in addition to the cells terminating in C1, there were also ganglion cells projecting to A1 from almost the entire extent of ipsilateral temporal retina.

The size of the LNS in LGNS-25 (fig. 19) is intermediate between that for LGNS-21 and -26. The labeling in C1 is as extensive as that in A1, if not slightly more so.

Like BCC-6, BCC-3 (fig. 20) was a cat from our colony used for a study to be reported elsewhere; this animal was not injected successfully with HRP. An autoradiograph from BCC-3 is included here because it supports our finding of ipsilateral projection from much of the central 20° of temporal retina. In BCC-3 lamina A1 is still broken up into the MNS and LNS, but the LNS is so large that

the overall labeling pattern in the LGN is almost normal. The terminal labeling in C1, although patchy, is also found at regions of the LGN corresponding to much of the central temporal retina. Thus, even in the absence of HRP data, one is led to conclude that significant numbers of cells from the central 20° of temporal retina sent axons to the ipsilateral LGN of BCC-3.

The autoradiographic findings described here confirm the HRP result that there is ipsilateral output from the central 20° of the Siamese temporal retina. Furthermore, these patterns of labeled retinal terminals show that many of the central ipsilateral cells must project to the LGN. (This makes it unnecessary to invoke mesencephalic contamination as the source of the unexpected ipsilateral HRP-filled cells.)

D. Comparison of ganglion cell density maps with pattern of retinal terminals in LGN

It is interesting to compare the ganglion cell density maps for the ipsilateral retinae of LGNS-21 and -26 in light of the autoradiographic data for these cats. As mentioned above, in LGNS-26 there is a relatively deep "valley" of ipsilateral density lying between the two density peaks near the horizontal meridian. The density ratios of the central maximum:minimum:peripheral maximum are 250:81:242 (3.1:1:3.0). The central and peripheral peaks may have projected to the MNS and LNS, respectively, and the "valley" of 81 cells/mm$^2$ (at an eccentricity of about 3 mm) might have corresponded to the region of the LGN in which terminal labeling is found only in lamina C1. In contrast to the results in LGNS-26, the labeled ganglion cell density profile is relatively flat along the horizontal meridian of LGNS-21, with central maximum:minimum:peripheral maximum ratios of

218:142:171 (1.5:1:1.2). In LGNS-21, there is heavy labeling of A1 as well as C1, and it may be that the density "valley" in the ipsilateral retina of LGNS-26 was "filled in" for LGNS-21 by the addition of cells projecting to the homolateral lamina A1.

# DISCUSSION

## The nature of the abnormality in the Siamese retinothalamic pathway

The initial studies of the retinogeniculate pathway in Siamese cats led to the assumption that the Siamese retina is divided into two vertically-oriented strips of exclusive unilateral projection; these strips were thought to be separated by a sharp decussation line located about 20° temporal to the zero azimuthal meridian (Guillery, '69; Guillery and Kaas, '71; Shatz, '77). Our study is the first published work to show that, in fact, there is bilateral projection to the thalamus from virtually the entire extent of temporal retina. We have found ipsilaterally-projecting cells central to the supposed 20° decussation line and contralaterally-projecting cells peripheral to this line. The "%-ipsilateral" maps show that there is a smooth change across the temporal retina in the relative proportions of cells projecting to the two thalami; these maps reveal a gradient-like increase in the percentage of ipsilateral retinothalamic cells as one proceeds temporally. Thus, as shown in figure 14, the Siamese defect is not simply a shift of the decussation line to a new position 20° into the temporal retina; not only is the line of equal projection to both hemispheres displaced far temporally, but the zone of transition from total contralateral projection to total ipsilateral projection is greatly spread out compared to the normal. Our demonstration of a smeared-out retinothalamic decussation pattern stands in strong contrast to the previous assumptions of a sharp boundary between the regions of ipsilateral and contralateral projection. The intermingling of contralateral and ipsilateral cells found here was raised as a possibility by Lund ('75), however, and has been found independently by Kirk ('76) and Stone et al. ('78) in their studies of the total retinofugal population in Siamese cats.

Projections of unexpectedly labeled ganglion cells

We must thus ask why the results of our study are so different from what would be expected on the basis of the previous work of Guillery and Kaas ('71). The main problem here is to try to determine the site of termination of the contralateral cells peripheral to 20° and of the ipsilateral cells central to 20°. One explanation for the difference between our results and those expected from previous findings might be that the ipsilateral and contralateral cells unexpectedly labeled here are actually retinomesencephalic neurons, whose terminals took up HRP diffusing to the midbrain, or whose axons were cut during the injection of HRP into the thalamus. It is known that damaged axons can transport sufficient quantities of HRP to give good staining of cell bodies (e.g., Bunt et al., '75; Halperin and Lavail, '75; Adams and Ware, '76; Kristensson and Olsson, '76). If contamination from axons projecting to the midbrain were involved here, it might still be possible that the projection to the LGN follows the pattern suggested by Guillery and Kaas ('71). The reason for rejecting the contribution of retinomesencephalic neurons to our results have been outlined above and in the previous paper (Cooper and Pettigrew, '78b); they include the absence of significant filling of the lower retina and of the contralateral temporal retina in normals, as well as the lack of staining of the smallest ganglion cells. In addition, as mentioned below, the autoradiographic evidence in this study confirms that much of the ipsilateral projection from the central 20° of temporal retina does indeed go to the thalamus (and, more particularly, to the LGN).

Finally, although this was not described above, we used a recording micropipette to inject lamina A in one Siamese cat (BCC-4) without the danger of cutting optic tract axons. In this case, we found HRP-labeled cells in both temporal retinae

at eccentricities from 0° to at least 6° along the horizontal meridian. This experiment again demonstrates bilateral retinothalamic projection from the central retina of Siamese cats.

If axons routed toward the midbrain do not seem to be the explanation for the unexpectedly labeled cells in our material, then where do these cells project? As far as the contralateral filled cells are concerned, it has already been noted that large cells make up an increasing proportion of the labeled contralateral cells beyond 20°. Likewise, the 50% decussation line for large cells is displaced temporally to that for the retinothalamic population as a whole. In the normal, it is also the case that the large cell decussation line is temporal to that for the rest of the retinothalamic cells, and it has already been pointed out (Cooper and Pettigrew, '78b) that these temporal-most large cells probably project to the MIN (see Sanderson, '71; Dreher and Sefton, '74; Mason, '75). Thus, it seems reasonable to suppose that many of the large cells peripheral to 20° in the Siamese cat likewise send axons to this thalamic nucleus. In fact, although Guillery and Kaas's formulation of the Siamese retina was based only on the examination of the pathway to the LGN, they did notice that the MIN was also affected by the Siamese defect. However, this cannot be the entire explanation for the demonstration of HRP-labeled cells in the contralateral temporal periphery, since except for the most temporal cells, which were almost invariably large, there were many small cells beyond the 20° line (see fig. 2A, for example). In the cell-size histograms centered at 15-20°, only 10% of the contralateral cells were large (9.1% for LGNS-26 and 12.4% for LGNS-25); also, as mentioned above, only 28% of the contralateral cells located more than 5 mm (about 25°) temporally in LGNS-26 were large cells. Since input to the MIN appears to be almost exclusively from Y-cells (Mason, '75), these small cells temporal to 20° presumably project elsewhere.

One possible site of termination for the contralateral cells temporal to 20° may be indicated by the fact that in the Siamese cat, the LNS of A1 often appears to be rather thinner than the overlying lamina A (e.g., LGNS-25, BCC-3, BCC-6, and cat 179 of Shatz ('77)). It may be that many of the contralaterally projecting fibers from the peripheral temporal retina fuse with the region of lamina A overlying the LNS. Since the aberrant temporal fibers would be from the same (contralateral) eye as the axons normally innervating A, they would be indistinguishable in autoradiographs from the normal fibers, but would contribute to an increased thickness of lamina A at the expense of the LNS of A1.

It is necessary also to consider the site of termination of the ipsilateral HRP-filled cells central to the 20° meridian. The autoradiographic evidence suggests that many of these ipsilateral cells do indeed send their axons to the LGN. In LGNS-21 and BCC-3, there is labeling of the ipsilateral LGN across virtually the entire extent of both lamina A1 and lamina C1. In LGNS-26 and BCC-6, the normal input to A1 is more restricted, but the ipsilateral terminals in C1 extend across most of the representation of the central and paracentral temporal retina. Such autoradiographic evidence is of importance for a number of reasons. First, it confirms and extends the results of the HRP experiments by showing ipsilateral projection to the LGN from most of the temporal retina. In fact, even in the absence of the HRP data, one would still be led to conclude that there was substantial ipsilateral projection from the central temporal retina in our Siamese cats. Secondly, some of the autoradiographs indicate that there is at least a rough correlation between the shape of the ipsilateral cell density maps and the distribution of retinal terminals in the LGN. It will be remembered that in LGNS-26, the ratios of central peak:valley:peripheral peak were 3.1:1:3.0, while in LGNS-21

they were 1.5:1:1.2. In LGNS-26, the label in the homolateral LGN extended across the representation of the central retina in C1 but not in A1; however, in LGNS-21, most of the lamina A1 was labeled as well. It is as if the addition of ipsilateral cells projecting to A1 in LGNS-21 went to "fill in" the "valley" formed by the baseline of cells projecting to C1 in LGNS-26.

## Ganglion cell classes and the Siamese abnormality

The autoradiographic data point to possible differential effects of the Siamese defect on the different ganglion cell classes. In LGNS-26 and BCC-6, it appears that the axons projecting to the C1-lamina maintain their proper ipsilateral projection over regions of retina in which axons directed toward the A1-lamina misproject contralaterally. (This trend is evident throughout most of the rostro-caudal extent of the LGN of both cats.) Of the eight Siamese cats receiving intraocular injections (LGNS-21, -25, -26 and BCC-2 through -6), none has shown significantly more extensive labeling of the LNS of A1 than of the C1-lamina. That is, C1 always showed as much or more normal ipsilateral input than the LNS. (In LGNS-26 and BCC-6, C1 was more widely labeled; while in the other cats, both laminae showed about the same extent of normal input.) Guillery and Kaas ('71) likewise found that the proportion of C1 receiving proper ipsilateral input often seemed to be greater than the proportion of A1. This tendency also appears to a certain extent in autoradiographs presented by Shatz ('77). The degree of normal labeling of C1 and the LNS of A1 is approximately equal in three of her cats (5R6, 179, and 6C2), while C1 receives substantially more normal input than A1 in two cats (6U5, fig. 6C, and especially WR1). In only one of Shatz's animals (7D2) was the normal input to the LNS somewhat more extensive than that for C1.

It should be emphasized that these comparisons between C1 and LNS of A1 must be made from coronal sections taken through the region of the horizontal meridian representation, since as one proceeds rostrally or caudally in the LGN, the curvature of the nucleus introduces radical differences in elevation between the A1 and C1 laminae in the same section (Sanderson, '71). (Also, as Guillery and Kaas ('71) pointed out, the posterior part of the LGN (corresponding to non-tapetal retina) may process retinal information differently than the rest of the LGN.) Since lamina C1 is supposed to receive only W-cell input (see above), the autoradiographic data suggest that the W-cells often preserve their normal ipsilateral projection to a greater degree than do the X- and Y-cells, which send axons to A1. Consistent with this suggestion is the fact that the 50% decussation line in the study of Stone et al. ('78a) tends to be shifted less temporally (1.7 to 3 mm) than that in our study (3.4 to 7.4 mm). Stone et al. ('78a) used tract-sectioned material to examine the total retinofugal population and thus included in their study W-cells projecting to the midbrain (Fukuda and Stone, '74); such cells would have been excluded from our study. This seemingly greater preservation of the normal ipsilateral projection in W-cells would appear to be only a tendency, however, in light of the exception in Shatz's cat 7D2, and more work will be needed to determine the proportion of cats in which the normal C1 labeling exceeds that in A1. In addition, the possibility of loss of X-cells in some Siamese retinae (see above and Stone et al. '78b) or of compression in the retinal projections to ipsilateral A1 (see below) must also be considered when evaluating this apparent tendency. However, our cats LGNS-26 and BCC-6 definitely show that there can be striking differences between the pattern of termination of the normal projections to C1 and A1.

A differential effect of the Siamese defect on the three ganglion cell classes is especially apparent in the case of the large cells; the data in the present study clearly show that these cells tend to misproject in higher proportions than the rest of the retinothalamic population. Of course, as previously noted, it is possible that many of the most temporal contralateral large cells project to the MIN. However, this differential effect must certainly involve the large cells sending axons to the LGN as well, since virtually all of the large cells at eccentricities less than 20° misproject contralaterally (see for example, figs. 2 and 14 or the cell-size histograms), and since Kelly and Gilbert ('75) have shown that at most eccentricities, all of the large cells project to the LGN (see also fig. 13 of the previous study). Because large cells presumably correspond to Y-cells (Boycott and Wassle, '74; Fukuda and Stone, '74; Kelly and Gilbert, '75; Cleland et al., '75), these data indicate that the Y-cells projecting to the thalamus are more affected by the Siamese defect than are the other cell classes. A similar result has been found independently in the studies of Stone et al. ('78) and Kirk ('76), which compared the Y-cells to the entire retinofugal population (retinothalamic and retinomesencephalic). It is interesting to note here that Lund ('75) proposed this greater susceptibility of Y-cells before any of these data were available.

## Bilateral projection from some retinal regions

At this point, one must ask why the intermingling of ipsilateral and contralateral cells in the temporal retina was not noticed by previous investigators (Guillery and Kaas, '71; Shatz, '77). In the first place, it should be mentioned that there is evidence for some bilateral overlap between abA1 and the LNS of A1 in a number of Shatz's ('77) autoradiographs (although she does not mention this).

In these sections (figs. 6D, 7F, 8A, 8B, 9A, 13A), there are regions in which the lateral end of abA1 overlaps the medial end of the LNS; this indicates the existence of both ipsilateral and contralateral projection from the section of temporal retina corresponding to the region of laminar overlap in the LGN. In terms of visual field, the amount of bilateral representation could be substantial in some cases (e.g., fig. 8A and 8B), since, owing to the magnification factor in the LGN, small distances in the region of laminar overlap could correspond to several degrees of visual field (Sanderson, '71; Guillery and Kaas, '71). Secondly, as shown above, the bilateral overlap is not always in the A-laminae, but often corresponds to overlap between a contralateral projection to abA1 and an ipsilateral projection to the C1-lamina. Guillery and Kaas ('71) and Shatz ('77) based their formulation on the retinal input to the A-laminae and thus ignored this often substantial projection from the central 20° to ipsilateral C1. Thirdly, much of the data of Guillery and Kaas ('71) were derived from multiunit electrophysiological recordings from the LGN. Such recordings could have been biased toward sampling large, Y-type cells (Fukuda and Stone, '74; Rowe and Stone, '76). We have shown that the large (presumably Y-) cells tend to misproject more than the rest of the retinothalamic cells. Thus, the recordings of Guillery and Kaas may have been biased toward the population of cells which shows the greatest defect across the temporal retina. It is also likely that these recordings did not include a significant sample of W-cells, which are rather difficult to record and which were not even known to exist at the time of the experiments (Stone and Hoffmann, '72; Cleland and Levick, '74). Finally, there does seem to be a genuinely large amount of variability in the pattern of the retinogeniculate projection in Siamese cats. For instance, there were no HRP-labeled cells in the ipsilateral central retina of LGNS-20. On the other

hand, the amount of ipsilateral autoradiographic label in lamina A1 of LGNS-21 and BCC-3 is so great as to be almost normal. (Indeed, Montero and Guillery ('78) have found a Siamese cat in which the rostral half of the LGN is entirely normal.) Except for Shatz's ('77) Siamese 6C2, in which the LNS and MNS almost fuse to give a continuous A1, none of the cats in the studies of Guillery and Kaas ('71) or Shatz ('77) showed ipsilateral labeling in A1 as extensive as that found in LGNS-21 or BCC-3. Thus, while we assume that the basic mechanisms underlying the chiasmal defect in Siamese cats are the same for all individuals, it appears that these mechanisms can be expressed to varying degrees in different cats.

## Mechanisms of the chiasmal error in Siamese cats

The question of the mechanism underlying the laterality errors in the Siamese cat naturally arises here. One explanation that has been discussed by Guillery and Kaas ('71) is a simple mechanical block deflecting some axons to the wrong hemisphere. Guillery and Kaas have rejected this possibility. They state that, given the relative imprecision in the retinotopic ordering of the axons in the optic nerve and chiasm (Overbosch, '27; Lashley, '34; Guillery and Kaas, '71), a simple mechanical block could not result in the rerouting of axons within a discrete, well-defined segment of temporal retina. But as shown in our study, the misrouting of optic axons to the thalamus is not in fact confined to a discrete strip, but occurs in a gradient-like fashion across the entire temporal retina. These new results could thus revive the possibility that a mechanical block is responsible for the chiasmal defect in the Siamese cat. However, the finding of a differential effect of the Siamese defect on different ganglion cell classes makes this possibility by itself rather unlikely, unless fibers of different cell classes

tend to follow rather different paths in the chiasm. Differential rates of outgrowth in combination with some sort of transient block could also provide a means of explaining these differential defects with a partly mechanical hypothesis.

One other type of data also tends to make a simple mechanical explanation unlikely. In the mink, there are a number of mutant gene combinations which reduce retinal pigment and also decrease the amount of ipsilateral projection from the retina (Sanderson et al., '74). Some of these gene combinations do not involve the C-locus, which is the site of mutation in the Siamese cat and other albino animals. From this evidence, Sanderson et al. ('74) concluded that the loss of retinal pigment per se must underlie the laterality defect in animals with hypopigmented retinae, since the mechanism of direct gene action is presumably different for the different gene combinations. The finding that the loss of retinal pigment itself is involved in the mis-specificiation of laterality again seems to make the mechanical block hypothesis unlikely (unless some chiasmal structure composed of melanin is involved).

Experiments in mice (Guillery et al., '73) and mink (Sanderson et al., '74) implicate long-range intercellular interactions in the specification of the laterality of optic axons. Our results from the Siamese cat indicate that these interactions affect the various classes of retinothalamic retinal ganglion cells differently. This point is also demonstrated by the fact that the different classes have different decussation patterns in normal cats (Stone and Fukuda, '74; Kirk et al., '76a,b; Cooper and Pettigrew, '78b). The smooth change across the Siamese temporal retina in the percentage of cells sending axons ipsilaterally may indicate that a gradient in the concentration of some laterality-specifying signal determines the crossed/uncrossed distribution of the retinal axons in normal and Siamese

cats (cf., Sperry, '63). Differential effects according to cell type might then result from differential sensitivities to the specifying signal. Alternatively, one might postulate that the distribution of the specifying signal changes with time during prenatal development and that the various ganglion cell types develop at different times. The finding in mice that the large ganglion cells tend to be "born" earlier than the other ganglion cells is consistent with this latter type of hypothesis (Sidman, '61). According to either of these hypotheses, the Siamese defect could result from errors such as mis-specification of "birthdates" of the cell classes, changes in the sensitivity of the various cell classes to the laterality-specifying signal, or errors in distribution of the signal itself. Sanderson et al. ('74) state that their finding of a variable distribution of retinal terminals in the LGN of hypopigmented mink makes it unlikely that a simple modification of a normal laterality-specifying gradient could be responsible for the albino abnormality. However, the possibility of compression of the retinal terminals in the LGN (or other redistributions of these terminals, see below) could result in a patchiness in the mink LGN which would not reflect exactly the positions of the misrouted retinal cells.

It is noteworthy that in all of the autoradiographs of the ipsilateral geniculates included in this study (as well as in those published elsewhere), there is a gap between the retinal terminals in the MNS and those in the more laterally placed LNS or C1. However, we never saw a corresponding gap in the distribution on HRP-labeled cells in our ipsilateral retinae. In most of our cats, the gap in the LGN is rather small (LGNS-21, -26, BCC-3, -6) and may correspond to a sufficiently small area of retina to be missed in our cell counting. (We think this is unlikely, however.) However, in cat LGNS-25, there was a more extensive

space between the MNS and the other segments of ipsilateral label in the LGN, in spite of the lack of a corresponding break in the distributions of ipsilateral HRP-filled ganglion cells. The retinal cells corresponding to this gap in the LGN could represent either cells projecting to other thalamic visual centers or retino-mesencephalic neurons with cut axons. (The reasons for discounting this last explanation are given above.) Alternatively, these autoradiographic results may indicate that there is some compression of the ipsilateral retinal terminals in the LGN, so that terminals usually bound for regions of the LGN where there is a gap may be routed to the nearby MNS or LNS. The possibility of compression of the retinal map in the LGN (especially the MNS) has already been suggested by Stone et al. ('78a). Such compression could result from a number of mechanisms. Results from prenatal eye enucleations in monkeys (Rakic, personal communication) show that the normal laminar distribution of the retinal terminals in the LGN depends on the presence of terminals from both eyes, which could indicate some interaction between the fibers from the two eyes. In addition, as mentioned by Stone et al. ('78a), the overlap of the ipsilateral and contralateral populations in the Siamese retina does not seem to result in intermingling in the LGN of the terminals from the two eyes. Rather, these terminals segregate into discrete laminae, as in the normal. (LGNS-21 seems to show this particularly well; the medial section of the LNS is a narrow, tongue-like projection below the abA1, the narrowness presumably being due to the misrouting to the opposite LGN of most of the axons from the central temporal retina.) It seems possible that competition for terminal space between fibers of the two eyes could result in contraction of the less numerous ipsilateral fibers into discrete islands in the LGN. Alternatively, there may be some minimal number of retinal fibers that

is required to define a region of domination by one eye. In this case, fiber-fiber interactions (Cook and Horder, '77) might cause coalescence of retinal terminals into patches of at least the requisite size. Compression of the ipsilateral eye's map in the Siamese LGN (especially in the MNS) might then be a consequence of the retraction or coalescence of the reduced number of ipsilateral fibers. Such mechanisms might also underlie the patchiness of the normal projection to lamina C1. It is of interest here that Guillery and Kaas (fig. 18, '71) found some evidence that the ipsilateral and contralateral visual field maps are not always in precise register in the Siamese LGN. More detailed recordings in the future may reveal a pattern of compression superimposed on the grossly normal topographic map in LGN of the Siamese cat.

## ACKNOWLEDGEMENTS

We are most grateful to Gary Blasdel, Sarah Kennedy, Phyllis Knudsen, and Monica Wengrowicz de Cooper for the excellent technical help which they provided at various times throughout the course of this work. Sheila and David Crewther kindly provided some of the cats used in this investigation. We appreciate our helpful discussions with John Allman, Joel Myerson, and Jonathan Stone, and we also thank Dr. Stone for making available to us his then unpublished manuscripts on the Siamese cat retina. In addition, we would like to thank William Levick for making us aware of the study of D. Kirk and for providing us with a copy of the relevant parts of Dr. Kirk's thesis. Lederle Laboratories provided the Flaxedil used in these experiments. Betty Hanson and Jane Chacon typed this manuscript.

This work was supported by the Spencer Foundation and grants (Nos. EY 1909 and MS 25852) from USPHS to J.D.P. M.L.C. held a National Science Foundation Predoctoral Fellowship.

# LITERATURE CITED

Adams, J. C. and W. B. Ware 1976 Origins of axons in the cat's acoustic striae determined by injection of horseradish peroxidase into severed tracts. J. Comp. Neurol., 170: 107-122.

Bishop, P. O., W. Kozak, and G. J. Vakkur 1962 Some quantitative aspects of the cat's eye: Axis and plane of reference, visual field co-ordinates and optics. J. Physiol., 163: 466-502.

Boycott, B. B. and H. Wässle 1974 The morphological types of ganglion cells of the domestic cat's retina. J. Physiol., 240: 397-419.

Bunt, A. H., A. E. Hendrickson, J. S. Lund, R. D. Lund, and A. F. Fuchs 1975 Monkey retinal ganglion cells: Morphometric analysis and tracing of axonal connections, with a consideration of the peroxidase technique. J. Comp. Neurol., 164: 265-286.

Cleland, B. G. and W. R. Levick 1974 Properties of rarely encountered types of ganglion cells in the cat's retina and an overall classification. J. Physiol., 240: 457-492.

Cleland, B. G., W. R. Levick, R. Morstyn, and H. G. Wagner 1976 Lateral geniculate relay of slowly conducting retinal afferents to cat visual cortex. J. Physiol., 225: 299-320.

Cleland, B. G., W. R. Levick, and H. Wässle 1975 Physiological identification of a morphological class of cat retinal ganglion cells. J. Physiol., 248: 151-171.

Cook, J. E. and T. J. Horder 1977 The multiple factors determining retinotopic order in the growth of optic fibers into the optic tectum. Phil. Trans. R. Soc. Lond. B, 278: 261-276.

Cooper, M. L. and J. D. Pettigrew 1977a The retinothalamic pathway in Siamese cats studied with horseradish peroxidase. Abstracts of Association for Research in Vision and Ophthalmology, Annual Meeting, May 1977, p. 86 (Abstract).

Cooper, M. L. and J. D. Pettigrew 1977b Naso-temporal division of retinothalamic pathway in normal and Siamese cats. Neurosci. Abstr., 3: 556.

Cooper, M. L. and J. D. Pettigrew 1978a A neurophysiological determination of the vertical horopter in the cat and owl. J. Comp. Neurol., submitted for publication.

Cooper, M. L. and J. D. Pettigrew 1978b The decussation of the retinothalamic pathway in the normal cat, with a note on the major meridians of the cat's retina. J. Comp. Neurol., submitted for publication.

Cowan, W. M., D. I. Gottlieb, A. E. Hendrickson, J. L. Price, and T. A. Woolsey 1972 The autoradiographic demonstration of axonal connections in the central nervous system. Brain Research, 37: 21-51.

Cunningham, T. J. and J. A. Freeman 1977 Bilateral ganglion cell branches in the normal rat: A demonstration with electrophysiological collision and cobalt tracing methods. J. Comp. Neurol., 172: 165-176.

Dreher, B. and A. J. Sefton 1974 Receptive field properties of cells in cat's medial interlaminar nucleus (MIN). The IUPS Satellite Symposium on the Visual Pathway, Structure and Function (1974).

Fukuda, Y. and J. Stone 1974 Retinal distribution and central projections of Y-, X- and W-cells of the cat's retina. J. Neurophysiol., 37: 749-772.

———— 1975 Direct identification of the cell bodies of Y-, X- and W-cells in the cat's retina. Vision Res., 15: 1034-1036.

Guillery, R. W. 1967 Patterns of fiber degeneration in the dorsal lateral geniculate nucleus of the cat following lesions in the visual cortex. J. Comp. Neur., 130: 197-222.

———— 1969 An abnormal retinogeniculate projection in Siamese cats. Brain Res., 14: 739-741.

———— 1970 The laminar distribution of retinal fibers in the dorsal lateral geniculate nucleus of the cat: A new interpretation. J. Comp. Neur., 138: 339-368.

Guillery, R. W., and V. A. Casagrande 1977 Studies of the modifiability of the visual pathways in Midwestern Siamese cats. J. Comp. Neur., 174: 15-46.

Guillery, R. W. and J. H. Kaas 1971 A study of normal and congenitally abnormal retinogeniculate projections in cats. J. Comp. Neur., 143: 73-100.

Guillery, R. W., G. L. Scott, B. M. Cattanach, and M. S. Deol 1973 Genetic mechanisms determining the central pathways of mice. Science, 179: 1014-1016.

Halperin, J. J. and J. H. LaVail 1975 A study of the dynamics of retrograde transport and accumulation of horseradish peroxidase in injured neurons. Brain Res., 100: 253-269.

Hickey, T. L. and R. W. Guillery 1974 An autoradiographic study of retinogeniculate pathways in the cat and fox. J. Comp. Neur., 156: 239-254.

Hubel, P. H. and T. N. Wiesel 1971 Aberrant visual projections in the Siamese cat. J. Physiol., 218: 33-62.

Hughes, A. 1975 A quantitative analysis of the cat retinal ganglion cell topography. J. Comp. Neur., 163: 107-128.

———— 1976 A supplement to the cat schematic eye. Vision Res., 16: 149-154.

Kaas, J. H. and R. W. Guillery 1973 The transfer of abnormal visual field representations from the dorsal lateral geniculate nucleus to the visual cortex in Siamese cats. Brain Res., 59: 61-95.

Kalil, R. E., S. R. Jhaveri and W. Richards 1971 Anomalous retinal pathways in the Siamese cat: An inadequate substrate for normal binocular vision. Science, 174: 302-303.

Kelly, J. P. and C. D. Gilbert 1975 The projections of different morphological types of ganglion cells in the cat retina. J. Comp. Neur., 163: 65-81.

Kirk, D. L. 1976 Projections of the visual field by the axons of cat retinal ganglion cells. Section 2: Decussation of optic axons in Siamese cats. pp. 1-17. Ph.D. Thesis, Australian National University.

Kirk, D. L., W. R. Levick, B. G. Cleland and H. Wässle 1976a Crossed and uncrossed representation of the visual field by brisk-sustained and brisk-transient cat retinal ganglion cells. Vision Res., 16: 225-232.

———— 1976b The crossed or uncrossed destination of axons of sluggish-concentric and non-concentric ganglion cells, with an overall synthesis of visual field representation. Vision Res., 16: 233-236.

Kölliker, A. 1899 Neue Beobachtungen zur Anatomie des Chiasma opticum. Festschr. der Phys. -Med. Gesellsch. Würzburg.

Kristensson, K. and Y. Olsson 1976 Retrograde transport of horseradish peroxidase in transected axons. 3. Entry into injured axons and subsequent localization in perikaryon. Brain Res., 115: 201-213.

Landmesser, L. and G. Pilar 1974 Synaptic transmission and cell death during normal ganglionic development. J. Physiol., Lond., 241: 737-749.

Lashley, K. S. 1934 The mechanism of vision. VII. The projection of the retina upon the primary optic centers in the rat. J. Comp. Neur., 59: 341-373.

Levick, W. R. 1972 Another tungsten microelectrode. Med. Electron. Biol. Engng., 10: 510-513.

Lund, R. D. 1975 Variations in laterality of the central projections of retinal ganglion cells. Exp. Eye Res., 21: 193-203.

———— 1978 Development and Plasticity of the Brain: An Introduction. Oxford University Press, Inc., New York.

Mason, R. 1975 Cell properties in the medial interlaminar nucleus of the cat's lateral geniculate complex in relation to the transient/sustained classification. Exp. Brain Res., 22: 327-329.

Montero, V. M. and R. W. Guillery 1978 Abnormalities of the cortico-geniculate pathway in Siamese cats. J. Comp. Neur., 179: 1-12.

Nikara, T., P. O. Bishop, and J. D. Pettigrew 1968 Analysis of retinal correspondence by studying receptive fields of binocular single units in cat striate cortex. Exp. Brain Res., 6: 353-372.

Overbosch, J. F. A. 1927 Experimenteel-anatomische onderzoekingen over de projectie der retina in het centrale zenuwstelsel. Thesis, H. J. Paris, Amsterdam.

Pettigrew, J. D. 1974 The effect of visual experience on the development of stimulus specificity by kitten cortical neurones. J. Physiol., 237: 49-74.

Rodieck, R. W., J. D. Pettigrew, P. O. Bishop, and T. Nikara 1967 Residual eye movements in receptive field studies of paralyzed cats. Vision Res., 7: 107-110.

Rowe, M. H. and J. Stone 1976 Properties of ganglion cells in the visual streak of the cat's retina. J. Comp. Neur., 169: 99-126.

Sanderson, K. J. 1971 The projection of the visual field to the lateral geniculate and medial interlaminar nuclei in the cat. J. Comp. Neur., 143: 101-118.

Sanderson, K. J., R. W. Guillery and R. M. Shackelford 1974 Congenitally abnormal visual pathways in mink (Mustela vison) with reduced retinal pigment. J. Comp. Neur., 154: 225-248.

Shatz, C. 1977 A comparison of visual pathways in Boston and Midwestern Siamese cats. J. Comp. Neur., 171: 205-228.

Sidman, R. L. 1961 Histogenesis of mouse retina studied with $H^3$-thymidine. In: The Structure of the Eye (G. K. Smelser, ed.), pp. 487-506. New York: Academic Press.

Sperry, R. W. 1963 Chemoaffinity in the orderly growth of nerve fiber patterns of connections. Proc. Nat. Acad. Sci., Wash., 50: 703-710.

Stone, J. 1965 A quantitative analysis of the distribution of ganglion cells in the cat's retina. J. Comp. Neur., 124: 337-352.

———— 1966 The naso-temporal division of the cat's retina. J. Comp. Neur., 126: 585-600.

———— 1978 The number and distribution of ganglion cells in the cat's retina. J. Comp. Neur., 180: 753-772.

Stone, J., J. E. Campion, and J. Leicester 1978a The nasotemporal division of retina in the Siamese cat. J. Comp. Neur., 180: 783-798.

Stone, J., and Y. Fukuda 1974 The naso-temporal division of the cat's retina re-examined in terms of W-, X- and Y-cells. J. Comp. Neur., 155: 377-394.

Stone, J., and K. P. Hoffman 1972 Very slow-conducting ganglion cells in the cat's retina. A major, new functional type? Brain Res., 43: 610-616.

Stone, J., M. H. Rowe, and J. E. Campion 1978b Retinal abnormalities in the Siamese cat. J. Comp. Neur., 180: 773-782.

Wilson, P. D., M. H. Rowe, and J. Stone 1976 Properties of relay cells in the cat's lateral geniculate nucleus. A comparison of W-cells with X- and Y-cells. J. Neurophysiol., 39: 1193-1209.

Wassle, H., W. R. Levick, and B. G. Cleland 1975 The distribution of the alpha type of ganglion cells in the cat's retina. J. Comp. Neur., 159: 419-438.

# FIGURE LEGENDS

Fig. 1 Schematic of expected results of our large HRP injections based on the previous formulations of the Siamese retinogeniculate pathway (Guillery and Kaas,'71; Shatz, '77). The shaded areas represent regions of anticipated HRP labeling. See Text for explanation of labeling patterns. The dotted lines show the location of the cuts made in some of the retinae. The vertical dashed line represents the supposed 20° decussation line. The ipsilateral retina has been inverted left-to-right to allow it to be superimposed with its contralateral partner.

Fig. 2 Uncounterstained whole mounts of contralateral ( top ) and ipsilateral ( bottom ) retinae of the Siamese cat LGNS-20. Arrow in upper figure lies approximately 20° into the temporal retina. ( The distance is calculated using 5.05°/mm (Hughes,'76).). Ipsilateral retina has been inverted in this and all subsequent figures so that both retinae lie in the same orientation. N, nasal; T, temporal. Cross = area centralis. Scale: 2 mm.

Fig. 3 Maps of HRP-filled ganglion cell density for LGNS-20. Dotted vertical lines represent approximate locations of decussation lines in the normal. The arrows at 20° are calculated using 5.05°/mm (Hughes,'76). The isodensity lines are in labeled cells/$mm^2$. Here, as in all subsequent density maps, the ipsilateral retina has been inverted left-to-right, so that temporal is to the left for both the ipsilateral and contralateral retinae.

Fig. 4 Electrode track through left visual cortex of LGNS-26. The representation of the ipsilateral visual field near the 17/18 border ( arrow ) shows that this was a "Boston" cat.

Fig. 5,6,7,8 Maps of retinothalamic cell density for LGNS-26,-21, -25,and-19, respectively. Symbols are as in figure 3.

Fig. 9 - 11 Isodensity maps of percentages of retinothalamic ganglion cells which project ipsilaterally.

Fig. 12 Cell-size histograms for corresponding points in the ipsilateral ( top ) and contralateral ( bottom ) temporal retinae of LGNS-26. The location of the region of cell counts is shown by the shaded rectangle in figure 9. Note change of scale for large cells.

Fig. 13 Cell-size histograms for the ipsilateral retinae of LGNS-25 (top) and LGNS-19 (bottom). The regions of the cell counts are shown by shaded rectangles in figures 11 and 10.

Fig. 14 Change in percentage of retinothalamic cells projecting ipsilaterally as one proceeds temporally along the horizontal meridian in normal and Siamese cats. The normal data is the same as in figure 8 of Cooper and Pettigrew,'78b.

Fig. 15 Dark-field autoradiograph of retinal terminals in normal LGN. Medial lies to the left. Scale: 1 mm.

Figs. 16-20 Similar autoradiographs for various Siamese cats. Scale: 1 mm.

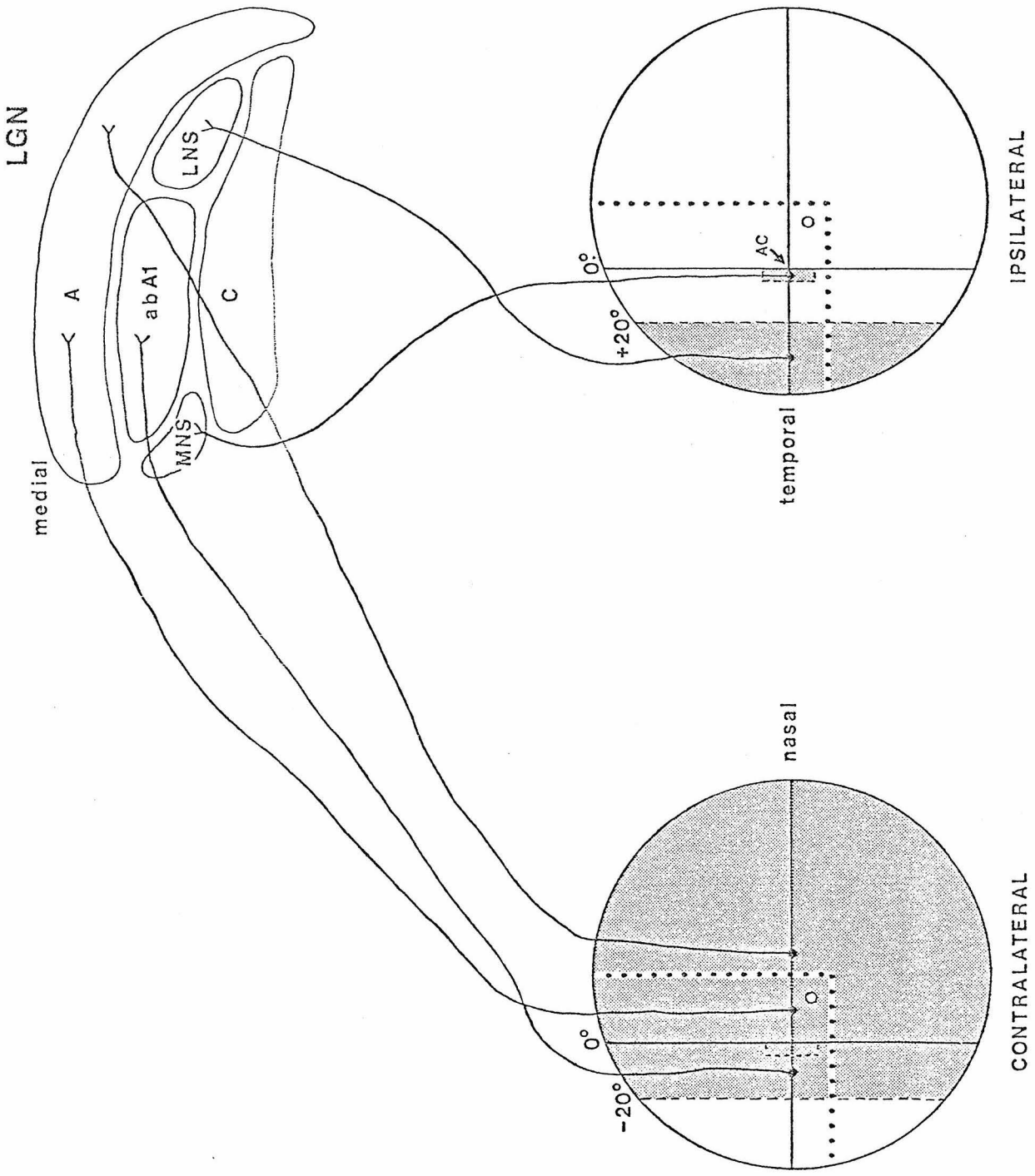
LGN
A
abA1
C
LNS
MNS
medial
temporal
nasal
0°
+20°
-20°
AC
IPSILATERAL
CONTRALATERAL

Figure 1

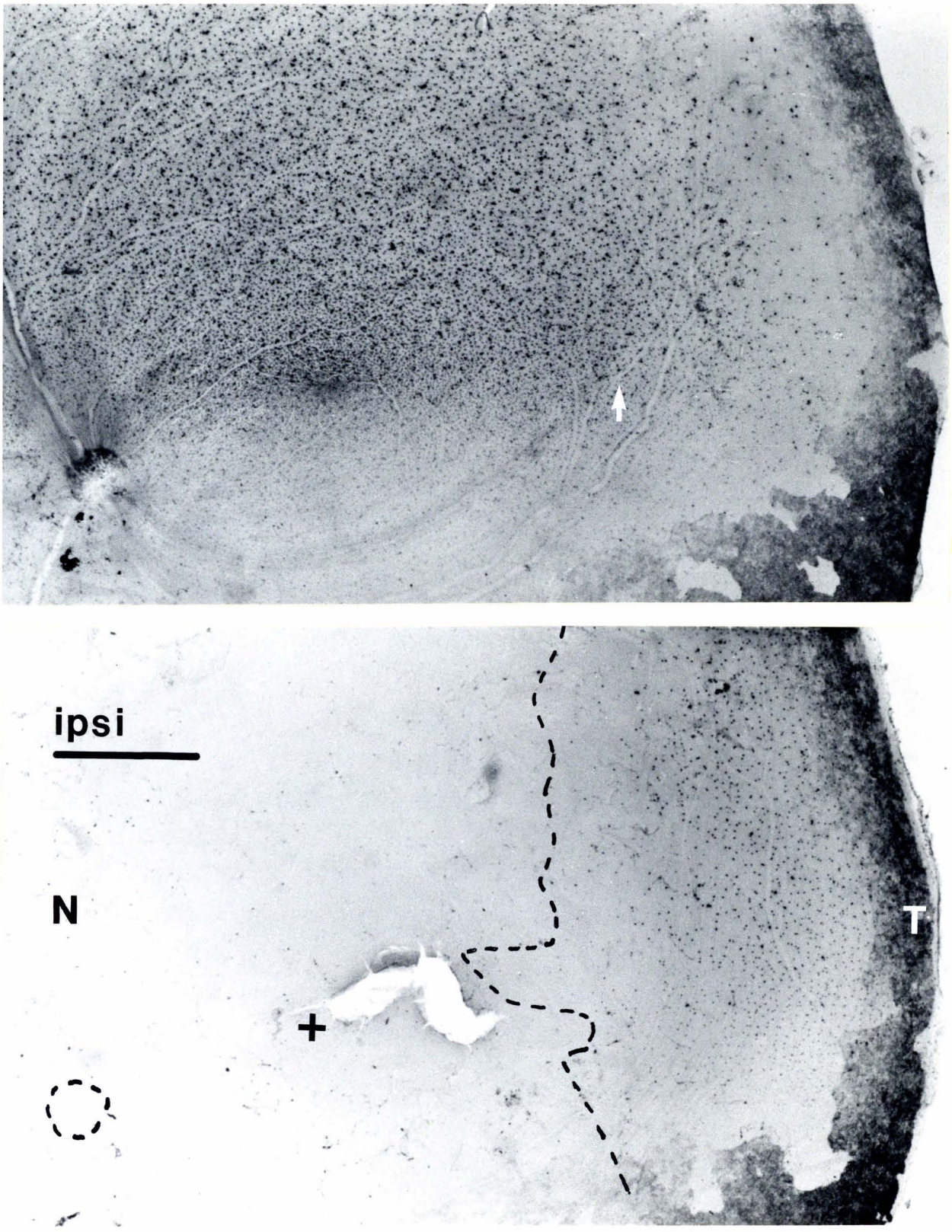


Figure 2

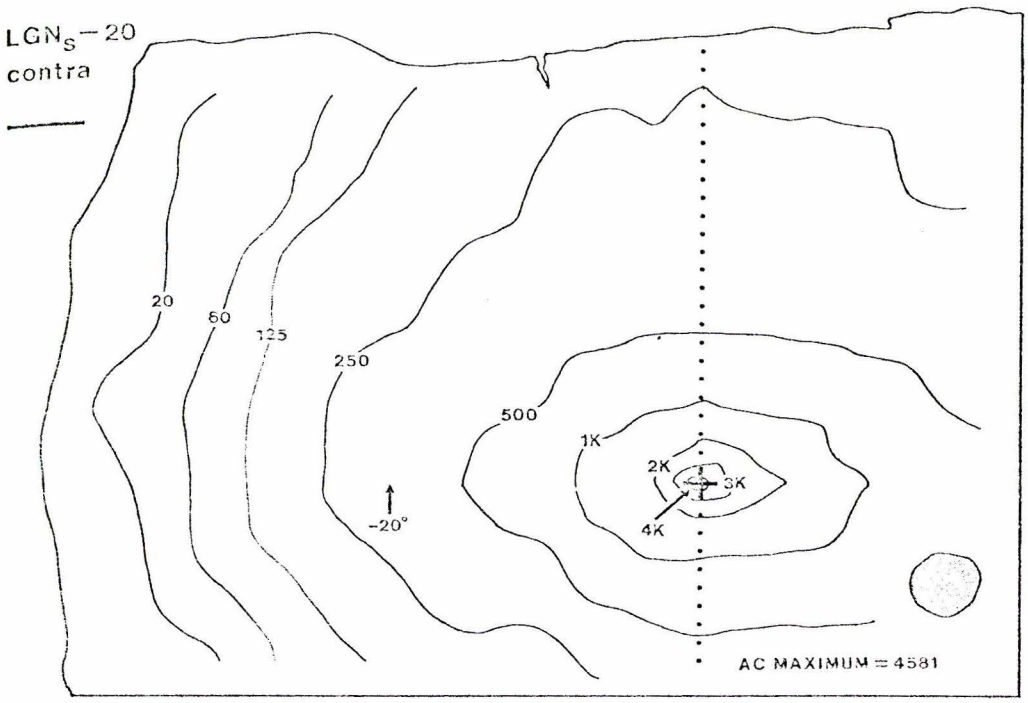
LGN$_S$–20
contra
20
60
125
250
500
1K
2K
3K
4K
–20°
AC MAXIMUM = 4581

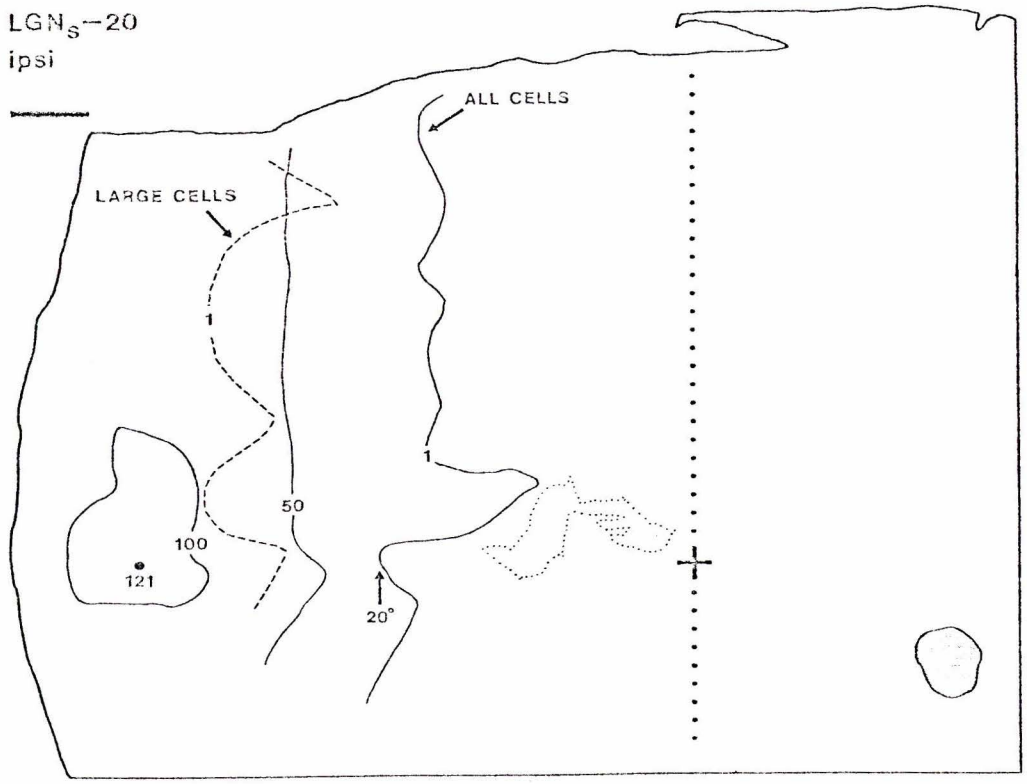
LGN$_S$–20
ipsi
ALL CELLS
LARGE CELLS
1
1
50
100
121
20°

Figure 3

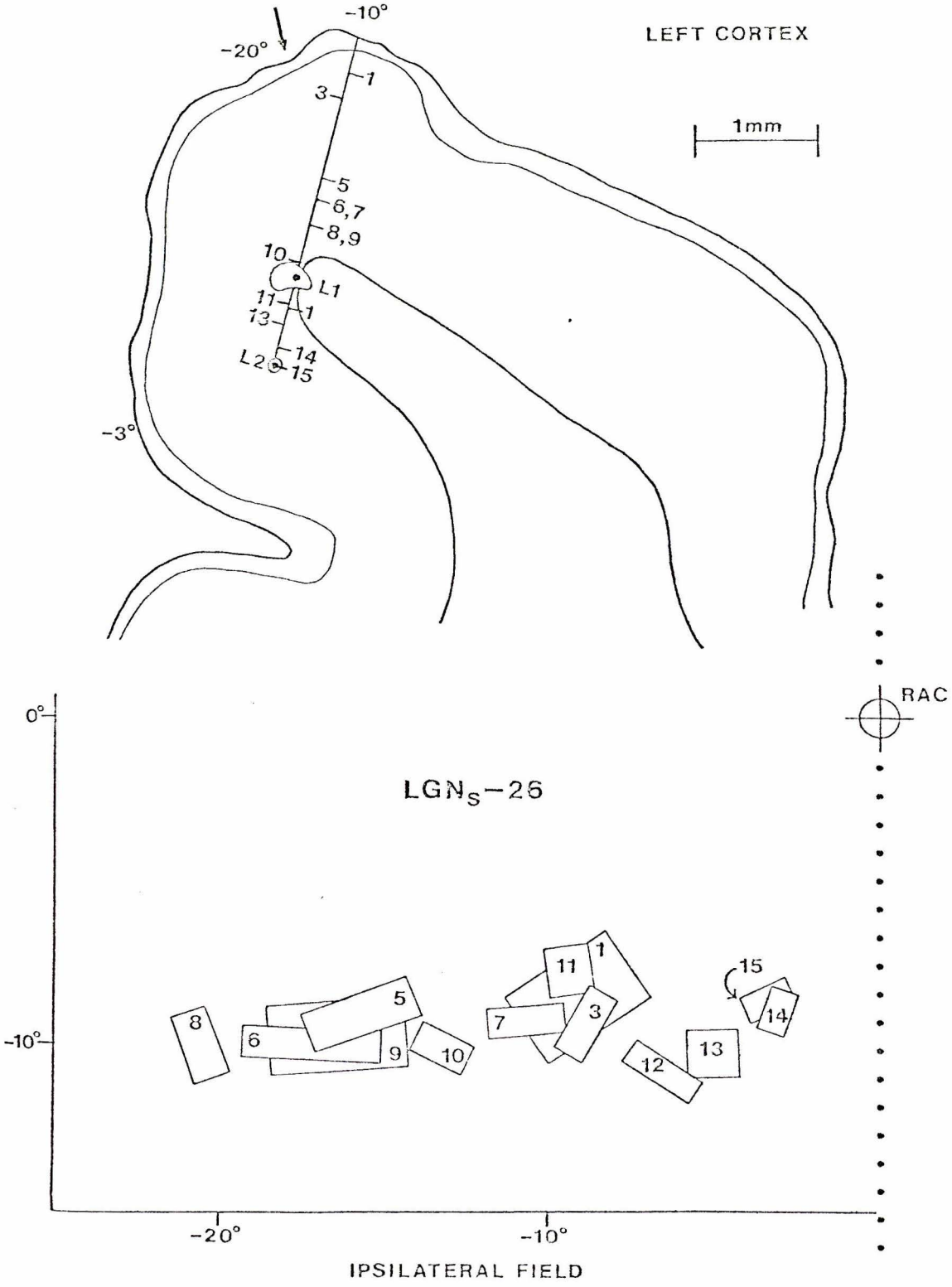
LEFT CORTEX
-10°
-20°
1mm
3
1
5
6,7
8,9
10
L1
11
13
1
L2
14
15
-3°
RAC
0°
LGN$_S$-26
-10°
8
6
5
9
10
7
11
1
3
12
13
15
14
-20°
-10°
IPSILATERAL FIELD

Figure 4

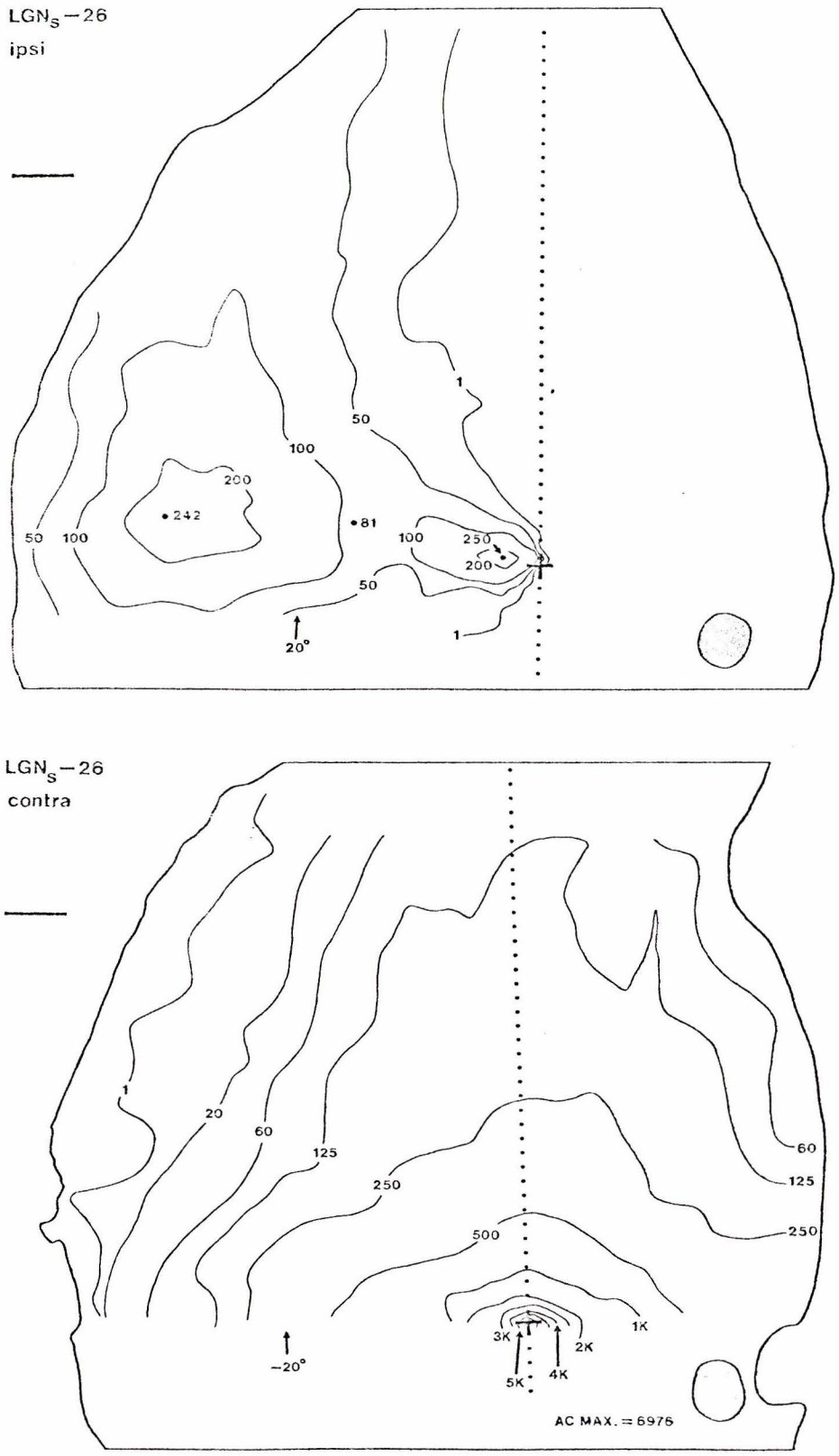
LGN$_S$ – 26
ipsi
1
50
100
200
• 242
• 81
50
100
100
250
200
50
1
20°
LGN$_S$ – 26
contra
1
20
60
125
250
500
60
125
250
1K
3K
2K
5K
4K
–20°
AC MAX. = 6976

Figure 5

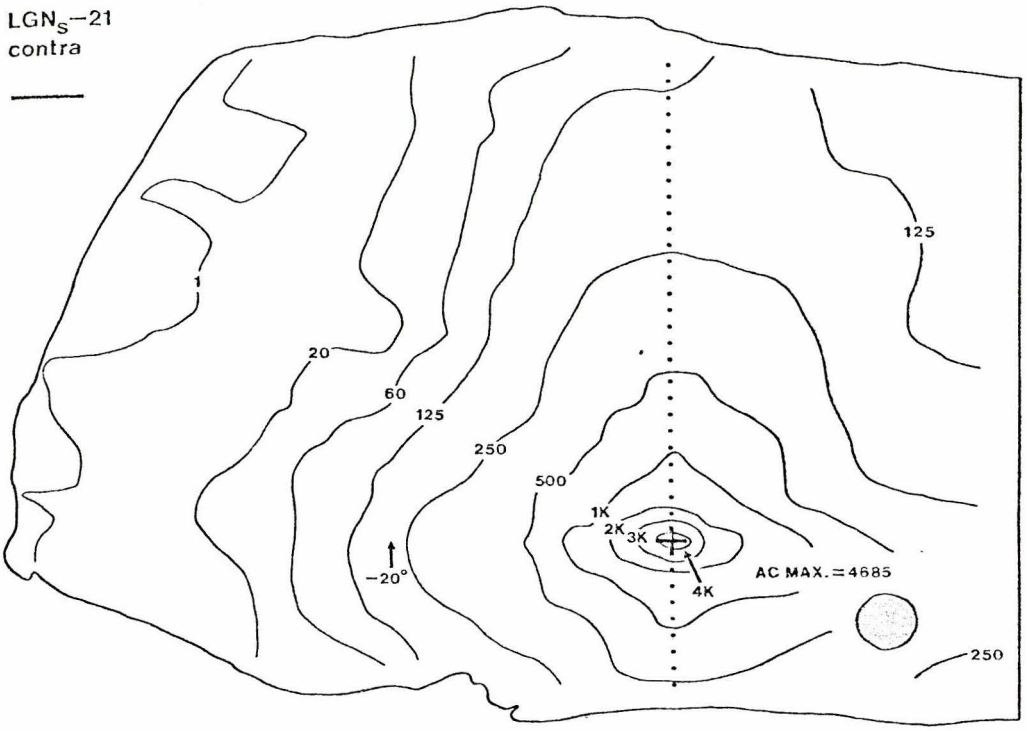
LGN$_S$–21
contra
1
20
60
125
250
500
1K
2K
3K
4K
AC MAX.=4685
–20°
125
250

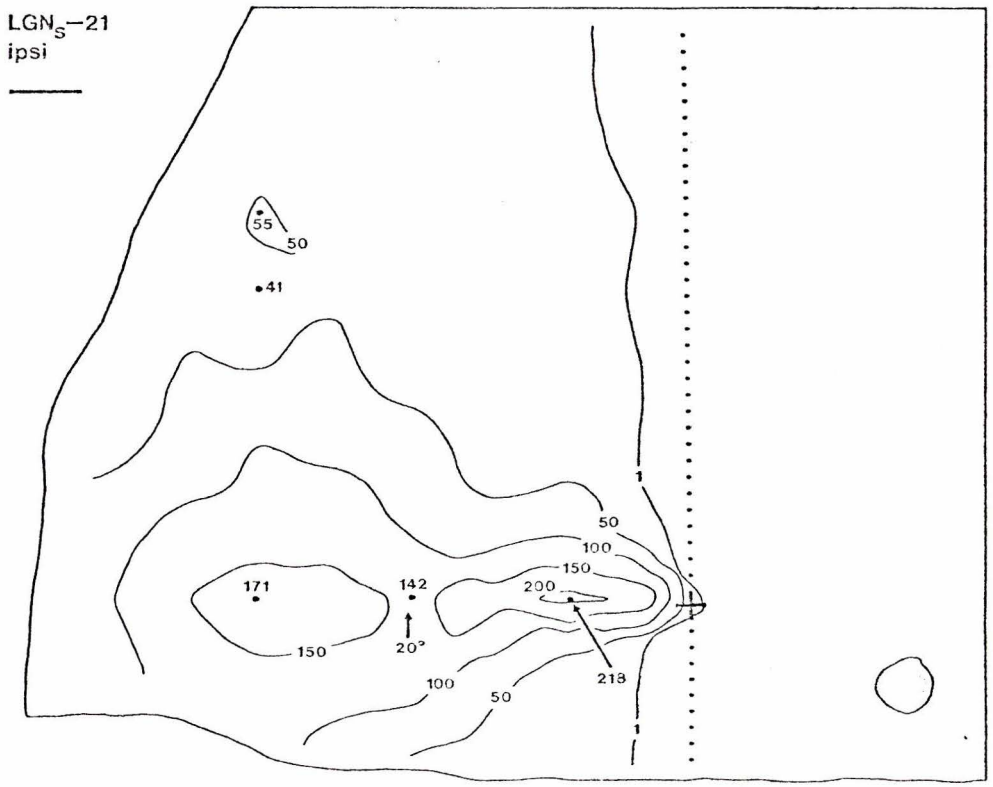
LGN$_S$–21
ipsi
55
50
41
1
50
100
150
200
171
142
150
20°
218
100
50
1

Figure 6

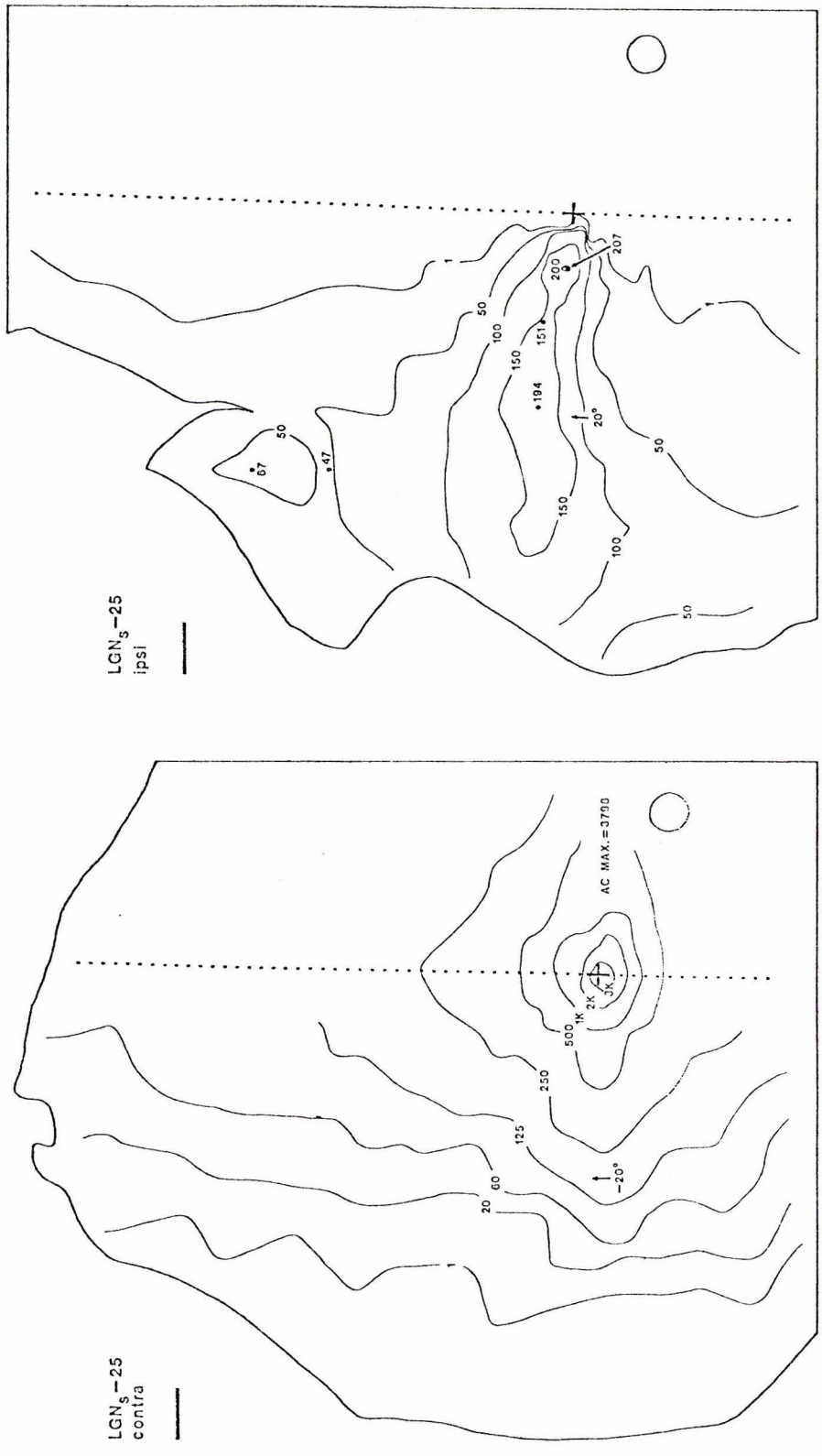
LGN$_S$-25
ipsi
50
100
150
151
200
207
194
67
47
20°
LGN$_S$-25
contra
AC MAX.=3700
1K
2K
3K
500
250
125
60
20
-20°

Figure 7

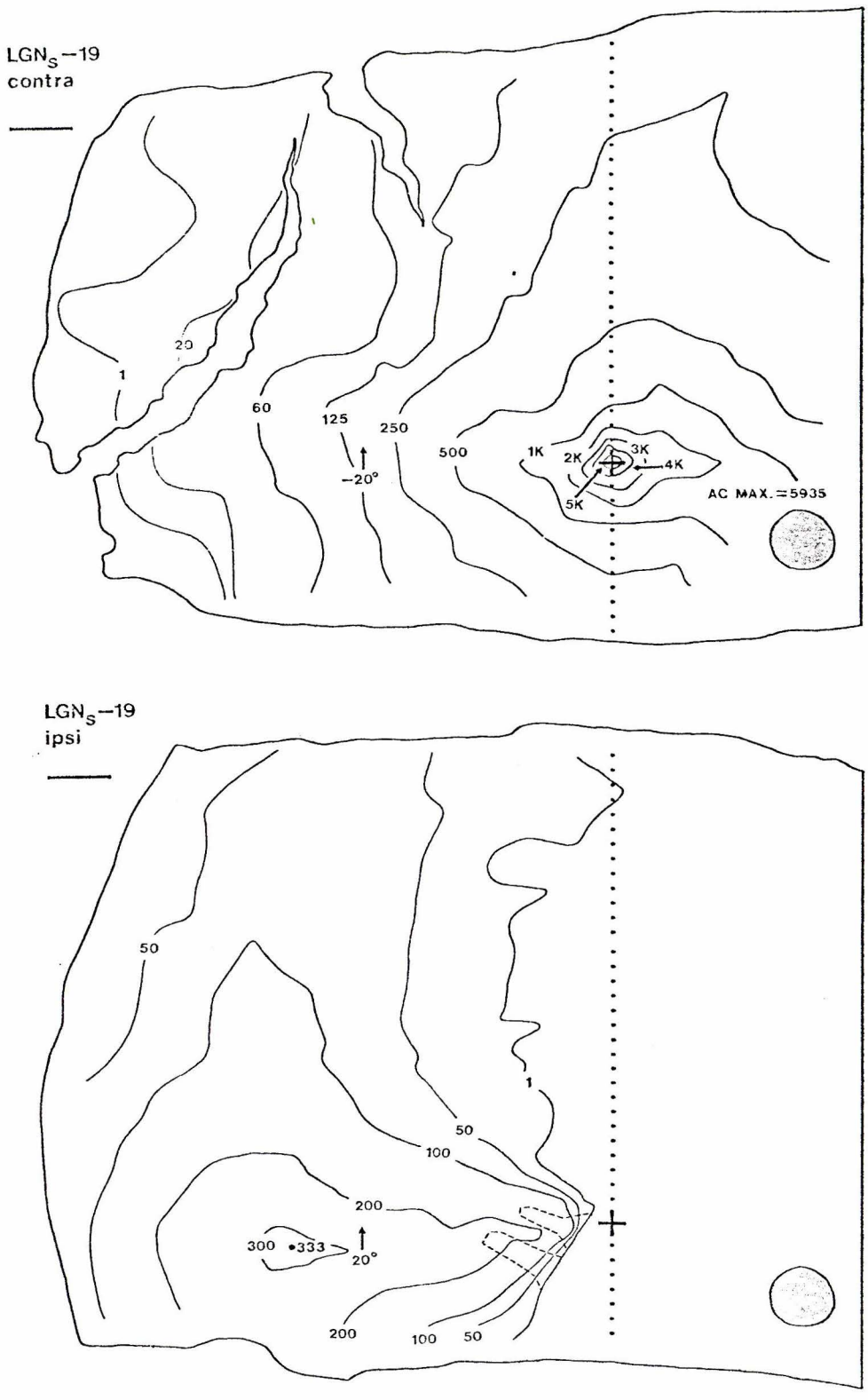
LGN$_S$–19
contra
1
20
60
125
250
500
–20°
1K
2K
3K
4K
5K
AC MAX.=5935
LGN$_S$–19
ipsi
50
1
50
100
200
300
•333
20°
200
100
50

Figure 8

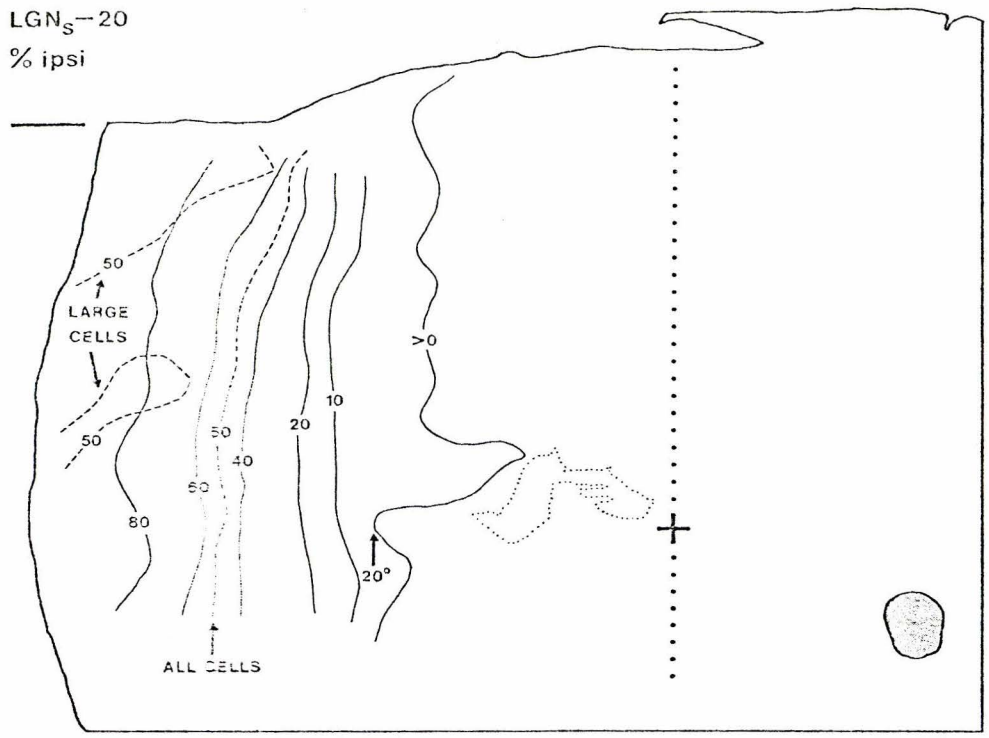
LGN$_S$–20
% ipsi
50
LARGE
CELLS
50
80
50
40
50
20
10
>0
20°
ALL CELLS

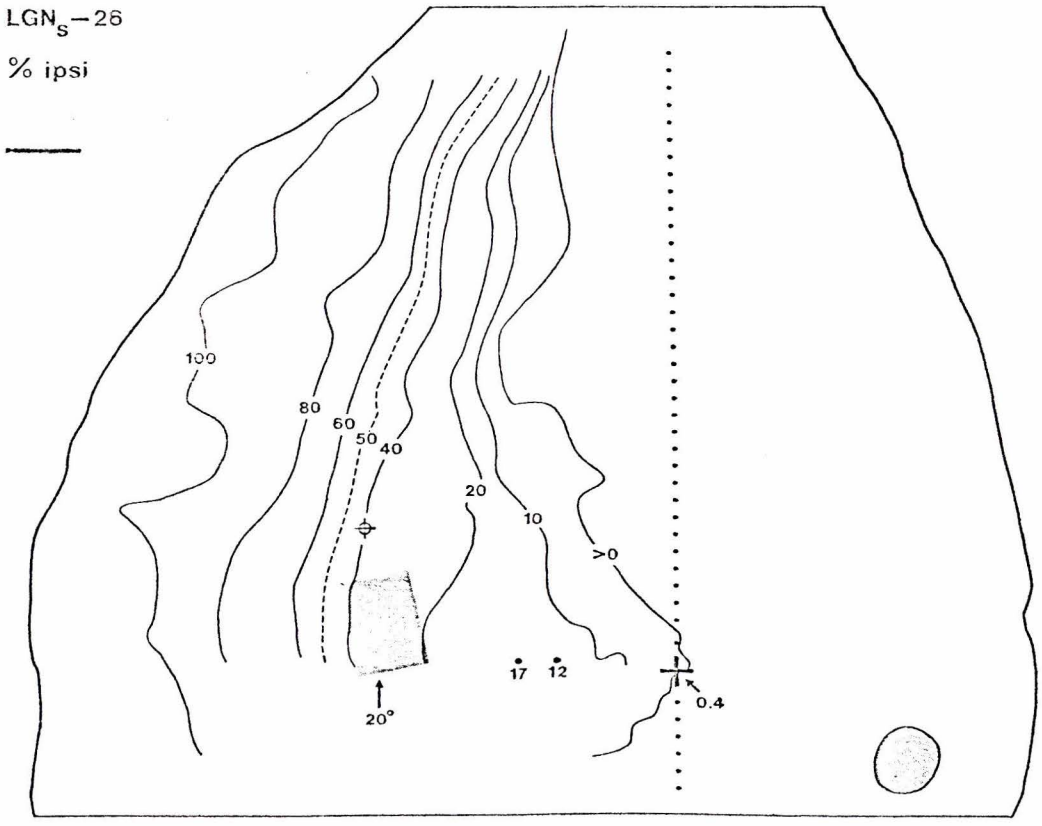
LGN$_S$–26
% ipsi
100
80
60
50
40
20
10
>0
17
12
0.4
20°

Figure 9

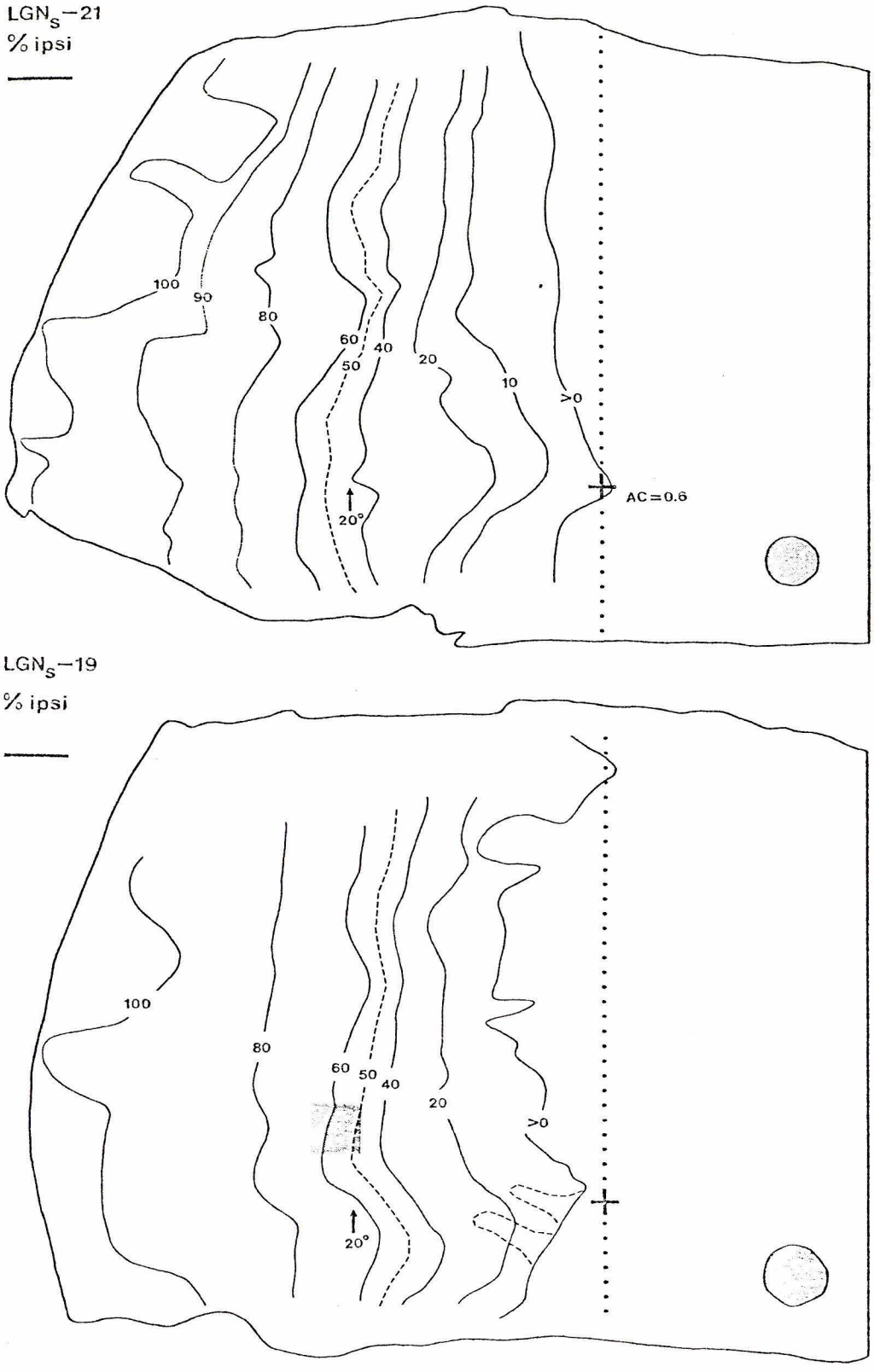
LGN$_S$–21
% ipsi
100
90
80
60
50
40
20
10
>0
AC=0.6
20°
LGN$_S$–19
% ipsi
100
80
60
50
40
20
>0
20°

Figure 10

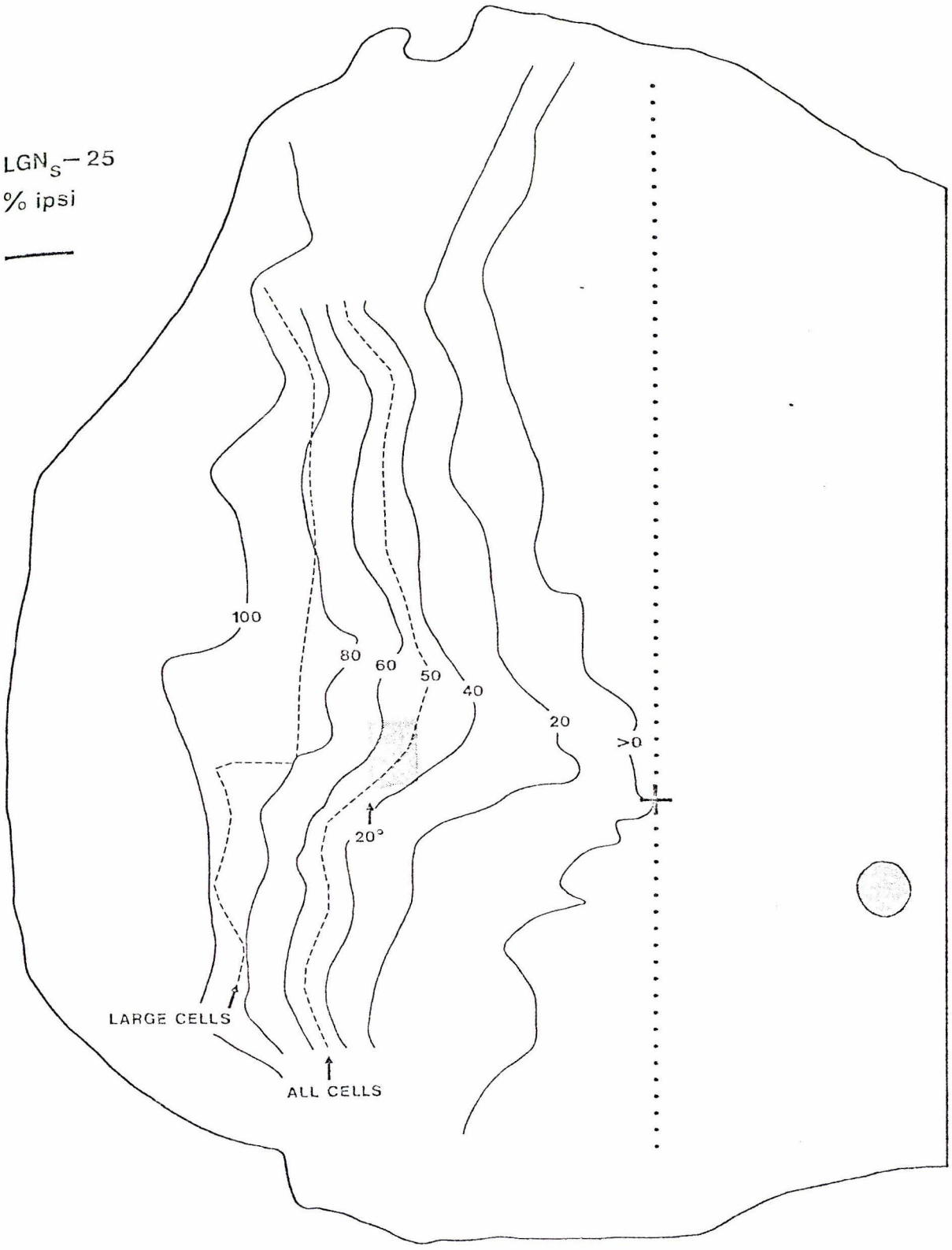


Figure 11

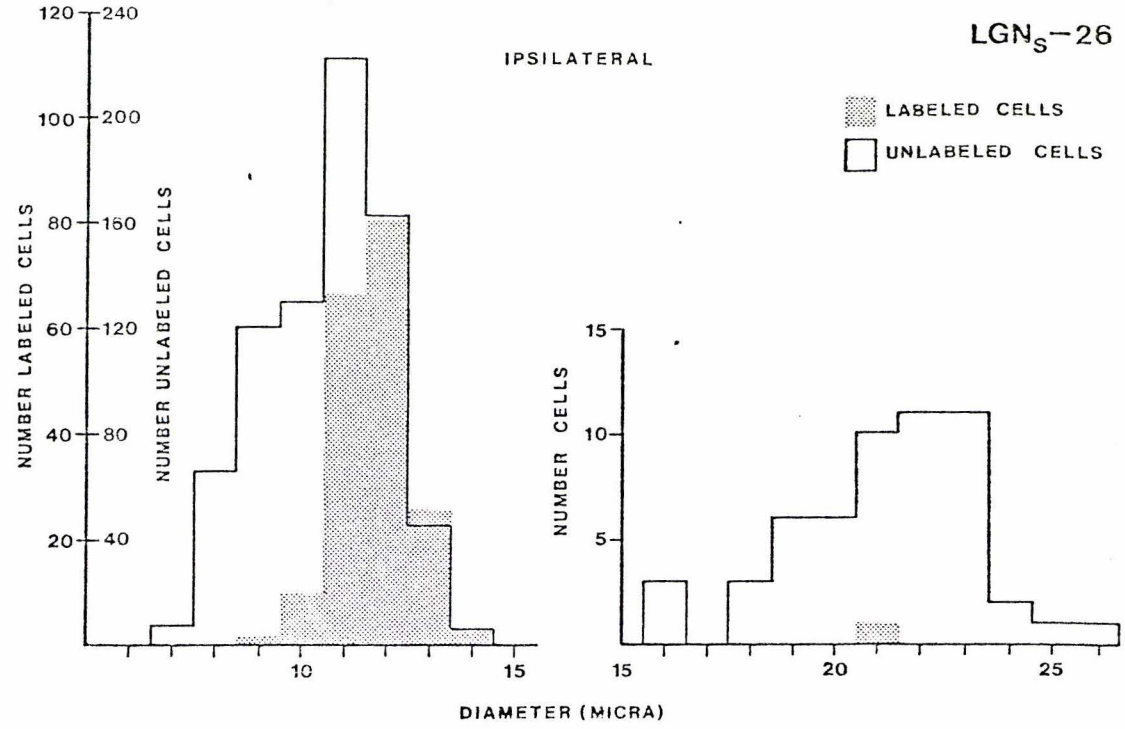
LGN$_S$–26
IPSILATERAL
LABELED CELLS
UNLABELED CELLS
NUMBER LABELED CELLS
NUMBER UNLABELED CELLS
NUMBER CELLS
DIAMETER (MICRA)

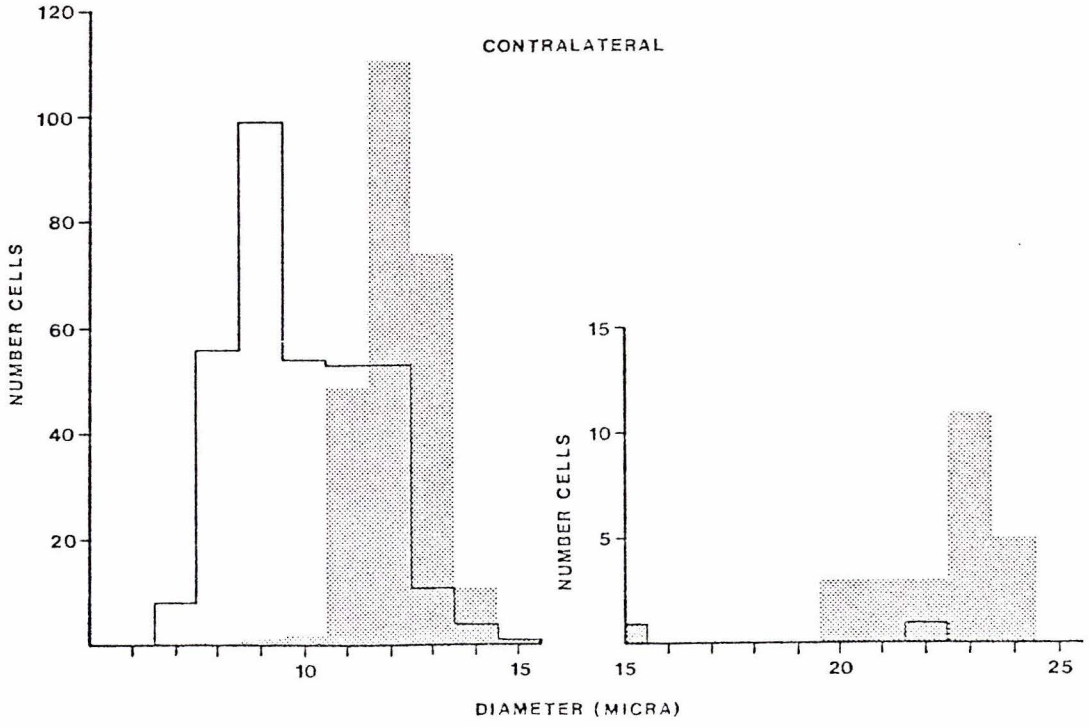
CONTRALATERAL
NUMBER CELLS
DIAMETER (MICRA)

Figure 12

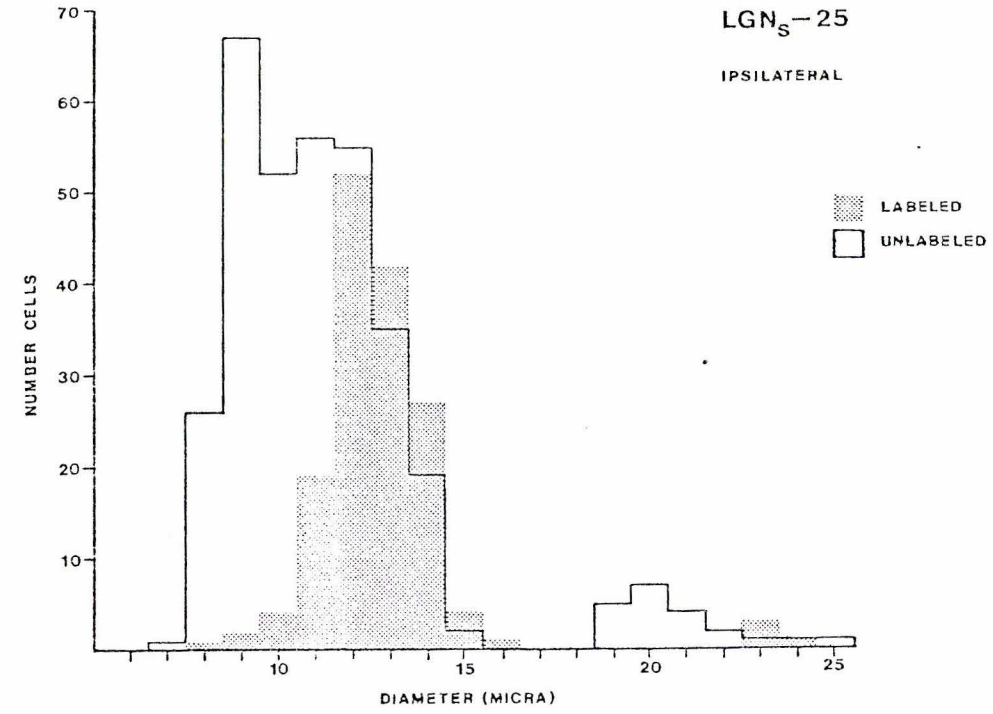
LGN$_S$–25
IPSILATERAL
LABELED
UNLABELED
NUMBER CELLS
DIAMETER (MICRA)
70
60
50
40
30
20
10
10
15
20
25

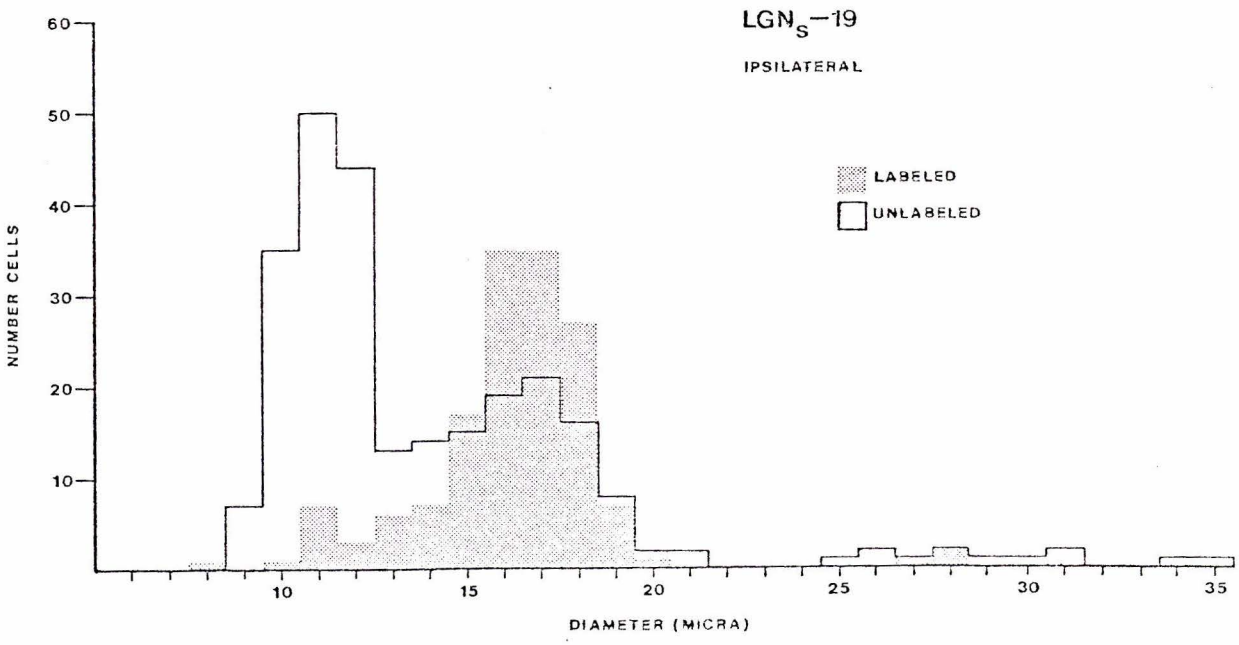
LGN$_S$–19
IPSILATERAL
LABELED
UNLABELED
NUMBER CELLS
DIAMETER (MICRA)
60
50
40
30
20
10
10
15
20
25
30
35

Figure 13

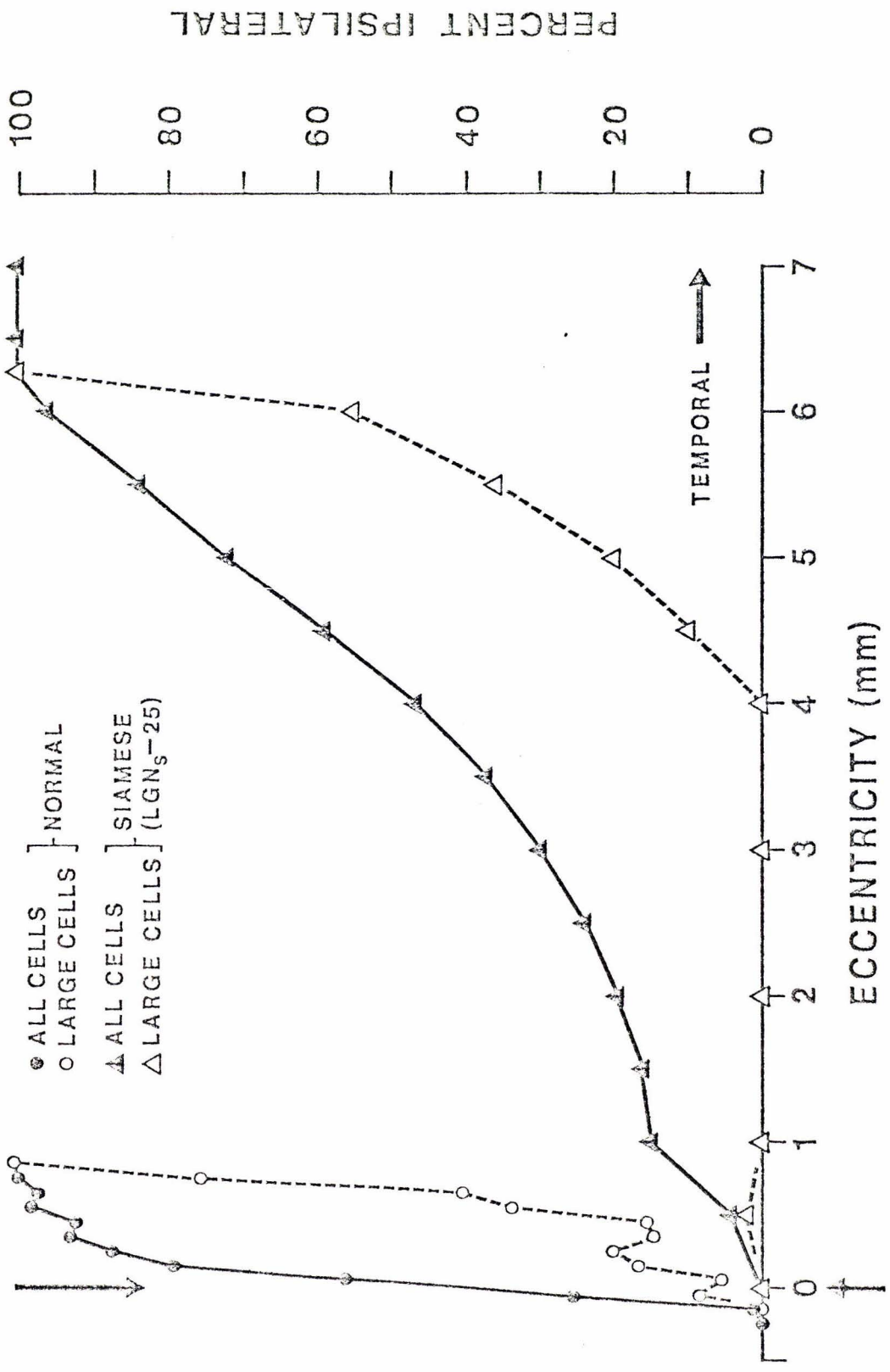
PERCENT IPSILATERAL
100
80
60
40
20
0
ECCENTRICITY (mm)
0
1
2
3
4
5
6
7
TEMPORAL
● ALL CELLS
○ LARGE CELLS
NORMAL
▲ ALL CELLS
△ LARGE CELLS
SIAMESE
(LGN$_S$-25)

Figure 14

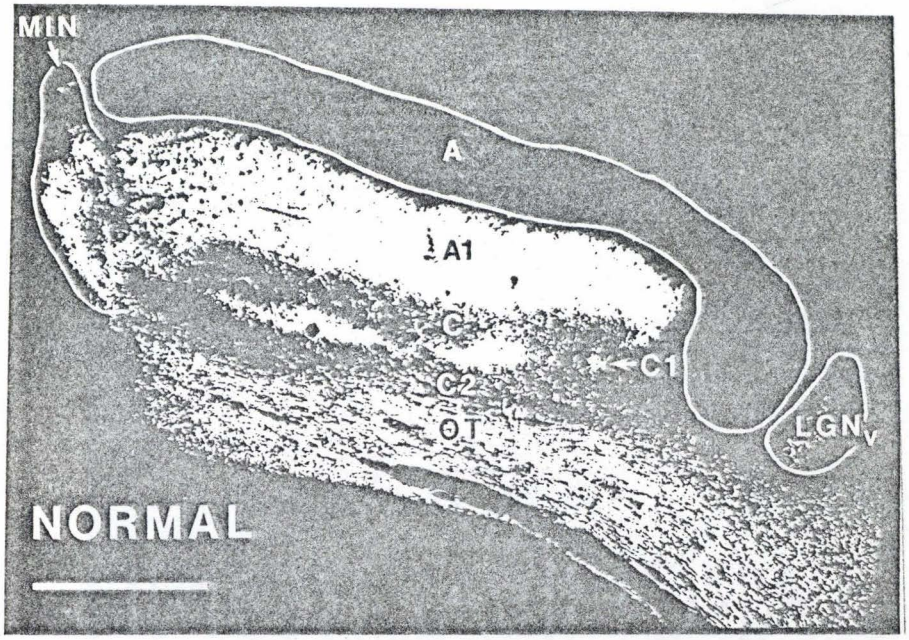


Figure 15

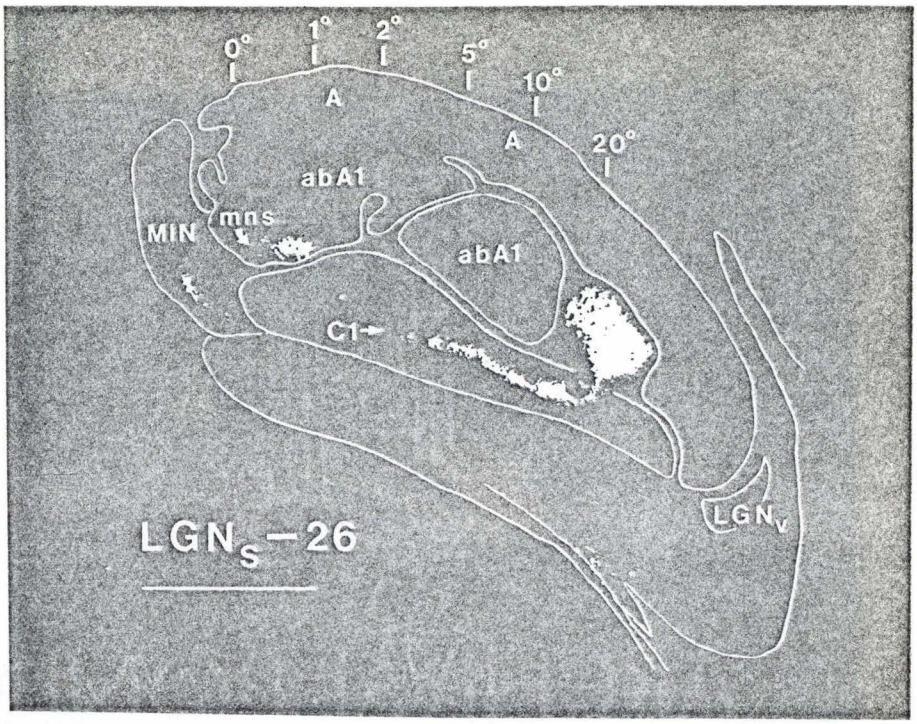


Figure 16

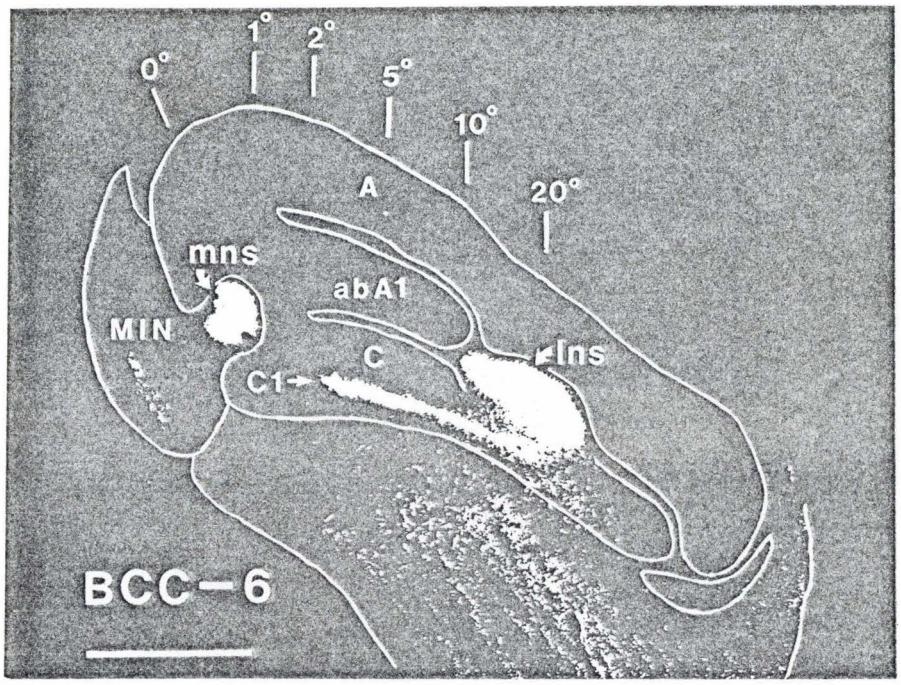


Figure 17

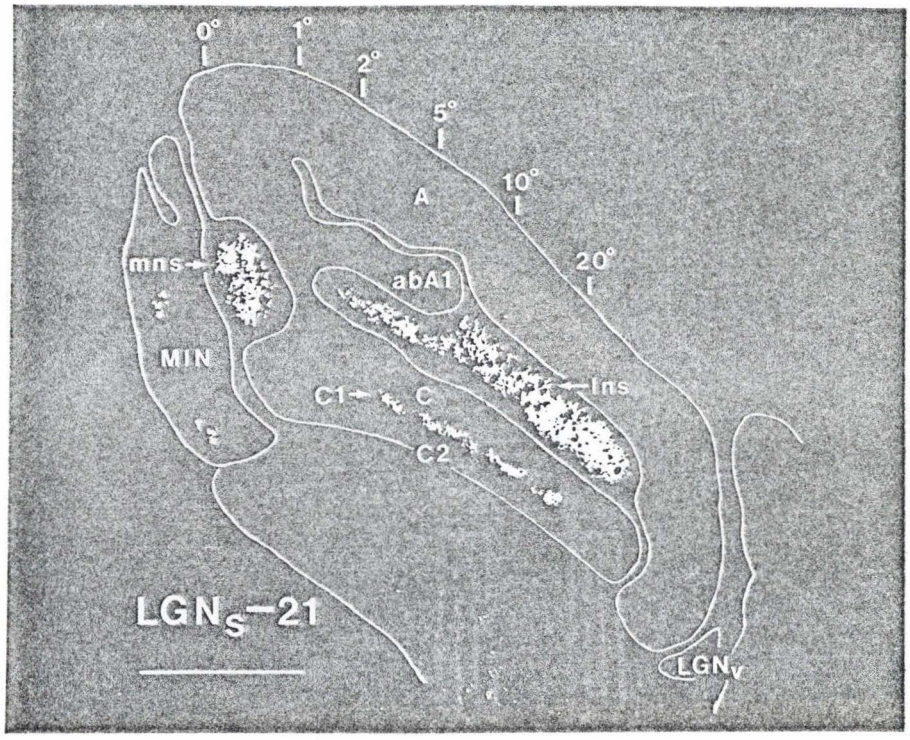


Figure 18

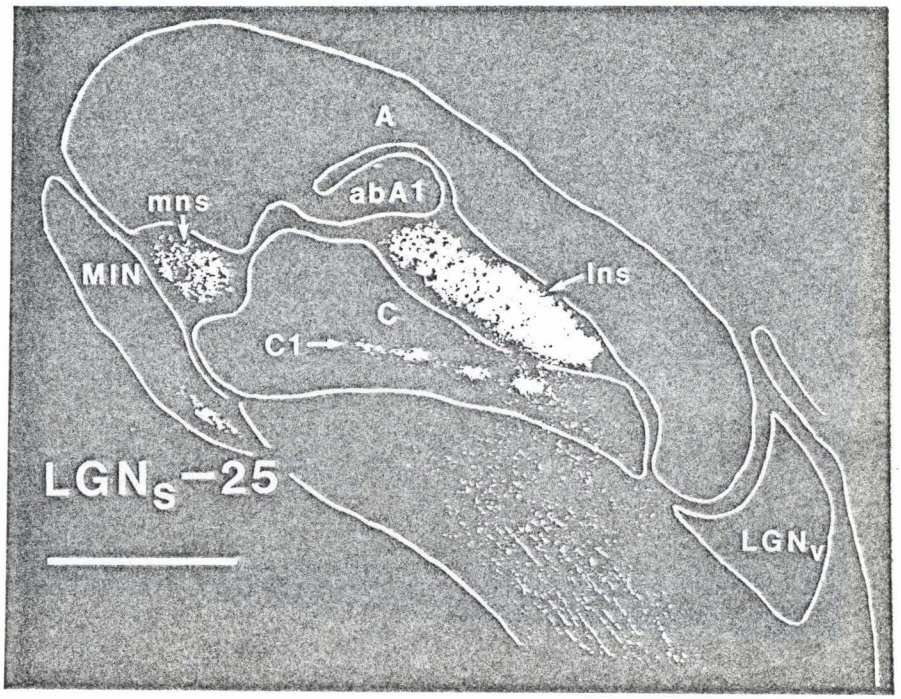


Figure 19

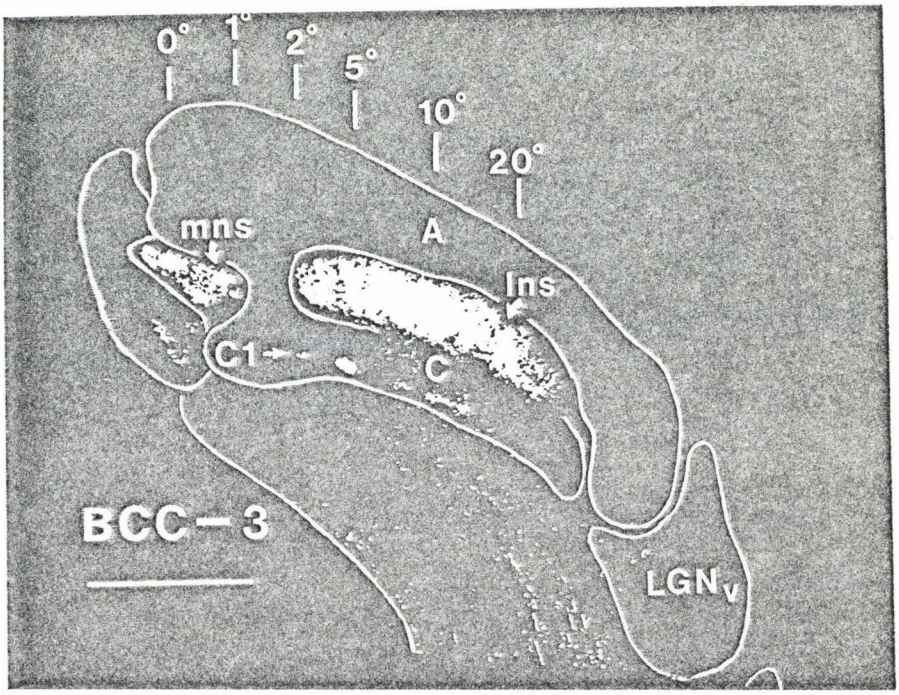


Figure 20

# CHAPTER 3

## A Neurophysiological Determination of the Vertical Horopter in the Cat and Owl

The horopter is defined as the locus of all points in space which stimulate corresponding points on the two retinae. Since each eye views space from a slightly different position, the correspondence revealed by the horopter's shape has always been of considerable interest, there being three approaches to its determination--theoretical (e.g., Aguilonius, 1613; Vieth, 1818; Müller, 1826), psychophysical (see Ogle, '32, '50, '62), and neurophysiological (Barlow, Blakemore and Pettigrew, '67; Nikara, Bishop and Pettigrew, '68; Joshua and Bishop, '70; Bishop, '73).

In the case of the horopter determined in the horizontal plane, all three approaches have led to reasonable agreement. Purely geometrical considerations give rise to a horopter in the shape of the Vieth-Müller circle, which passes through the nodal points of both eyes and through the fixation point. Psychophysical studies (where the horopter is established by finding a series of points each of which is seen as lying in the same direction when viewed by each eye separately) yield a similar, but slightly flattened curve. This slight flattening, called the Hering-Hillebrand deviation from the Vieth-Müller circle, probably reflects the way in which the wiring pattern from each retina onto binocular cortical neurons departs from the geometrical ideal.

Since, as pointed out by Shipley and Rawlings ('70), "corresponding points are such, ultimately, by virtue of a cortical correspondence," one might hope that single unit recordings from cortical neurons could be used to define the horizontal horopter physiologically. Indeed, Joshua and Bishop ('70) have performed this physiological experiment in the cat and report a result very similar to the Hering-Hillebrand deviation described psychophysically for humans (Hillebrand, 1893; and see Ogle, '50, '62).

In spite of the agreement as to the general form of the horopter in the horizontal dimension, there is dispute concerning the shape of the vertical horopter. Helmholtz's measurements led him to conclude that the vertical horopter in the mid-sagittal plane is a straight line tilted away from the observer (Helmholtz, 1867, '25). This analysis has been rejected by more recent authors (Ogle, '62; Shipley and Rawlings, '70) who have assumed that this horopter is oriented in the fronto-parallel plane. In spite of this, a new series of measurements in humans tends to support Helmholtz's original formulation (Nakayama, Tyler and Appelman, '77; Nakayama, Appelman and Tyler, MS in preparation).

We were led into a physiological study of the vertical horopter by trying to reconcile some apparent contradictions in the literature of the visual physiology of the cat. A previous study in the LGN has shown that the representation of the zero (azimuthal) meridian in this structure is indeed vertical in the paralyzed cat (Sanderson, '72). However, it has been shown that, at the time of paralysis, the eyes cyclorotate about an antero-posterior axis so that the twelve o'clock position of each eye is about 5° more medial than its normal position. (Henceforward this rotation will be referred to simply as "intorsion" and its opposite as "out-torsion" (Bishop, et al., '62; Hubel and Wiesel, '62; Nelson, Kato and Bishop, '77).) It was difficult to see how ocular intorsion under paralysis could leave the neural representation of the zero meridian as vertical. However, this problem can be resolved by a consideration of the projection of each eye's zero meridian into three-dimensional space, rather than by analysis in the fronto-parallel plane of the tangent screen where the data are collected. If it were assumed that the cortical representations of the two eyes' zero meridians were out-torted with respect to each other in the alert, unparalyzed cat, such out-torsion

would imply that cortical binocular units with receptive fields on the upper-field zero meridians would have uncrossed disparities with respect to the fixation point, while lower-field units would have crossed disparities. Assuming that binocular units with fields on the two zero meridians are the neural substrate for binocular correspondence in the mid-sagittal plane, the presumed out-torsion would result in a vertical horopter passing through the fixation point and tilted away from the cat. A schematic representation of such a horopter is shown in figure 1.

In order to test this hypothesis, we have recorded binocular cortical units at various elevations on or near the 17/18 border, which represents the zero meridian in the cat. After correction for the eyeball cyclotorsion induced by paralysis, our results indicate that the vertical horopter is indeed tilted away from the cat, as Helmholtz first proposed for humans. A similar method of analysis applied to data on binocular neurons recorded from the visual Wulst of Speotyto cunicularia leads also to a tilted vertical horopter for this terrestrial owl species. A preliminary report of this work has been presented elsewhere (Cooper and Pettigrew, '78).

## METHODS

### Cat Preparation

The main objective of each experiment was to map the representation of each eye's zero meridian in the cortex of the paralyzed cat. This was done by plotting the receptive fields of binocular cortical neurons at various elevations near the zero meridian. The general outline of the recording procedures has been described elsewhere (Nikara et al., '68; Pettigrew, '74) and will be reviewed here.

Six normal adult cats were used in this study. For four of the six all phases of the experiment were successfully completed and a vertical horopter

constructed. Surgical anesthesia was induced with 5% fluothane in a mixture of nitrous oxide and oxygen (2:1) and maintained with 1% fluothane. After tracheal and I.V. cannulation, the fluothane was discontinued; the cats were then transferred to a stereotaxic head-holder and paralyzed with 40 mg of Flaxedil (gallamine triethiodide). The cats were force-ventilated (minute volumes 40% greater than those recommended on the Harvard App. Chart) with a mixture of nitrous oxide, oxygen, and carbon dioxide (80%:20%:0% initially and 75%:22.5%:2.5% during recording). Infusion at 4.3 ml/hr of a paralytic solution containing Flaxedil (1.2 mg/ml) and d-tubocurarine (0.12 mg/kg/ml) in 0.3% saline/8% dextrose began shortly after initial paralysis and continued until the end of the experiment. This paralytic mixture was chosen to maximize ocular stability (Rodieck, Pettigrew, Nikara and Bishop, '67). The corneas were protected with contact lenses of zero power with radii of curvature chosen to produce sharpest focus of the projected fundus (see below).

Dual Recording

After opening the scalp, two craniotomies were made in order to uncover the visual cortex of the left hemisphere (except in LGN-33, in which the right cortex was used). The anterior craniotomy exposed the 17/18 border from approximately HC A15 to P5, while the posterior opening was made far laterally at about P8 in order to uncover the upper field zero meridian representation (Tusa, Palmer, and Rosenquist, '78). In an effort to eliminate systematic errors due to slow eye drifts during the course of the experiments, we recorded simultaneously from two tungsten-in-glass electrodes (Levick, '72). One electrode was placed far anteriorly in order to record units at approximately -30° in the visual field; the other track was used to map the zero meridian at about +10°. Each electrode was angled so as to remain on or near the 17/18 border for as long as possible during the course of the track. In

addition to this check on eye position provided by the near-simultaneous comparison of upper- and lower- field units, the absolute position of the eyes was also determined regularly by the projection technique described below. In two animals, after a sufficient number (at least five) of reliably plotted binocular units was recorded from one track, a third electrode track was placed between the first two in order to map zero meridian units at approximately -10 to -15° in the visual field. All receptive field data for each cat were collected within a 24 hr period, the first two tracks usually being completed in one 12-hr session. In LGN-36, all of the data were collected within a period of two hours. Receptive fields for binocular units were plotted on a tangent screen 57 cm from the animal. Conventional stimulation and recording techniques were used (Nikara et al.,'68; Pettigrew, '74).

Monitoring Eye Position

As indicated above, eye movements were minimized by continuous infusion of paralytic agents. In addition, one animal (LGN-36) was bilaterally sympathectomized. We were able to measure residual eye movements by positioning a fiber optic light pipe in front of the cat's eyes. The bright fiber optic light, being reflected from the cat's tapetum, was focused by the animal's own optics onto the tangent screen. In this way a clear image of the fundus was obtained on the same screen used for plotting units (see fig. 3). Eye movements were monitored by noting the drift in certain retinal blood vessel intersections. Generally, two or three pairs of intersections symmetrically placed on both sides of the area centralis were traced on the tangent screen. Each pair served as a baseline to determine residual torsions of the eye (Nelson et al., '77). In addition, lateral or vertical eye movements could be determined from the corresponding displacements of the landmark intersections. With good optics, this light pipe method allows very accurate

monitoring of eye position. The wide extent of fundus projected by this method usually allows all the retinal landmarks to be drawn at the same time (see fig. 3). If care is taken to replace the light pipe in the same position for each measurement, torsional movements can be measured to within 0.3° and translational displacements to 0.2° or less. In later experiments a modification enabled a bent fiber optic to be left in place in front of each eye for the duration of the experiment without affecting receptive field plots (Pettigrew, Cooper and Blasdel, MS in preparation). With this modification it became a routine matter to check each eye's position immediately upon plotting each unit's receptive fields.

Besides ease of measuring torsion and of drawing a wide area, our method of projecting the fundus has two other advantages, the first being that it allows accurate focusing of the cat's eyes on the tangent screen. This is done by testing contact lenses of various curvatures until the blood vessels are in sharp focus on the screen. Secondly, the area centralis can be plotted easily, since it appears as a darker green area against the yellow background of the tapetum and since a large number of blood vessels are visible simultaneously as they converge towards the area centralis. Thus the position of the area centralis can be determined to within 1° at the time of the experiment and with even greater accuracy post mortem, when the extensive drawing of retinal blood vessels can be related to the vessels on a retinal whole mount in which the area centralis is stained (see below).

Once the proper contact lenses were in place, they generally were not disturbed during the course of the experiment. This avoided any changes in eye position due to eye toilet (Nelson et al., '77). The short duration of the recording sessions insured maintenance of clear optics without the need for periodic cleaning of the eyes.

Estimation of the Visual Pole

In a study such as this, where accurate determination of receptive field elevation is important, it is necessary to have a good estimate of the position of the horizontal meridian passing through the area centralis. In order to verify and refine the estimate of the area centralis position made by projection of the fundus, the right lateral geniculate nucleus of each animal was filled with horseradish peroxidase (HRP) on the day before the recording session. Forty to fifty hours later, after the completion of the cortical recordings, the experimental animal was perfused and both retinae removed and reacted with benzidine in order to reveal the HRP retrogradely transported to the retinal ganglion cells. Whole mounts of these retinae allowed direct demonstration of the naso-temporal decussation of the retinothalamic pathway, as well as clear visualization of the area centralis. Each whole mount was photographed while still wet. Not only do the retinal blood vessels stand out clearly in such photographs (see fig. 2), but use of hydrated whole mounts avoids errors due to tissue shrinkage. Color transparencies of the whole mounts were projected on a screen at approximately 50X magnification and the position of the area centralis with respect to various blood vessel intersections was noted. By relating the blood vessel pattern on the whole mounts to that of the detailed tangent screen drawing of each fundus made in the living animal, it was possible to determine the position of the area centralis on the tangent screen to within 0.5°. In this way we were able to estimate accurately the position of the horizontal meridian during our recording sessions. A more detailed description of the HRP injection procedure, as well as a quantitative description of the decussation of the retinothalamic pathway in normal and Siamese cats, will be published elsewhere (Cooper and Pettigrew, MSs in preparation).

Estimation of Torsion

The conclusions of this study depend not only on the accurate determination of the cortical representation of the zero meridian in the paralyzed cat, but also on reliable measurement of the amount of ocular intorsion induced by paralysis. Our method of determining eye-rolling takes advantage of the fact that the cat's pupil has a slit shape. Before the HRP injection, photographs of each cat's eyes were taken in moderately bright light in order to obtain a measure of the normal position of the slit pupils. Minimal restraint without drugs was used to obtain these photographs. On the day of the recording session (after the ketamine used in the previous day's HRP injection had worn off), the experimental cat was placed in the stereotaxic head-holder, and the paralyzing infusion was started. We then waited for at least 2-3 hours before photographing the pupils of the paralyzed animal. This delay was included in order to let the eyes stabilize after the comparatively large drifts which occur during the first two hours of paralysis (Nelson et al., '77). Immediately after the photographing of the eyes, the pupils were dilated with a fast-acting anti-muscarinic agent (cyclopentolate hydrochloride) or intravenous atropine, and the blood vessel pattern of each eye was drawn on the tangent screen. As little time as possible was allowed to elapse between the photographing of the pupils and the drawing of the fundi in order to make sure that the eye position did not change between the two procedures. These initial fundus drawings thus provided a baseline of known eye position, and all subsequent residual cyclotorsions or translations were corrected to this initial determination of eye position. The eye torsion induced by paralysis was estimated by projecting the photographs of the eyes on a screen (5X magnification) and measuring the angle between the pupils before and after paralysis. Care was taken to use only

photographs which were directly frontal to the animal so as to avoid errors due to a tilt of the cat's head. Each of the authors determined the eye torsion independently, without any previous agreement on a convention for doing so. The two authors' values for mean eye torsion agreed to within 10% for every cat, showing that this simple method for determining eye-rolling is suitably precise. Nelson et al. ('77) have questioned the accuracy of this photographic technique. However, our mean value of 8.7° net intorsion for both eyes agrees well with the 10° value obtained with the same method by Bishop et al. ('62), and with the 9.2° value found by Nelson et al. ('77) using mean interocular orientation disparity of cortical units (see table 1). (Our convention has been to use positive angles for intorsion and negative angles for out-torsion.)

We have collected other data indicating the accuracy of our photographic technique. In two experiments (LGN-34 and 36), the cyclopentolate was allowed to wear off; thus the pupils had again assumed a slit shape by 17 to 20 hours after the initial determination of eye position. At this time we photographed the pupils and then redilated them in order to plot the positions of the landmark blood vessels. In this way we obtained two independent estimates of the amount of residual torsion occurring subsequent to the estimate of eye position at the beginning of the recording sessions. In the case of LGN-34 (table 1), the residual torsion was determined to be -1.8° by the slit-pupil photographic method and -1.9° by use of retinal landmarks. In LGN-36, use of the slit pupils gave a residual rolling of -1.4°, while a value of -1.6° was obtained from the fundus drawing. Thus, these two different and independent methods of measuring residual torsion of the eyes yielded very similar estimates of this torsion. We therefore feel that our photographic method is both valid and precise.

In making our corrections for eyeball rolling during paralysis, we have assumed that this torsion occurs about the visual axis of the eye. Measurements from the pupil photographs show that the axis of eyeball rotation runs approximately through the center of the slit pupil, since the tops of the pupil converge by about the same amount as the bottoms diverge. In addition, use of the fundus projection technique allowed small amounts of residual torsion around the area centralis to be measured in some cats after paralysis (e.g., LGN-34 and LGN-36, see table 1). Both of these measurements show that it is at least approximately correct to treat the area centralis as lying on the axis of rotation during paralysis.

Owl Preparation

In addition to our experiments in cats, we have also attempted to determine the form of the vertical horopter in a terrestrial, diurnal owl, the burrowing owl (Speotyto cunicularia). The burrowing owl is a small bird; our specimen had a height (ground-to-eyes) of about 15 cm when erect. The owl, weighing 185 gm, was anesthetized with an i.m. injection of 2.5 mg ketamine hydrochloride. We immobilized the bird's head by cementing the beak to a rigid metal bar. After removing the crown feathers and parting the scalp and temporalis muscles, we used dental cement to fix the back of the skull to two metal bars which were attached to the frame from which the owl was painlessly suspended. After making the appropriate craniotomies, we inserted two electrodes into the right visual Wulst; one penetration was placed anteriorly and the other posteriorly, in an effort to record simultaneously from the zero meridians in the upper and lower fields. We switched frequently from one track to the other; as in the cats, this was done in order to avoid systematic differences in mean field separation between the two tracks due to the slight eye movements in the unparalyzed owl (see below). The owl faced a tangent screen placed 57 cm

in front of its eyes; recording and stimulation procedures were identical to those used above for the cats and for owls in previous studies (Pettigrew and Konishi, '76; Pettigrew, '78).

Due to the small degree of eye movement in the owl (Steinbach and Money, '73; Pettigrew and Konishi, '76), it was not necessary to paralyze the bird during the recording session. After fixing the owl's head, we observed the eye movements with an ophthalmoscope for a period of one-half hour. These eye movements consisted of occasional fast flicks of about 0.5° in amplitude, after which the eye returned to the starting point. In addition we noted slow drifts, also of about 0.5° amplitude, which occurred over the order of minutes. We did not observe any larger movements in response to attempts to startle the owl (approaching objects, noises, rapping the beak). After this observation period, the positions of the foveae and pecten tips were plotted on the tangent screen by means of a reversible ophthalmoscope. We measured the effect of ketamine on eye position in the owl by leaving an ophthalmoscope fixed in front of each eye while administering a 2.5 mg dose of ketamine (this after the original dose had worn off). By 5 min after the injection of the ketamine, each eye had diverged by about 0.5°. We did not notice any significant net torsion between the two eyes as a result of the administration of ketamine, although our accuracy for monitoring torsion between the eyes was only to within about 3°. We could not observe any effect of the ketamine by 1.5 hrs after the injection; at this time the eyes had returned to their pre-injection positions. The return of the bird's responsiveness to external stimuli also indicated that the ketamine was no longer effective by this time. All of the units used in this study were plotted after this test dose of ketamine had worn off; no more anesthetic was needed during recording. Thus it is possible to discount any effect

of anesthetic on the results of this experiment. The owl was recovered after the experiment.

## RESULTS

### Cat

As mentioned above, our main experimental objective was to determine the position of the zero meridian for each eye, since we have assumed that the zero meridian is the physiological substrate for the horopter in the mid-sagittal plane. Our procedure has been to record binocular units at several H-C levels close to the 17/18 border. In this way we have recorded the receptive field positions of binocular units at several elevations on or near the zero meridian. Table 1 contains a summary of our data base of binocular units. We have recorded a total of 129 well-isolated binocular units from 11 tracks in 4 cats. Our calculations of the zero meridians are based on 70 units; the others were discarded because they were too far from the vertical meridian or because they did not give a sufficiently reliable receptive field plot in one of the eyes. All of the units selected for analysis were within 5° of the zero meridian in order to avoid the systematic changes in field separation which occur with increasing horizontal eccentricity (Joshua and Bishop, '70). The only exception to this was LGN-36, in which the placement of the electrode tracks necessitated using fields in the 5°-strip from 3°-8° azimuth.

### Binocular Receptive Field Separation at Different Elevations

Figure 3 is a drawing of those receptive field plots used for analysis as they appeared on the tangent screen for LGN-34. There were four clusters of receptive fields on the tangent screen, each cluster corresponding to one of the cortical penetrations. As would be expected from previous descriptions of the topography of the cat visual cortex, the most anterior track

corresponded to the unit at the lowest visual field elevation, while the most posterior track corresponded to the fields at the highest elevation (Talbot, '40; Hubel and Wiesel, '62; Bilge, Bingle, Seneviratne and Whitteridge, '67). Because of the fact that the eyes diverge slightly under paralysis (Bishop et al., '62), the areae centrales and receptive field pairs were somewhat separated on the tangent screen. However, it is evident from the figure that all of the tracks gave units lying quite close to the zero meridian. This figure also makes it clear that the receptive field separation of binocular pairs was roughly the same at all elevations. In other words, despite the cyclorotation which had occurred during paralysis, the zero meridians of each eye appeared to be parallel. The angle between the zero meridians was next determined more precisely, as described in the following section.

Formal Calculation of the Zero Meridian

In order to calculate the zero meridian we have adopted the method developed by Bishop and his colleagues, which makes use of the separation of receptive field pairs for binocular units (Nikara et al.,'68; Sanderson and Sherman, '71; Joshua and Bishop, '70). Figure 4 demonstrates the manner in which we have calculated the two zero meridians from the positions of the binocular receptive field pairs (all corrected for residual eye movements, both translational and torsional). The parameter of interest here is D, the distance on the tangent screen between the two zero meridians at each elevation. However, since we do not have a direct way here to determine the absolute position of each eye's zero meridian at every elevation, we must instead determine B, the distance (at each visual field elevation) from the vertical line through one eye's blind spot to the zero meridian of that eye. (The vertical through the blind spot is taken as the perpendicular to the line passing through the centers of the two optic disk projections.)

If we assume that the two eyes are symmetrical, then it is evident that $2B + D = A$, where $A$ is the distance on the screen between the centers of the two blind spots. Rearranging the equation gives $B = (A - D)/2$. In the absence of an estimate for $D$, we must calculate the separations ($d$) of the receptive field pairs for the binocular units; we then assume that the mean value of $d$ for each elevation will equal $D$, the separation of the zero meridians at that elevation. That is, we assume that the average field separation gives the separation of corresponding points on the tangent screen. It then becomes possible to calculate a value of $B$ for each receptive field pair, i.e., $B = (A - d)/2$.

Figure 5 is a plot of $(A - d)/2$ versus elevation for each binocular unit of LGN-34. This figure is thus a plot of the distance from the vertical through the blind spot to the estimated zero meridian for each data point. The linear regression line (solid) through the data points therefore is the experimentally determined zero meridian for one eye. (By symmetry, the other eye will have a zero meridian which is the mirror image of this plot. The dotted lines in the figure represent the 95% confidence limits for the linear regression estimate of the zero meridian.) In the case of cat LGN-34 under paralysis, the angle between the experimental zero meridian for one eye and the vertical through that eye's optic disk was found to be $+0.75 \pm 0.95°$, the positive value indicating that the zero meridian in the lower field is slightly farther from the line through the blind spot than is the upper field meridian. Table 2 gives the estimates of $\theta_p$, the angle between one eye's zero meridian and the vertical, for all of the experimental cats under paralysis. The value of $2\theta_p$ equals the net angle of shearing between the two zero meridians in the paralyzed animals. The absolute value of this shearing is never greater than 1.5°, and the mean value is +0.24° .

(The positive angle means that the two vertical meridians are slightly crossed in the lower field). The above data thus confirm Sanderson ('72), who used a different method but also found that the zero meridians for the two eyes are parallel and (by symmetry) vertical in the paralyzed cat.

Torsion

We have found, in support of the results of others, that under paralysis each eye cyclorotates inward from its position in the alert, unparalyzed cat. Table 1 gives the measured values for $\theta_n$, the net torsion between the two eyes induced by paralysis. These data show that there is an average net intorsion of +8.7° (S.D. = 4.7°) due to paralysis. This value is in good agreement with the estimates of cyclotorsion obtained by others (10°, Bishop et al., '62; about 10°, Hubel and Wiesel, '62; 9.2°, Nelson et al., '77). The cat we have used for illustration, LGN-34, showed a net intorsion of +14.1° ± 2.0°. The error of 2° is the 95% confidence limit for the difference between the inter-pupillary angle before paralysis (11 photographs) and this angle after paralysis (6 photographs).

Estimation of Zero Meridians in Life

Because of the intorsion produced by paralysis, it becomes necessary to correct the value of $2\theta_p$ for each cat in order to obtain the value for the angle between the two zero meridians in the unparalyzed state. If it is assumed that the axis of rotation corresponds to the visual axis through the fixation point, out-torsion of the eye will shift the upper retina temporally and thus will shift the lower portion of the zero meridian nasally (i.e., away from the blind spot) on the tangent screen. This correction thus corresponds, for the right eye, to rotation by an angle of $(\theta_n/2)$ in the clockwise direction as one faces the tangent screen. Figure 6 shows the zero meridians for the two eyes of LGN-34 after correcting for the intorsion.

induced by paralysis. In order to construct this figure, the data points in figure 5 were rotated around the fixation point by $\theta_n/2 = 7.05°$. The parameter $r^2$ in figure 6 is the square of the correlation coefficient for the linear regression estimate of the corrected zero meridian. The value of $r^2 = 0.93$ indicates that the experimental data for each zero meridian are approximated quite well by a straight line. After correction for torsion, the net angle between the zero meridians in LGN-34 is +15.6° ± 3.9°. The calculated values for the angles between the two eyes' zero meridians in the unparalyzed state are given in table 2 for all our cats; the mean angle is +10.0°. All of the experimental cats except LGN-28 had zero meridians with a significant degree of such shearing, and all except LGN-28 had $r^2 > 0.9$, indicating that the zero meridian is indeed a straight line over the range of eccentricities studied here. In LGN-28 the zero meridians were sheared by an angle of +2.0° with respect to each other in the alert cat, but the large error limit of 5.3° makes it unlikely that this degree of shearing was significant. The small value of $r^2$ in this animal does not indicate that the experimental data points did not fall on a fairly straight line (which, by inspection, they did), but rather reflects the fact that $r^2$ becomes a poor index of the straightness of a line as that line approaches vertical or horizontal.

Spatial Implications of Sheared Zero Meridians

As is evident from figure 6, the correction for torsion under paralysis implies that the zero meridians in the lower visual field are crossed with respect to the fixation point, while the upper field meridians are uncrossed. That is, a point on the lower field zero meridian for one eye is farther from the vertical through the optic disk for that eye than a point on the upper field zero meridian. Since points on the two zero meridians are assumed

to be corresponding points (in the stereoscopic sense of the word), this result indicates that corresponding points in the lower field are crossed with respect to the fixation point, and corresponding points in the upper field are uncrossed.

As schematized in figure 7, receptive fields on the tangent screen which are crossed relative to the fixation point correspond to depths in front of the plane of fixation. On the other hand, uncrossed points correspond to depths behind the fixation plane. Because points on the zero meridians are assumed to be corresponding, and because the vertical horopter is the locus of corresponding points in the mid-sagittal plane, it should be possible to calculate the vertical horopter for each of our experimental cats by projecting corrected data points like those in figure 6 onto the mid-sagittal plane. By virtue of the finding that the two zero meridians are crossed in the lower field, the vertical horopter in the lower visual field will be closer to the animal than the fixation point. Conversely, since the zero meridians are found to be uncrossed in the upper field, the horopter in the upper field will be farther away from the animal than the fixation point.

The finding that the zero meridians on the tangent screen are themselves straight lines implies that their projection into space will yield a horopter which is also a straight line (see Appendix).

Determination of a Vertical Horopter for a Particular Animal

The experimentally determined vertical horopter for LGN-34 is depicted in figure 9. This horopter has been calculated using a pupillary separation of 3.8 cm (as measured from photographs of LGN-34); the fixation point has been set arbitrarily at 57 cm, the distance between the animal and the tangent screen. It can be seen that the experimentally determined horopter for LGN-34

is a straight line tilted approximately 13° from the horizontal. The line is closer to the animal in the lower visual field and farther away in the upper field; the horopter line reaches the animal at a point about 13.5 cm below the eye. Thus, for the assumed fixation distance of 57 cm, the vertical horopter is far from being a fronto-parallel line and is in fact considerably tilted from vertical.

By virtue of the significant crossing of the vertical meridians in LGN-33 and LGN-36, these cats would also be found to have tilted horopter lines in the unparalyzed, alert state.

Owl

Dual Recording

We made two electrode penetrations into the right visual Wulst of the burrowing owl, S05. One track was placed near the posterolateral margin of the Wulst and the other near the anterolateral margin in an effort to record units at elevations on the zero meridian equally spaced above and below the horizontal meridian (see Pettigrew and Konishi, '76; Pettigrew, '78). In fact, however, the posterior track yielded units whose fields fell almost exactly on the horizontal meridian, the fields of the anterior track lying an average of 16° below. The fields on both penetrations clustered around an azimuth of 10°.

A total of 27 units was studied in the owl, of which 19 had binocular plots reliable enough to include in the data analysis. The nine units on the posterior track had a mean azimuth of 10.6° (range 7.2° to 12.1°, S.D. = 1.6°) and a mean elevation of -1.0° (range +0.1° to -2.1°, S.D. = 0.8°). All of the receptive field pairs in this penetration were uncrossed on the tangent screen and had a mean separation of +1.3° (range 0.6° to 1.8°, S.D. = 0.3°). There was no systematic vertical separation between members

of the receptive field pairs in this posterior track; the mean vertical separation between the fields for the nine binocular units was -0.1° (negative indicating that the ipsi field was higher than the contra field). The range of vertical separations was from -0.4° to +0.4° with a S.D. of 0.3°.

The anterior track yielded ten reliably plotted binocular units, with a mean azimuth of 8.7° (range 7.2° to 10.2°, S.D. = 1.0°), and a mean elevation of -16.1° (range -13.5° to -20.9°, S.D. = 2.5°). All of the receptive field pairs for this penetration were crossed on the tangent screen, with a mean receptive field separation of -1.0° (range -0.4° to -1.8°, S.D. = 0.4°). The mean vertical separation for the fields of the ten binocular units was 0.0°, with a range from -0.4° to +0.8° and a S.D. of 0.3°. The mean for this track is not significantly different from that for the posterior track ($p > 0.05$ for a two-tailed "t"- test).

Calculation of Zero Meridians and Horopter

The linear regression analysis for the zero meridians of SO5 is shown in figure 8. The data in this figure are represented in a manner slightly different from that used for the cat data in figure 5. (for which $(\underline{A}-\underline{d})/2$ is graphed against elevation). Figure 8 is a plot of the receptive field separation, $\underline{d}$, versus elevation for each binocular unit. The slope of this regression line yields directly the angle between the two zero meridians. (For the plot of $(\underline{A}-\underline{d})/2$, the slope yields one-half this angle.) We have found that the net angle between the zero meridians in the unparalyzed burrowing owl is $+8.3° \pm 1.5°$, and that, as in the cat, receptive fields on the lower part of the zero meridian are crossed with respect to fields on the upper part of the zero meridian. The experimental data for the owl's zero meridian are fit fairly well by a straight line, as demonstrated by the value of $r^2 = 0.89$.

The experimental vertical horopter for the owl S05 has been calculated in the same manner as for LGN-34, that is, by projecting the receptive fields for each binocular unit into space. This experimental horopter is shown in figure 9. (The fact that the owl fields do not lie on the zero meridian does not invalidate their use in calculating the angle between the zero meridians, since both penetrations were at about the same azimuth. However, in order to depict the horopter here we have assumed that there is no change in mean field separation with horizontal eccentricity. This assumption can be questioned in light of the horopter deviations mentioned above for man and cat.) The major result of this calculation is clear, viz., that the vertical horopter in the burrowing owl is not fronto-parallel, but rather is tilted quite far from the vertical. This result is implicit in the finding that the vertical meridians are torted with respect to each other, with the upper-field meridians being divergent compared to the lower-field meridians.

## DISCUSSION

### Position of cat's eyes in paralysis

Our finding from cortical recordings in the paralyzed cat that the zero meridians are parallel and vertical (by symmetry) both confirms an earlier conclusion based upon geniculate recording (Sanderson, '72) and reaffirms Bishop's view that one can specify with considerable accuracy and reproducibility the position of the cat's eyes in paralysis (Bishop et al., '62; Vakkur et al., '63). In four cats we found that angle between the zero meridians under paralysis was $0.24^\circ \pm 0.96^\circ$ (mean and standard deviation of the mean). In other words, if there has been no interference with the eyes, if eye-bars and other paraphernalia which might displace them have been removed, and if a non-depolarizing neuromuscular block has been instituted for some time, it may now be safe to assume that the zero

meridians of each eye are parallel and vertical in the normal cat (within the confidence limits specified), in addition to being somewhat divergent.

Position of cat's eyes in life

Inter-subject variability: Having established that the zero meridians are parallel and vertical in paralysis, it is possible to estimate their relationship in life provided one has information about the amount of intorsion which occurs with paralysis. The value which we have obtained for torsion (mean = 8.7°, S.D. of mean = 4.7°) is in good agreement with those obtained in a number of other studies (e.g. Bishop et al.,'62, 10°; Nelson, Kato and Bishop, '72, 9.2°). The two findings in paralysis of a net intorsion and of parallel vertical zero meridians indicate that in life the zero meridians are neither parallel, nor vertical. Rather, when seen on the tangent screen they are crossed, or out-torted, with respect to one another. In other words, our hypothesis of a tilted horopter for the cat is confirmed (see below).

It should be noted, however, that there is considerably more variance in the data pertaining to the amount of ocular torsion occurring under paralysis than there is in the data on the angle between the zero meridians in paralysis. One cat (LGN-28) out of the four that we studied showed very little torsion with paralysis, so we are not entitled to conclude that it would have had a significantly tilted horopter in life. We cannot be certain why this particular cat should be so different from the other three, all of which would show highly significant tilts in life, but there are a number of possible explanations. For example, it may be that cats exert active control over counter-rotatory torsional eye movements and that LGN-28 was maintaining its eyes in an extreme position when the pre-paralysis photos were taken; we did not attempt to control for this possibility.

On the other hand, some subjects just may not have tilted vertical horopters. This appears to be the case in man, since Helmholtz found a much smaller angle between the zero meridians of myopic subjects than between those of normals. (Hering, who was myopic, had an angle close to zero; p. 413, Helmholtz, 1925.) Using the insights provided by this study, Cynader (personal communication) has been able to deduce from analysis of slit-pupil data that visually deprived cats probably lack tilted vertical horopters.

The tilted vertical horopter and psychophysics

On the basis of simple psychophysical experiments, Helmholtz (1867, '25) proposed over one hundred years ago that the vertical horopter is a tilted line passing through the observer's fixation point and his feet. Helmholtz based his suggestion on data concerning the divergence of the upper ends of the apparent vertical meridians for the two eyes. These data had been obtained in monocular measurements by Volkmann and in Helmholtz's own measurements using the criterion of single vision. Subsequent investigators have rejected the results of both Volkmann and Helmholtz as being due to "idiosyncratic excyclotorsions of Volkmann's and of Helmholtz' own eyes about the anterior-posterior axis" (Shipley and Rawlings, '70; Ogle, '62). These authors have implied that the vertical horopter is fronto-parallel. However, recent experiments in man using the nonius method have confirmed Helmholtz' original result and show that the zero meridians for the two eyes are indeed crossed. These experiments further show that this top-outwards divergence of the zero meridians is not due to eyeball cyclotorsion (Nakayama et al., '77, and MS in preparation). Breitmeyer, Julesz and Kropfl ('75) and Julesz, Breitmeyer and Kropfl ('76) have also obtained psychophysical data which support the hypothesis of a tilted horopter. These workers have found that random-dot stereograms with crossed disparities are fused at

shorter durations in the lower visual field, while stereograms with uncrossed disparities have shorter required durations in the upper field.These data indicate that the stereoscopic mechanisms of the human visual system are biased toward greater distances in the upper visual field.

Our principal finding supports and extends Helmholtz's suggestion concerning the vertical horopter. We find that the vertical meridians for the two eyes are extorted with respect to each other (i.e., divergent at the top, convergent at the bottom) in both the cat and the burrowing owl. This result implies that the vertical horopter is tilted away from the animal in both of these species. It is interesting to note that although our conclusions are novel for both the cat and burrowing owl, our raw data for the cat merely confirm the previously published observations of others. Indeed, we could have drawn our main conclusion concerning the cat from data already present in the literature (although we have done our own experiments in order to ascertain whether the error inherent in our physiological methods is sufficiently small so as not to obscure the proposed phenomena). As mentioned above, our estimate of the amount of inward cyclotorsion under paralysis in the cat is in good agreement with other findings. And the observations that the zero meridians are parallel in paralysis also has been noted already (Sanderson, '72). However past investigators have tended to see a conflict between the physiological results for the zero meridians and the suggestions of eye rolling during paralysis. For instance, Sanderson ('72) argued that there could be no significant rolling of the cat's eyes because of the fact that the zero meridians are vertical under paralysis. We have combined these seemingly contradictory data and have tried to show that they are in fact not conflicting. The apparent conflict arises from restricting one's consideration to the flat tangent screen, when in fact

the visual system of the cat (and owl, and man) is designed to operate in depth. If one projects the crossed zero meridians (which result from the combination of our physiological and photographic data) from the two-dimensional tangent screen into three-dimensional space, one can appreciate that the data for the physiological mapping of the zero meridians and the photographic correction for torsion are not in conflict, but rather complement each other to give a behaviorally meaningful construction for the vertical horopter.

Adaptive significance of a tilted vertical horopter

We have found that the vertical horopter is tilted in both the cat and burrowing owl. Why would it be of advantage to these animals to have such a horopter line in place of the fronto-parallel line which is usually proposed for humans? Inasmuch as the horopter is the locus in space of corresponding points, it is also the locus of points around which stereoscopic processing of visual information is possible. Stereoscopic mechanisms operate over only a relatively narrow range of depths in front of or behind the horopter curve. (This range may be determined by the spread of optimal disparities of single neurons around the mean (Barlow et al., '67; Nikara et al., '68; Joshua and Bishop, '70; van der Heydt, Adorjani, Hänny and Baumgartner, '78).) Thus the position of the horopter in space indicates the region in which the animal is able to use stereopsis, which is the most accurate mechanism of depth discrimination.

Both the cat and burrowing owl are small terrestrial predators. In these species, given a fixation point on or near the horizon, most objects of interest (e.g., prey) will be on the horizon or in the lower field closer than the horizon. If the horopter were fronto-parallel, the animals would be denied the use of stereoscopic processing in the lower field, which is just the region where precise depth judgments would be of greatest usefulness. A horopter line passing near the feet and slanted toward the fixation point

would allow the stereoscopic mechanism to operate in the behaviorally significant region of lower visual field between the animal and its horizon.

For a given angle $\theta_u$ between the zero meridians, the point at which the horopter intersects the coronal plane through the animal's eyes depends on the pupillary distance ($P$, see Appendix) and is given by $(P/[2 \tan (\theta/2)])$. For a cat with the average pupillary separation of 3.8 cm (Bishop et al., '62) and an angle of +10° between the zero meridians (see table 2), the horopter would intersect the coronal plane at a point about 22 cm below the eyes. This compares favorably with the height of a cat, which can vary from about 10 to 30 cm, depending on whether the cat is crouching or standing erect. In the burrowing owl S05 the eyes were about 15 cm above the ground in the normal posture; we estimate the horopter for S05 to pass somewhere between 16 and 23 cm below the eyes, using $P$ = 2.8 cm and $\theta = 8.3° \pm 1.5°$. In man, according to Helmholtz ('25), the angle between the apparent vertical corresponding meridians is about 2.5°, which for a pupillary separation of 6.5 cm (reasonable for an adult) means that the horopter line should pass somewhere about 150 cm (5 ft) below the eyes. These calculations show that in all three of these species the horopter line intersects the vertical plane through the eyes at a point near the observer's feet. We do not wish to make too much of the exact numbers resulting from these calculations, since the data used are obviously approximate, and the calculated horopter is therefore subject to error. (For instance, a change from 2.5° to 2° for the angle between zero meridians in the human will shift the intersection point from 150 cm to 190 cm below the eyes.) However, these rough calculations do indicate that the horopter line indeed passes in the vicinity (loosely defined) of the observer's feet, just as Helmholtz proposed.

Of possibly greater interest than the exact point of intersection with the coronal plane is the angle which the horopter line makes with the horizontal. Figure 10 shows the vertical horopter lines calculated for a cat with $\underline{P}$ = 3.8 cm and $\theta_u$ = +11° as fixation distance varies from 25 to 50 to 100 cm (all of which are reasonable fixation distances for a cat). It can be seen that as fixation distance increases, the horopter becomes flatter, and its angle with the horizontal decreases. In the limit of fixation at infinity, the horopter will itself be horizontal. The large range of convergent eye movement possible in the cat and man (Hughes, '72; Stryker and Blakemore, '72) thus implies that the horopter angle in these species may vary over a considerable range. On the other hand, in the burrowing owl, with its relatively restricted range of eye movements, the horopter angle probably varies relatively much less as a result of changes in fixation distance, although it could conceivably be varied by counter-rotatory cyclotorsional eye movements. We do not have any direct evidence bearing on this point, but Steinbach, Angus and Money ('74) have measured cyclo-rotatory eye movements in one eye of an owl subjected to tilt.

As might be expected from the Results section, the slope of the horopter depends critically on the angle between the two eyes' zero meridians. The experimental errors in estimating the net angle between the zero meridians in life thus place limits upon the accuracy with which we have been able to determine the slope of the horopter for our experimental animals. Since in all of our animals (except LGN-28) the net angle in life between the zero meridians has been greater than the 95% confidence limits (see table 2), we can validly conclude that the vertical horopter would be tilted in all of these animals. However, the large amount of eye movement in the cat raises the possibility that this animal can vary the slope of its vertical

horopter not only by changing fixation distance, but also by actively cyclo-rotating its eyes. For instance, by keeping its fixation point constant while increasing the angle between the zero meridians (by out-torting the eyes to make the zero meridians even more divergent at the top), the cat would be able to flatten its horopter line. This could be a mechanism for adjusting for varying height above the ground, although we have made no systematic attempt to determine whether in fact the cat does have active control of cyclotorsional eye movements. This possibility is schematically illustrated in figure 11 and is supported by the data of Table 1, in which the angle between the slit-pupils shows a greater variance (both inter- and intra-animal) before paralysis. It is known that in man convergence is accompanied by out-torsion of the eyes (Allen, '54).

Comparison with related physiological studies

Joshua and Bishop ('70) found that the mean field separation for midline binocular units lying 16-30° below the horizontal meridian was 2-3° smaller than the separation for units in the central region. However, we did not find any great difference between the mean separations of far inferior fields and those closer to the horizontal. One reason for this discrepancy may be that Joshua and Bishop's ('70) data for the far inferior field consisted of only a few area 17 cells from 2 out of 19 cats. In contrast, some of our recordings were from area 18. Another factor involved here may be the small residual torsions during the course of an experiment; these movements would affect the separation of far inferior fields considerably. We took special care to monitor and correct for these torsions. However, it should be noted that even if more extensive studies were to confirm the finding of a significant decrease in mean separation for the far peripheral lower field, this would only indicate that the zero meridians in the lower field were already crossed in the paralyzed animal. Thus, in this case, a tilted horopter would be indicated

even before correction for eye rolling. The correction for torsion under paralysis might then result in a horopter even more tilted than that in the animal with parallel zero meridians under paralysis. It is worth mentioning in this regard that the experimentally measured field separations on the midline might have two components, one corresponding to the actual anatomy of the retinocortical pathway, and the other representing the exact amount of eye rolling which has occurred under paralysis.

An adequate account of ocular torsion, in conjunction with the present findings, may also help to explain discrepancies in the literature concerning the precise values for receptive field disparity variation in area 17. For example, Nikara et al. ('68) obtained a standard deviation of 0.5° for receptive fields close to the visual pole, whereas Barlow et al. ('67) found a value of 1.5° for fields with eccentricities between 5° and 15°. Joshua and Bishop ('70) observed a systematic increase in disparity variation with increasing horizontal eccentricities and thought that this would be sufficient to account for this difference in values. However, while the increase in disparity variation with horizontal eccentricity is in the right direction to help make up the discrepancy, it is not sufficient, according to a recent study by van der Heydt et al. ('78). Perhaps the remaining difference can be accounted for by the fact that Barlow et al. ('67) corrected for cyclotorsion back to the pre-paralysis state and therefore would have introduced systematic changes in receptive field disparities with changes in vertical eccentricity as well. (This would result because the zero meridians are crossed if one corrects back to the unparalyzed state.) Since the data of Barlow et al. ('67) are pooled from quite a wide range of eccentricities, it seems possible that correction for the systematic changes occurring along both axes would bring about even closer agreement with the other studies.

The horizontal meridians

The finding that the zero azimuthal meridians are out-torted in the unparalyzed cat raises a question concerning the horizontal meridians in the paralyzed and unparalyzed conditions. During a physiological experiment on a paralyzed cat, the horizontal meridian is usually taken simply as the perpendicular to absolute vertical, or as the parallel to the line between the centers of the blind spots (Bishop et al., '62). In this case, out-torsions of the eyes to correct for the effects of paralysis would induce vertical disparities between the receptive fields of binocular units on the horizontal meridian. However, if it is assumed that the units on the horizontal meridian should have no net vertical disparity in the unparalyzed animal, then the intorsion under paralysis should result in measurable vertical separations for horizontal meridian units plotted on the tangent screen; in particular, the receptive field for the contralateral eye should be higher than the receptive field for the ipsilateral eye. This prediction has been verified by van der Heydt et al. ('78), who have found a progressive change in vertical disparity with increasing horizontal eccentricity, a change exactly accounted for by the photographically measured ocular cyclotorsion.

Hughes ('77) has pointed out further evidence that the horizontal meridian of the cat's eye is not in the horizontal plane during paralysis. In a paralyzed cat the angle between the horizontal plane and the plane through area centralis and blind spot ($\psi$B of Bishop et al., '62) is greater than the angle in a retinal whole mount between the horizontal visual streak and the line through area centralis and optic nervehead (24.4°, Bishop et al.,'62; 22.2°, Vakkur et al.,'63; 25.2°, Hammond quoted in Hughes, '75, versus 16.6°, Hughes, '75; 16.2°, Wässle et al., '75). In other words, in the paralyzed cat the horizontal visual streak of each eye is tilted approximately 7° from

true horizontal, close to the amount needed if the 4-5° out-torsion of the unparalyzed state were to bring the visual streak in alignment with the horizon.

Helmholtz ('25, p. 411) showed that even though the angle between apparent vertical corresponding lines was 2° 40' (in one human observer), the angle between the retinal horizons was only 0° 18'. A similar result has been obtained by Nakayama et al. (MS in preparation). This indicates that if the apparent vertical and horizontal meridians were projected onto a tangent screen, they would not be exactly perpendicular (although the meridians themselves would be <u>seen</u> as perpendicular in space). The same situation would presumably apply to the cat, so that the out-torsion of the zero meridians in the unparalyzed animal need not imply a relative rotation between the horizontal meridians for the two eyes. This implication that the horizontal meridian of the eyeball and the eyeball's zero azimuthal meridian are not at right angles is one reason that we have carefully avoided equating the terms "zero meridian" and "vertical meridian" in this paper. The important question of the relationship between the various major meridians of the cat's eye has been taken up by McIlwain ('77) and will be addressed more fully by us with reference to the naso-temporal division (Cooper and Pettigrew, MS in preparation).

In the burrowing owl we have found a result similar to that of Helmholtz; the vertical meridians for the owl's two eyes were tilted by 8.3° with respect to each other, yet there was no significant net vertical separation for fields in the posterior track. These fields were centered around an azimuth of 10.6° along the horizontal meridian. This result, incidentally, is an internal control against the possibility that our finding of tilted zero meridians in the owl is due to torsion of the owl's eyes. If there were a net torsion of 8.3° between the two eyes, then fields lying 10.6° along the horizontal

meridian should have the ipsilateral receptive field about 1.5° higher than the contralateral field. In fact, calculation of the mean vertical separation for the units on the posterior track showed that, on the average, the ipsilateral field was higher than the contralateral field by only 0.1° (S.D. = 0.3°, see Results); in no case was there more than 0.4° of vertical separation between the two fields of a binocular unit. Furthermore, the mean vertical separation for the anterior track was not significantly different from that of the posterior track, and there was no significant vertical disparity between the projections of the two areae centrales of the owl. These findings confirm our contention that our result in S05 was not due to rolling of the owl's eyes during our recording session. (A net rotation of 8.3° would seem unlikely in any event, given the small amount of movement possible for the eye of the burrowing owl.)

Conclusion

During the last two decades, single unit recording techniques have been used extensively in the study of the function of the visual system. The ultimate aim of this application of recording methods is to try to understand the physiological mechanisms underlying the wealth of psychophysical data which has been accumulated. In this paper we have presented physiological data bearing on a psychophysical construct, the vertical horopter. Our results, based on the simple application of electrophysiological recording methods, reveal an underlying connectivity of extraordinary precision and give hope that these methods will contribute much more concerning the physiological basis of perception.

ACKNOWLEDGMENTS

The authors would like to thank K. Nakayama and C. W. Tyler for helpful discussions and for making available copies of their manuscripts on the vertical horopter in man. Lederle Labs supplied the Flaxedil used in these experiments. Sarah Kennedy and Phyllis Knudsen helped with the track reconstructions, and Betty Hanson typed this manuscript. Gary Blasdel also provided technical assistance. This research was supported by grants MH 25852 and EY 1909 from USPHS to J.D.P. M.L.C. held a National Science Foundation Predoctoral Fellowship.

LITERATURE CITED

Aguilonius, F. 1613 Opticorum Libri Sex. Plantin, Antwerp.

Allen, M. J. 1954 The dependence of cyclophoria on convergence, elevation and the system of axes. Am. J. Optom. 31: 297-307.

Barlow, H. B., C. Blakemore, and J. D. Pettigrew 1967 The neural mechanism of binocular depth discrimination. J. Physiol. 193: 327-342.

Bilge, M., A. Bingle, K. N. Seneviratne, and D. Whitteridge 1967 A map of the visual cortex in the cat. J. Physiol. 191: 116p-118p.

Bishop, P. O. 1973 Neurophysiology of binocular single vision and stereopsis. In: Handbook of Sensory Physiology, Vol. VII/3, R. Jung, ed. Springer-Verlag, Berlin, pp. 255-305.

Bishop, P. O., W. Kozak, and G. J. Vakkur 1962 Some quantitative aspects of the cat's eye: axis and plane of reference, visual field coordinates and optics. J. Physiol. (London), 163: 466-502.

Breitmeyer, B., B. Julesz, and W. Kropfl 1975 Dynamic random-dot stereograms reveal up-down anisotropy and left-right isotropy between cortical hemifields. Science 187: 269-270.

Cooper, M. L., and J. D. Pettigrew 1978 The vertical horopter in the cat. Abstracts of Association for Research in Vision and Ophthalmology Meeting, Sarasota, Florida, p. 173 (Abstract).

Helmholtz, H. 1867 Handbuch der Physiologischen Optik, Leopold Voss, Leipzig.

_____ 1925 Treatise on Physiological Optics, Vol. III, Columbia Univ. Press for Opt. Soc. Am., J. P. C. Southall, ed., New York. Translation of 3rd German edition (1909-1911).

Hillebrand, F. 1893 Die Stabilität der Raumwerte auf der Netzhaut. Z. Psychol. Physiol. Sinnesorg. 5: 1-60.

Hubel, D. H., and T. N. Wiesel 1962 Receptive fields, binocular interaction and functional architecture in the cat's visual cortex. J. Physiol. (Londo 160: 106-154.

Hughes, A. 1972 Vergence in the cat. Vision Res., 12: 1961-1994.

_____ 1975 A quantitative analysis of the cat retinal ganglion cell topography. J. Comp. Neur., 163: 107-128.

Joshua, D. E., and P. O. Bishop 1970 Binocular single vision and depth discrimination. Receptive field disparities for central and peripheral vision and binocular interaction on peripheral single units in cat striate cortex. Exp. Brain Res., 10: 389-416.

Julesz, B., B. Breitmeyer, and W. Kropfl 1976 Binocular-disparity-dependent upper-lower hemifield anisotropy and left-right hemifield isotropy as revealed by dynamic random-dot stereograms. Perception, 5: 129-141.

Levick, W. R. 1972 Another tungsten microelectrode. Med. Electron. Biol. Engng., 10: 510-513.

McIlwain, J. T. 1977 Orientation of slit pupil and visual streak in the eye of the cat. J. Comp. Neurol., 175: 337-344.

Müller, J. 1826 Zur vergleichenden Physiologie des Gesichtssinnes des Menschen und der Thiere. Cnobloch, Leipzig.

Nakayama, K. 1977 Geometric and Physiological Aspects of Depth Perception in Three Dimensional Image Processing, S. Benton (Ed.), Proc. Soc. Photo Optical Inst. Engineers.

Nakayama, K., C. W. Tyler and J. Appelman 1977 A new angle on the vertical horopter. Abstracts of Association for Research in Vision and Ophthalmology Meeting, Sarasota, Florida, p. 82 (Abstract).

Nelson, J. I., H. Kato, and P. O. Bishop 1977 Discrimination of orientation and position disparities by binocularly activated neurons in cat striate cortex. J. Neurophysiol., 40: 260-283.

Nikara, T., P. O. Bishop, and J. D. Pettigrew 1968 Analysis of retinal correspondence by studying receptive fields of binocular single units in cat striate cortex. Exp. Brain Res., 6: 353-372.

Ogle, K. N. 1932 An analytical treatment of the longitudinal horopter. J. Opt. Soc. Am., 22: 665-728.

_____ 1950 Researches in Binocular Vision. Sanders, Philadelphia.

_____ 1962 The optical space sense. In: The Eye, Vol. 4, Pt. II. H. Davison, ed. Academic Press, New York, pp. 211-417.

Pettigrew, J. D. 1974 The effect of visual experience on the development of stimulus specificity by kitten cortical neurones. J. Physiol., 237: 49-74.

Pettigrew, J. D. 1978 Binocular visual processing in the owl's telencephalon. Proc. Roy. Soc. B, in press.

Pettigrew, J. D., and M. Konishi 1976 Neurons selective for orientation and binocular disparity in the visual Wulst of the barn owl (Tyto alba). Science, 193: 675-678.

Rodieck, R. W., J. D. Pettigrew, P. O. Bishop, and T. Nikara 1967 Residual eye movements in receptive field studies of paralyzed cats. Vision Res., 7: 107-110.

Sanderson, K. J. 1972 Does rolling of the eye occur in the anaesthetized paralysed cat? Vision Res., 12: 1045-1050.

Sanderson, K. J., and S. M. Sherman 1971 Nasotemporal overlap in the visual field projected to the lateral geniculate nucleus in the cat. J. Neurophysiol. 34: 453-466.

Shipley, T., and S. C. Rawlings 1970 The Nonius horopter. I. History and theory. Vision Res., 10: 1225-1262.

Steinbach, M. J., R. G. Angus, and K. E. Money 1974 Torsional eye movements of the owl. Vision Res., 14: 745-746.

Steinbach, M. J., and K. E. Money 1973 Eye movements of the owl. Vision Res., 13: 889-891.

Stryker, M., and C. Blakemore 1972 Saccadic and disjunctive eye movements in cats. Vision Res., 12: 2005-2013.

Talbot, S. A. 1940 Arrangement of visual field on cat's cortex. Am. J. Physiol., 129: 477-478.

Tusa, R. J., L. A. Palmer, and A. C. Rosenquist 1978 The retinotopic organization of area 17 (striate cortex) in the cat. J. Comp. Neurol., 177: 213-236.

Vakkur, G. J., P. O. Bishop, and W. Kozak 1963 Visual optics in the cat, including posterior nodal distance and retinal landmarks. Vision Res., 3: 289-314.

van der Heydt, R., Cs. Adorjani, P. Hänny, and G. Baumgartner 1978 Disparity sensitivity and receptive field incongruity of units in the cat striate cortex. Exp. Brain Res. 31: 523-545.

Vieth, G. U. A. 1818 Ueber die Richtung der Augen. Ann. Phys. 58: 233-251.

Wässle, H., W. R. Levick, and B. G. Cleland 1975 The distribution of the alpha type of ganglion cells in the cat's retina. J. Comp. Neurol. 159: 419-438.

# APPENDIX

The geometrical relationships which determine the slope and position of the vertical horopter are made explicit in figure 12 and the equations below.

In figure 12A the zero meridians of the right (RE) and the left (LE) eye are out-torted with respect to each other by angle $\theta$, and the eyes are fixating point F. Consider 2 planes; one, LEFLE'B, inclined to contain the zero meridian of the left eye, and another, REFRE'B, with a different inclination to contain the zero meridian of the right eye. The intersection of these two planes with each other in the midsagittal plane (BF), is the vertical horopter, which can be seen to be tilted away from the subject. When these two inclined planes intersect a coronal plane, such as a tangent screen, the projections of the zero meridians of each eye can be seen to intersect with angle $\theta$.

Consider the coronal plane containing both eyes (fig. 12B). The point, B, at which the vertical horopter intersects this plane can be determined from the pupillary separation, P, and the angle of shear between the zero meridians, $\theta$, in the following way:

$$\tan(\theta/2) = \frac{P}{2H}$$

$$H = \frac{P}{2\tan(\theta/2)} \qquad \text{Eq. 1}$$

Note that H is independent of the fixation distance, f. When applied to the burrowing owl, for which P = 2.8 cm and $\theta = 8.3°$, this equation gives a surprisingly good estimate (19.3 cm) of the owl's actual ground-to-eye distance (which varies, according to posture and head bobbing, from 15 cm, standing quietly, to about 20 cm, at the height of a "bob").

The inclination of the vertical horopter ($\phi$), can be derived by considering the midsagittal plane containing the points M (the midpoint between the eyes), F (the fixation point), and B (the point where the vertical horopter intersects the coronal plane through the eyes):

$$\tan \phi = \frac{H}{f} \quad \text{(from fig. 12c)}$$

$$= \frac{P}{2f \tan (\theta/2)} \quad \text{(from Eq. 1)}$$

$$\phi = \arctan\left[\frac{P}{2f \tan (\theta/2)}\right] \qquad \text{Eq. 2}$$

It can be seen that if $\theta$ is constant, H is also constant (from Eq. 1), and $\phi$ is inversely proportional to the fixation distance. The change in $\phi$ which occurs with variation of f and constant $\theta$ is depicted in figure 10 for a cat with P = 3.8 cm, $\theta = 11°$ and f = 25, 50, 100 cm.

On the other hand, if f is kept constant and $\theta$ is varied, then both H and $\phi$ vary inversely with $\theta$. This situation is illustrated in figure 11 where the same cat is shown for f = 50 and $\theta = 0°, 2°, 5°, 10°$.

TABLE 1

| Cat | # units studied | #units used | #tracks | Area 17 or 18? | Angle between pupils before paralysis | Angle between pupils after paralysis | Net torsion $\theta_n$ | Residual torsion from pupils | Residual torsion from fundus |
|---|---|---|---|---|---|---|---|---|---|
| LGN-28 | 24 | 17 | 2 | 17 | +12.4° ± 3.3° (5) | +14.2° ± 1.0° (4) | +1.8° ± 4.1° | | |
| LGN-29 | - | - | - | - | +13.0° ± 1.4° (6) | +19.4° ± 1.1° (2) | +6.4° ± 2.6° | | |
| LGN-33 | 35 | 14 | 3 | 17 | +9.7° ± 6.0° (5) | +19.4° ± 2.5° (9) | +9.7° ± 4.9° | | |
| LGN-34 | 34 | 23 | 4 | 18 | +2.0° ± 2.1° (11) | +16.1° ± 0.9° (6) | +14.1° ± 2.0° | -1.8° | -1.9° |
| LGN-35 | - | - | - | - | +8.2° ± 1.0° (16) | +14.9° ± 0.6° (5) | +6.7° ± 1.0° | | |
| LGN-36 | 36 | 16 | 2 | 18 | +7.1° ± 1.2° (23) | +19.4° ± 0.4° (3) | +13.4° ± 1.8° | -1.4° | -1.6° |
| Mean ± Standard Deviation of Mean | | | | | +8.7° ± 4.0° | +17.2° ± 2.4° | +8.7° ± 4.7° | | |



Our estimate of the angle between the slit-pupils before and after paralysis is shown here for each cat. The standard deviation of this estimate is included in every case, and the number of photographs used to determine each angle is shown in parentheses. A positive value for the inter-pupillary angle indicates that the slit-pupils were convergent at the top. Note that there is more variance in the pre-paralysis estimates of inter-pupillary angle than in those obtained after paralysis.

The net torsion, $\theta_n$, is the difference between the inter-pupillary angles before and after paralysis. A positive value of $\theta_n$ indicates that the eyes intorted under paralysis, so that the tops of the slit-pupils converged even more than in the unparalyzed state. The 95% confidence limit for $\theta_n$ is included for each cat.

Our estimate of $\theta_n$ for LGN-36 varies slightly from the difference between the inter-pupillary angle, since in this case we obtained eye position baselines from blood vessel intersections plotted several hours after the initial drawing

Table 1 (legend continued)

of the fundus. A slight residual intorsion had occurred between the times these two fundus drawings were made.

In two cases (LGN-34 and LGN-36) additional estimates of residual torsion after paralysis were obtained by two methods--measurement of inter-pupillary angle and projection of the fundal pattern of blood vessels. Note the good agreement between these two independent estimates.

TABLE 2

| Cat | $\theta_p$ | $2\theta_p$ | $\theta_u$ | $r^2$ |
|---|---|---|---|---|
| LGN-28 | $+0.07° \pm 0.59°$ | | $+2.0° \pm 5.3°$ | 0.47 |
| LGN-33 | $+0.07° \pm 0.75°$ | | $+9.8° \pm 6.4°$ | 0.94 |
| LGN-34 | $+0.75° \pm 0.95°$ | | $+15.6° \pm 3.9°$ | 0.93 |
| LGN-36 | $-0.41° \pm 0.96°$ | | $+12.6° \pm 3.7°$ | 0.93 |
| Mean $\pm$ S.D. of mean | $+0.12° \pm 0.48°$ | $+0.24°$ | $+10.0°$ | |

$\theta_p$ is the angle in the paralyzed cat between the linear regression estimate of the zero meridian of one eye and the vertical through the blind spot for that eye. The error value shown for $\theta_p$ is the 95% confidence limit for the angle obtained from this regression calculation of the zero meridian.

$\theta_u$ denotes the angle between the two zero meridians in the unparalyzed cat and is calculated from the equation $\theta_u = 2\theta_p + \theta_n$, where $\theta_n$ is the net torsion between the two eyes induced by paralysis (see Table 1). The error value for $\theta_u$ is the sum of the 95% confidence limits for $2\theta_p$ and for $\theta_n$. A positive angle for $\theta_u$ indicates that the zero meridians are crossed in the lower field.

The parameter $r^2$ represents the square of the correlation coefficient for the linear regression estimate of one eye's zero meridian in the unparalyzed state. For LGN-34, this zero meridian was determined by rotating by an angle of $\theta_n/2 = 7.05°$ all of the data points obtained in the paralyzed state (see fig. 5); the center of rotation was taken as the presumed fixation point. The estimated zero meridian for one eye was then the linear regression line through the corrected data points (see fig. 6). A similar calculation was performed for the other cats.

FIGURE LEGENDS

Fig. 1 Diagram to show how it is possible for the zero meridians of both eyes to be out-torted with respect to each other and yet for the neural representation of both zero meridians, considered together, to remain vertical.

If binocular neurons have receptive fields upon each zero meridian, then binocular correspondence will be defined by the locus of points in space where the projections of the two zero meridians intersect. The nature of this intersection is shown in this figure.

The projection of the zero meridian from the left eye into space is represented by the inclined plane, LEFLE'B. A similar plane, REFRE'B, with a different inclination, can be drawn for the right eye. The intersection of these two planes in the midsagittal plane (assuming symmetrical fixation of both eyes upon F) is given by the line BF, which is therefore the vertical horopter. Note that this line is tilted away from the subject and is totally contained within the midsagittal plane.

The angle of shearing between the zero meridians, $\theta$, becomes apparent when one considers a coronal plane, such as the tangent screen, upon which the projections of the zero meridians are seen to cross over one another, with divergence in the upper field and convergence in the lower field. For the sake of clarity in the figure the angle, $\theta$, has been exaggerated from the values likely to be found in life.

Fig. 2 Fresh retinal whole-mount, just following reaction for horseradish peroxidase (HRP) retrogradely transported to ganglion cells, but prior to dehydration and mounting. Combined dark-field and light-field illumination has been employed to improve the visibility of the blood vessel pattern, which is

(Fig. 2 legend continued)

used to estimate the projection of the area centralis in relation to the blood vessel pattern in a drawing of the projected fundus (see fig. 3).

This retina was ipsilateral to an injection of HRP into the lateral geniculate, and ganglion cells (particularly the large α-cells) stained with reaction product can be seen to the temporal side of the naso-temporal decussation.

This monochrome was prepared from a color photograph actually used for estimations in these experiments.

Fig. 3 Raw data from one experiment to determine the zero meridians in a paralyzed cat. The receptive fields of binocular neurons are shown as they were plotted on the screen during recording, before small corrections were applied for residual eye movements occurring during the experiment. Eye movements were monitored by projecting the tapetal fundus of each eye onto the screen with the fiber-optic technique described in Methods. This projection technique also allowed detailed drawings to be made of the blood vessel pattern on the same screen where receptive fields were plotted. (For clarity, only part of the pattern drawn for the right eye during the experiment is shown in the figure.) These drawings could then be related, after the experiment, to the blood vessel pattern in retinal whole mounts in which labeled ganglion cells marked the area centralis and naso-temporal decussation (fig. 2). By triangulation from a number of blood vessel intersections the position of the area centralis on the whole mount could be related to its position on the screen (shown by crosshairs) with an accuracy of about 0.5°

Four electrode tracks in Area 18 near the 17/18 border yielded four pairs of receptive field clusters at a variety of vertical eccentricities close to the

(legend continued)

(Fig. 3 legend continued)

midline. The zero meridians are obviously close to parallel and vertical. This is analyzed more quantitatively in the following figures.

Fig. 4 Figure illustrating our method for calculating the positions on the tangent screen of the zero meridians (vertical lines) for the two eyes. It is desired to determine the distance, D, between the zero meridians at each elevation. However, since there is no a priori way here to estimate the position of each zero meridian at each elevation, we instead calculate B, the distance on the tangent screen between the zero meridian of one eye and the vertical line through the blind spot (stippled circle) of that eye. In practice we have determined B for each binocular unit by using the separation, d, of the unit's two receptive fields. If one uses A to denote the distance on the tangent screen between the centers of the two blind spots, it can be seen that, for each unit, $B = (A - d)/2$.

The crosses in this figure represent the projections of the visual poles of the two eyes.

Fig. 5 Figure depicting the zero meridian for the right eye of LGN-34 in the paralyzed state. This meridian was calculated according to the method outlined in figure 4 and is shown lying in the plane of the tangent screen. The stippled circle represents the projection of the blind spot of the right eye, while the vertical axis corresponds to the vertical through the blind spot. The vertical solid line is the linear regression estimate of the zero meridian and is drawn through the calculated data points (filled circles) for the binocular units; the dotted lines represent the 95% confidence limits for the slope of this regression line. Under paralysis, the zero meridian made an angle of $+0.75^\circ$ with the vertical and intersected the horizontal meridian at a point 16.1 cm from the line through the blind spot.

Fig. 6 Diagram showing the zero meridians for the two eyes of LGN-34 after correction to the unparalyzed, alert state. As in the preceding figure, this drawing is made in the plane of the tangent screen. The corrected zero meridian for the right eye was determined by rotating the data points in figure 5 around the fixation point by an angle of $\theta_n/2 = 7.05°$, where $\theta_n$ denotes the net torsion between the two eyes occurring under paralysis. In order to correct for the paralysis-induced intorsion, each eye must be out-torted, which corresponds to rotating the points in figure 5 in a clockwise direction. The zero meridian for the left eye has been drawn as the mirror image of that for the right eye.

We have assumed in our calculations that cyclotorsion occurs around the visual axis (see Methods for partial justification of this assumption). Note however that sheared meridians will result from any axis of cyclotorsion which produces a coronal rotational component visible in frontal photographs of the slit-pupils.

The value of $\Delta$ in this figure gives the horizontal distance between each corrected data point and the midsagittal plane. It can be seen that the two eyes' zero meridians are crossed in the lower field, the net angle between them being 15.6°. The dotted lines represent 95% confidence limits for the corrected zero meridians; $r^2$ is the square of the correlation coefficient for the linear regression line through the data points in the unparalyzed animal.

Fig. 7 Figure illustrating how one can translate into space the tangent screen positions of a unit's receptive fields. The fields for the left eye are shown in broken lines, while the fields for the right eye are shown unbroken; the depths in space at which each pair of fields superimpose are shown by stippling. The line joining stippled and unbroken fields is the intersection of the

(legend continued)

(Fig. 7 legend continued)

horizontal and midsagittal planes.

The fields of the horizontal unit are crossed with respect to the fixation point on the screen; when projected onto the midsagittal plane, they correspond to a depth in front of the fixation plane. Conversely, the vertical unit, with uncrossed fields, translates into a depth beyond the plane of fixation.

Fig. 8 Diagram demonstrating the calculation of the angle between the zero meridians for the unparalyzed burrowing owl SO5. The separations on the tangent screen of the receptive fields of binocular units are plotted against elevation on the screen. (A negative value for the field separation indicates that the receptive fields were crossed on the screen.) The slope of the linear regression line (solid) through the data points yields directly the angle between the meridians of the two eyes (+8.3°). The dotted lines represent the 95% confidence limits for the slope of the regression line. It is apparent that, as in the cat, the zero meridians for the owl are crossed in the lower field.

Fig. 9 Data points for individual binocular neurons from owl SO5 and cat LGN-34, projected into space. Each point shows the distance at which the receptive fields of a given binocular neuron would be superimposed. Upper field units have more divergent receptive fields, and therefore more distant points of superimposition, than lower field units.

The points have been treated as if they all fell in the midsagittal plane (i.e., they all had zero azimuth), although this is not strictly correct for SO5, whose sample of units was collected at a horizontal eccentricity of around 10°.

(legend continued)

(Fig. 9 legend continued)

In the case of the cat, five units had receptive field separations which were too divergent (and therefore points too distant) for them to be included in the figure.

The sloping line for the owl is the regression line through the points in space. The line for the cat is the regression line through the projections into space of the average field position of each of the four data point clusters in figure 6. These sloping lines thus correspond to the experimentally calculated vertical horopters for S05 and LGN-34.

Fig. 10 Effect of varying fixation distance upon the tilt of the vertical horopter, other parameters being held constant. The calculations for the figure are based upon an "average cat" with a pupillary separation of 3.8 cm, an angle of 11° out-torsion between the zero meridians, and an eye height (nodal point-to-ground) of 20 cm. Vertical horopters are shown for fixation distances of 25, 50, and 100 cm. See the Appendix for the basis of the calculations and for demonstration that only the slope of the horopter varies with changing distance if other parameters, such as the angle of out-torsion between the zero meridians, are held constant. See also Nakayama ('77).

Fig. 11 Effect upon the vertical horopter of changes in $\theta$, the shearing of the zero meridians, when fixation distance is held constant at 50 cm. Same "average cat" as figure 10 with $\underline{P}$ = 3.8 cm.

When the zero meridians are parallel ($\theta = 0°$) the vertical horopter is fronto-parallel, at right angles to the visual axis. With increasing amounts of out-torsion of the zero meridians, the vertical horopter becomes increasingly tilted.

(legend continued)

(Fig. 11 legend continued)

While it is known that cats can change fixation distance (see text), it has not been shown that cats actively counter-cyclorotate their eyes to produce changes in shearing of the zero meridians. However, this possibility seems very likely, in view of the large variance we have obtained in our estimates of cyclotorsion in the unparalyzed cat (see Table 1). We have illustrated the conditions of changing eye-to-ground height in which we would hypothesize active cyclotorsion would be most useful to the cat in adjusting the vertical horopter.

See Appendix for derivation of the relation between $\theta$ and eye-to-ground height.

Fig. 12 See Appendix for explanation.

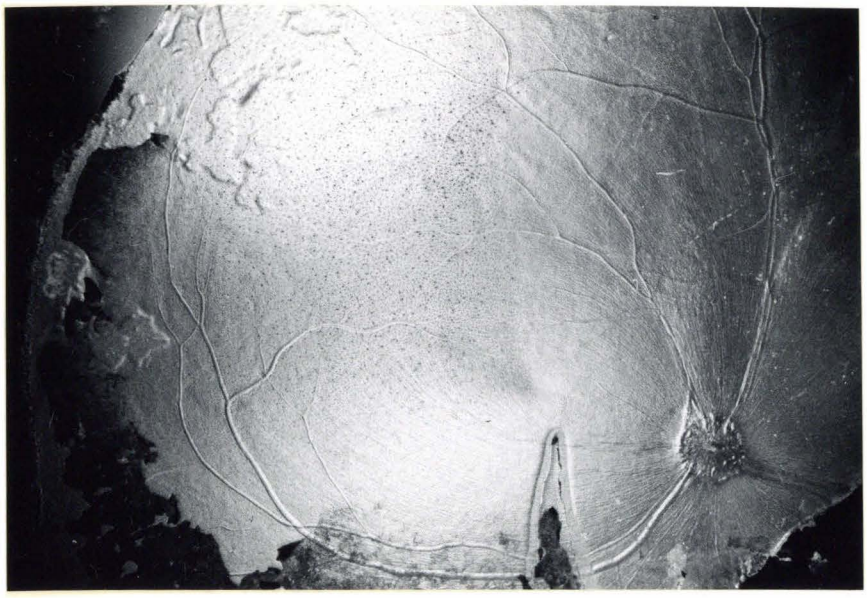

Figure 2

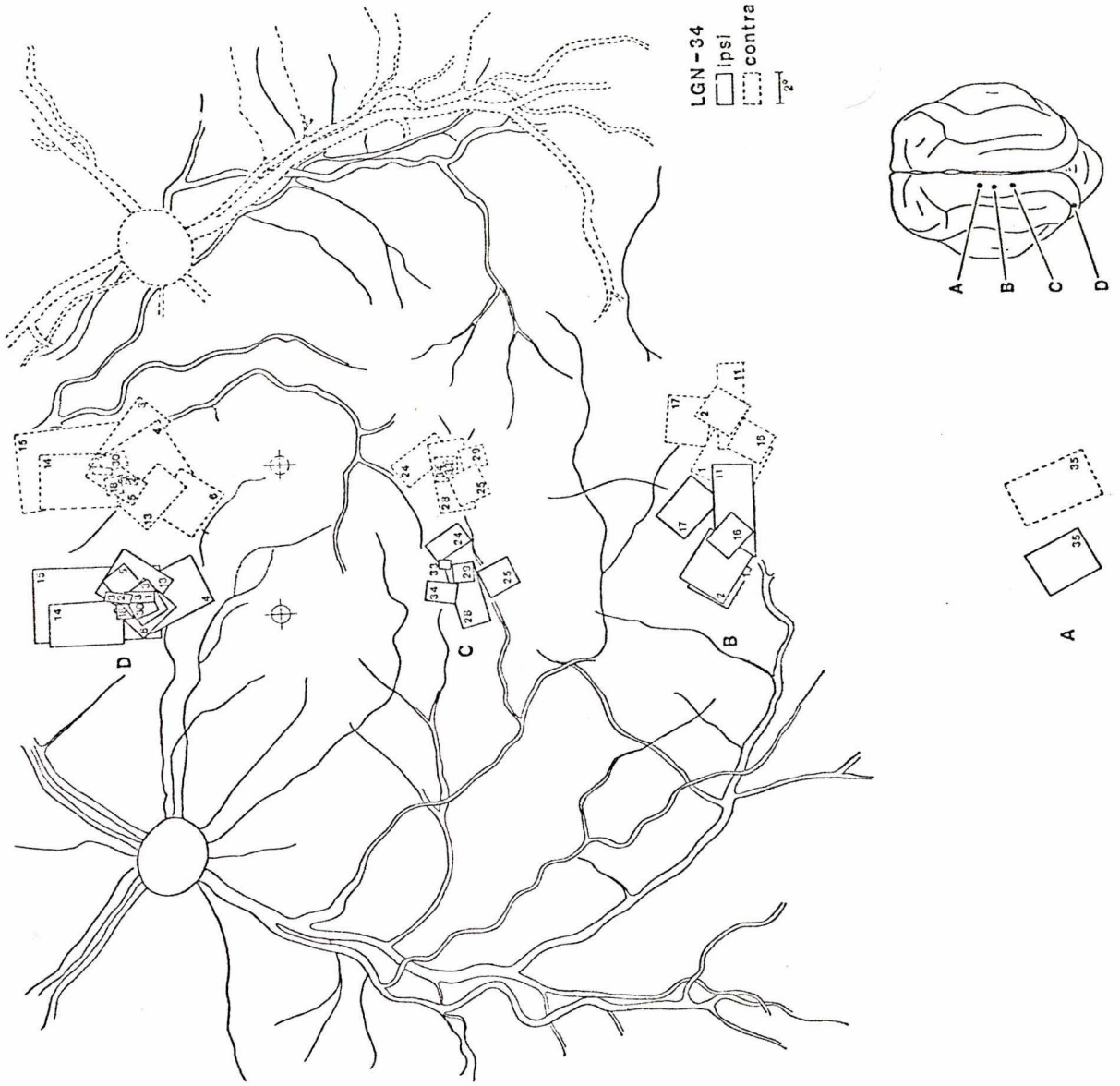


Figure 3

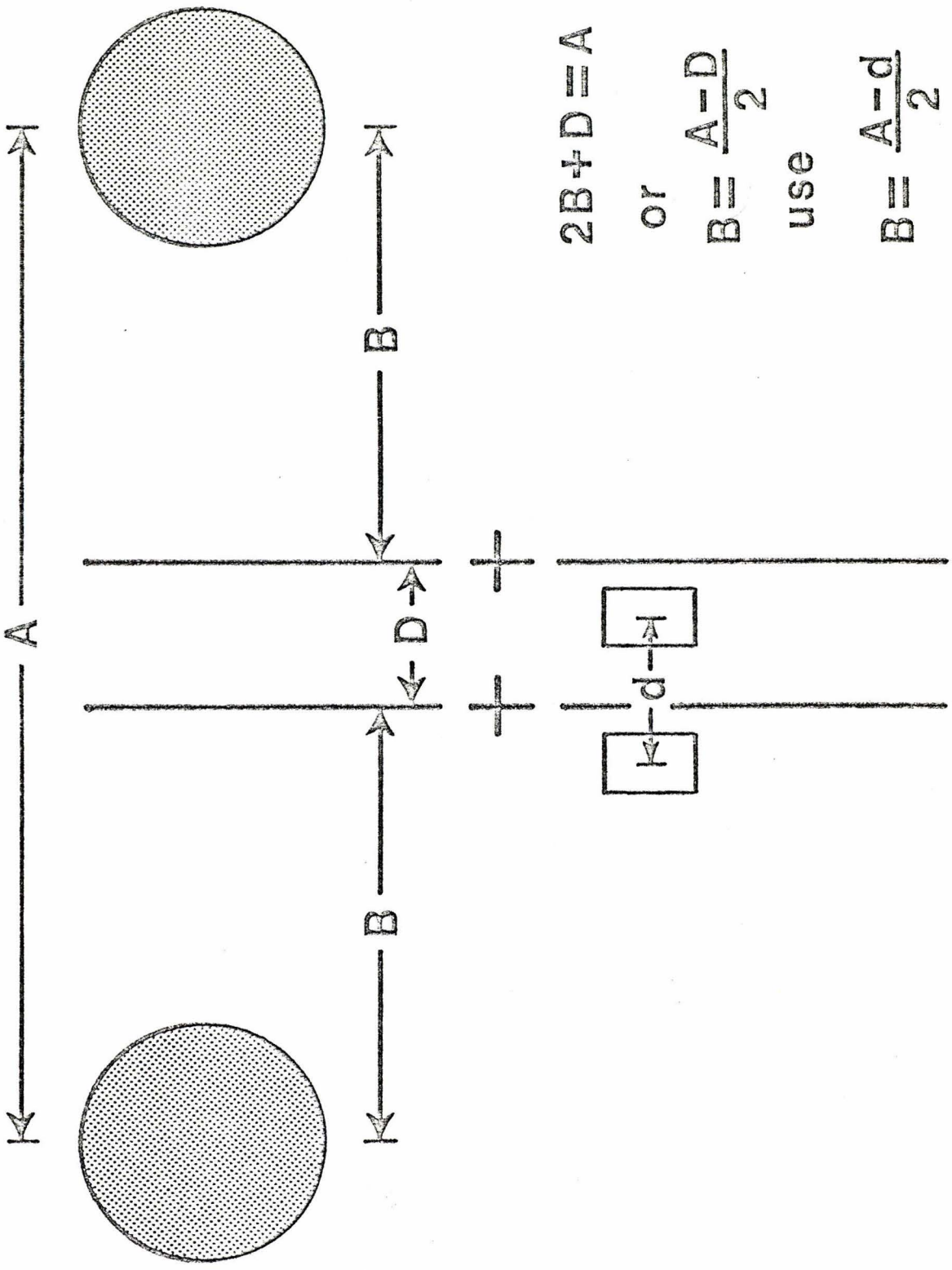


Figure 4

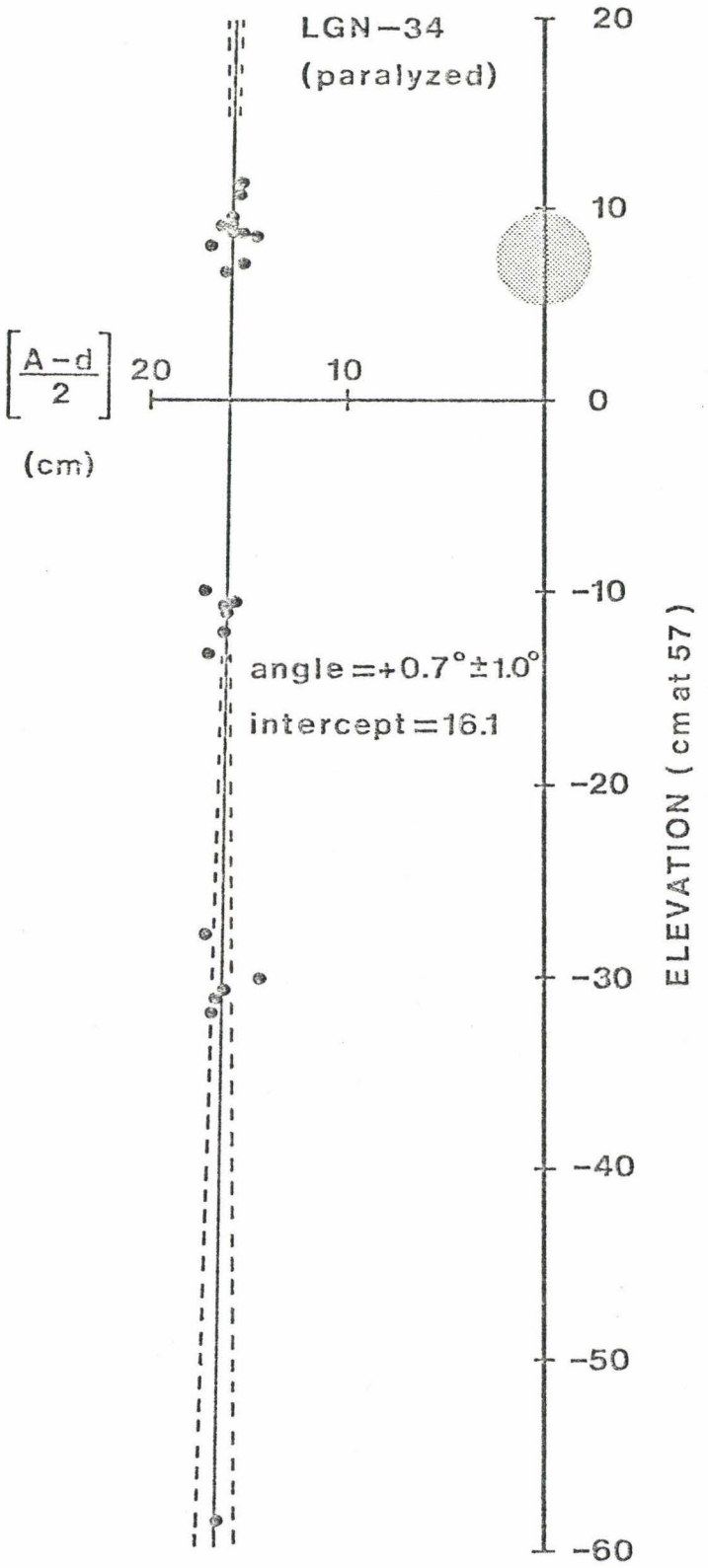
LGN–34
(paralyzed)
20
10
0
-10
-20
-30
-40
-50
-60
ELEVATION ( cm at 57 )
[A-d/2]
20
10
(cm)
angle = +0.7° ± 1.0°
intercept = 16.1

Figure 5

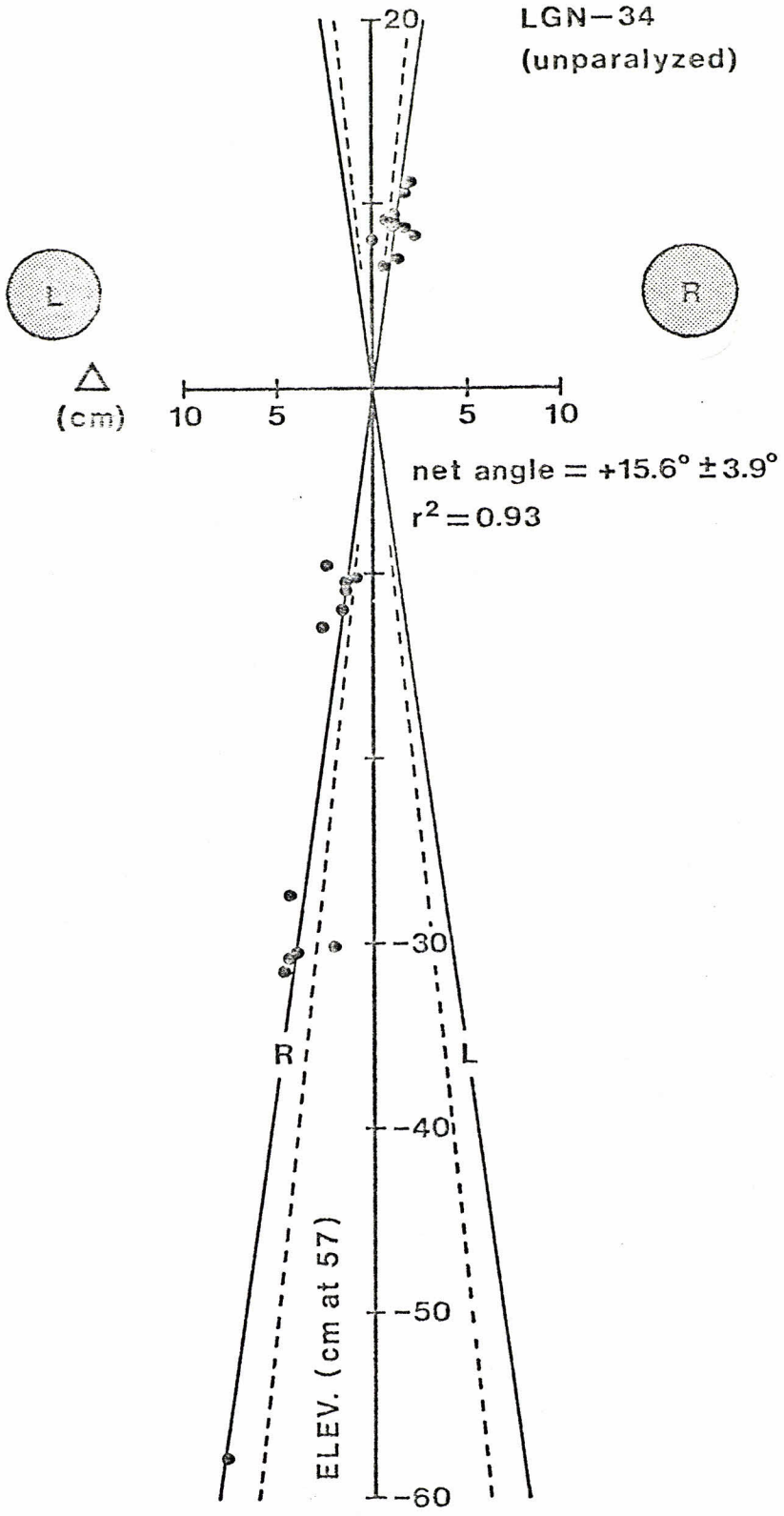
LGN–34
(unparalyzed)
L
R
△
(cm)
10
5
5
10
20
net angle = +15.6° ±3.9°
r² = 0.93
-30
-40
-50
-60
R
L
ELEV. (cm at 57)

Figure 6

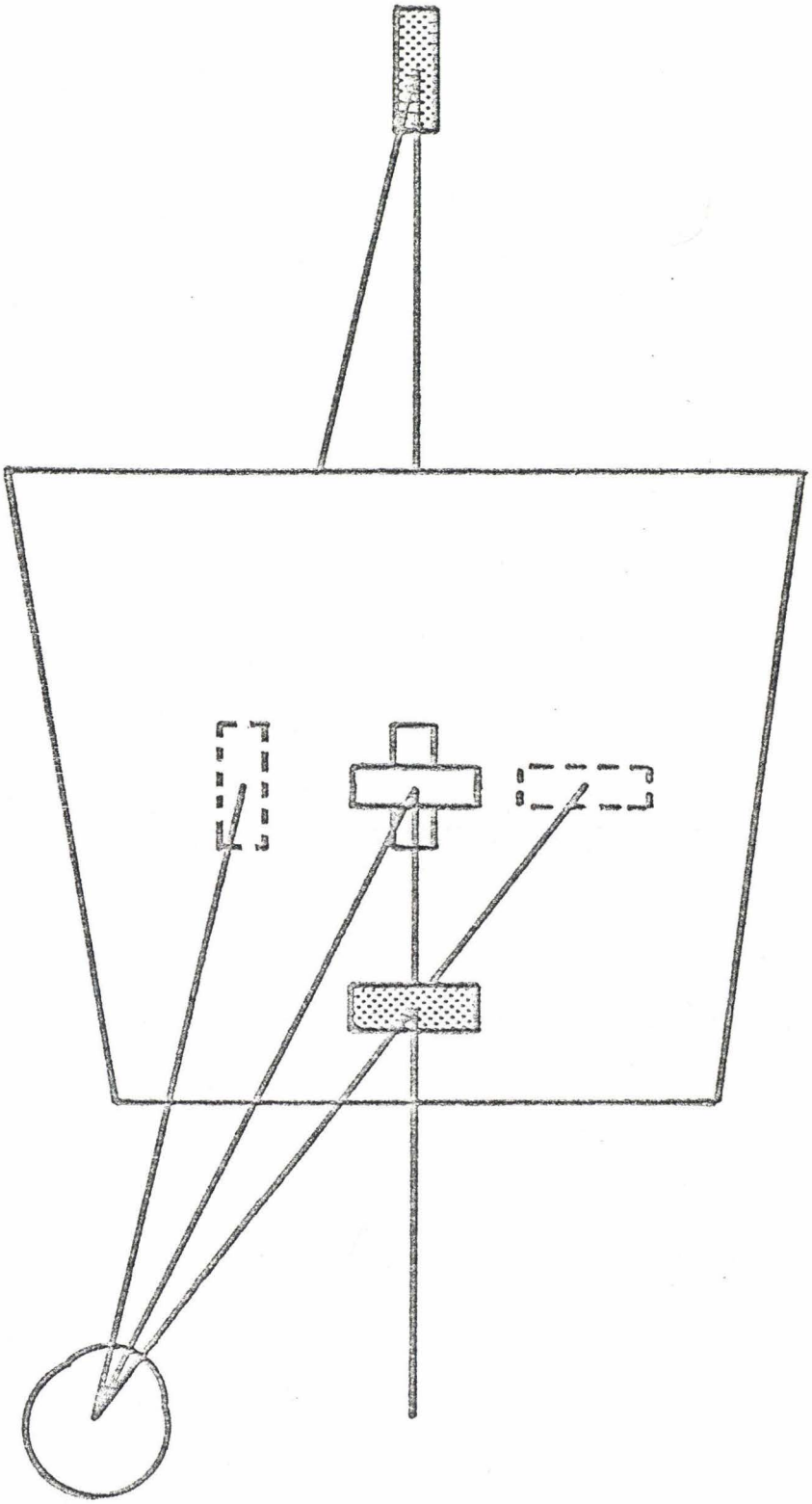

Figure 7

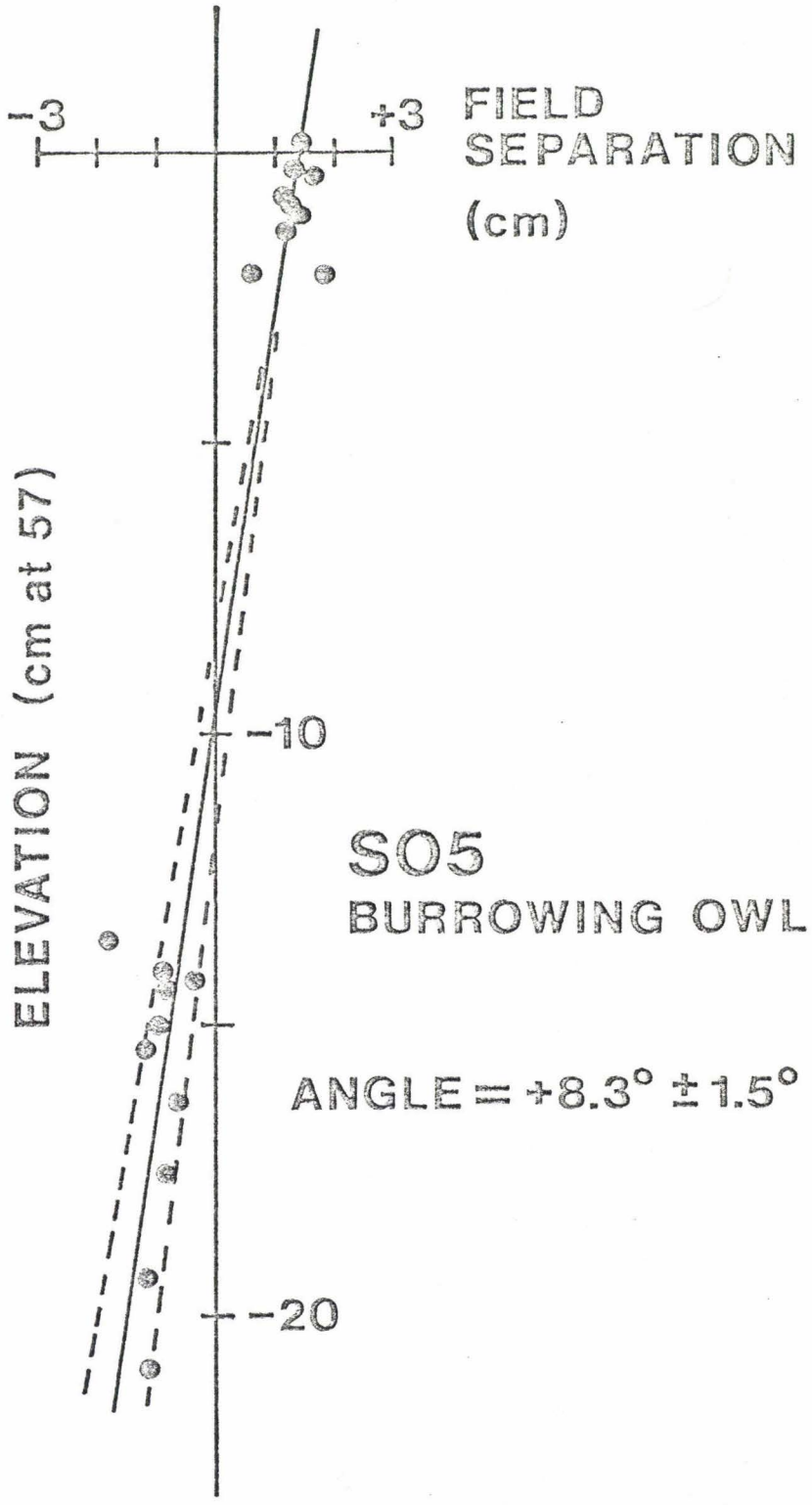
-3
+3
FIELD
SEPARATION
(cm)
ELEVATION (cm at 57)
-10
-20
SO5
BURROWING OWL
ANGLE = +8.3° ± 1.5°

Figure 8

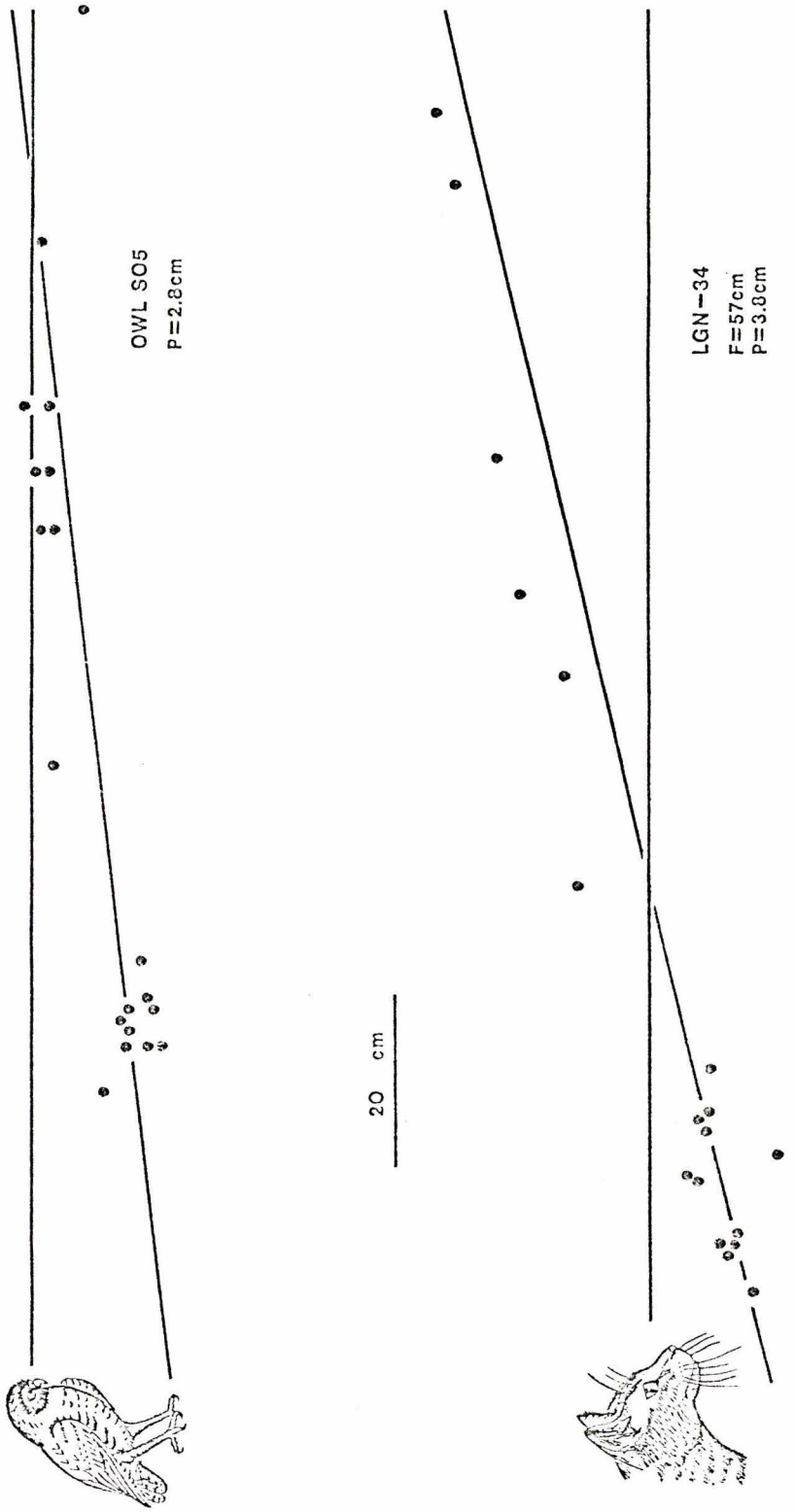


Figure 9

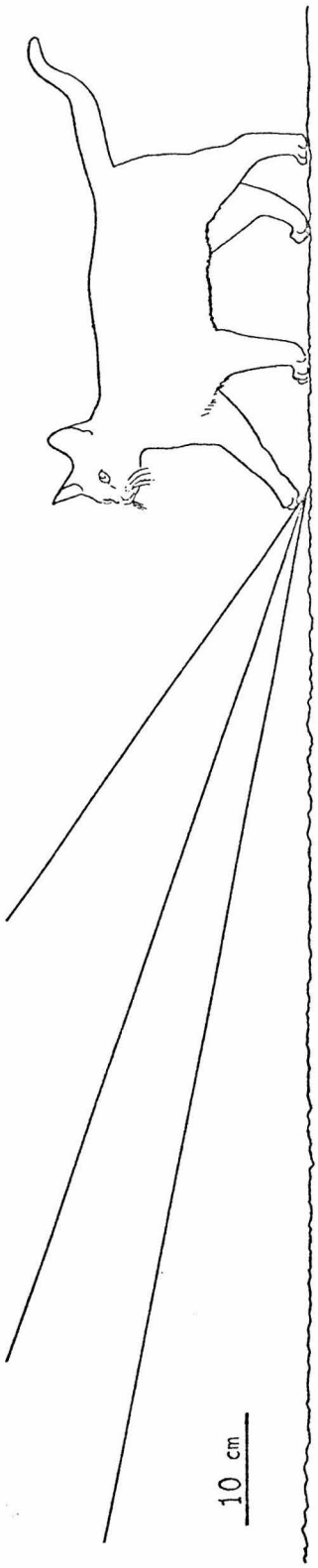


Figure 10

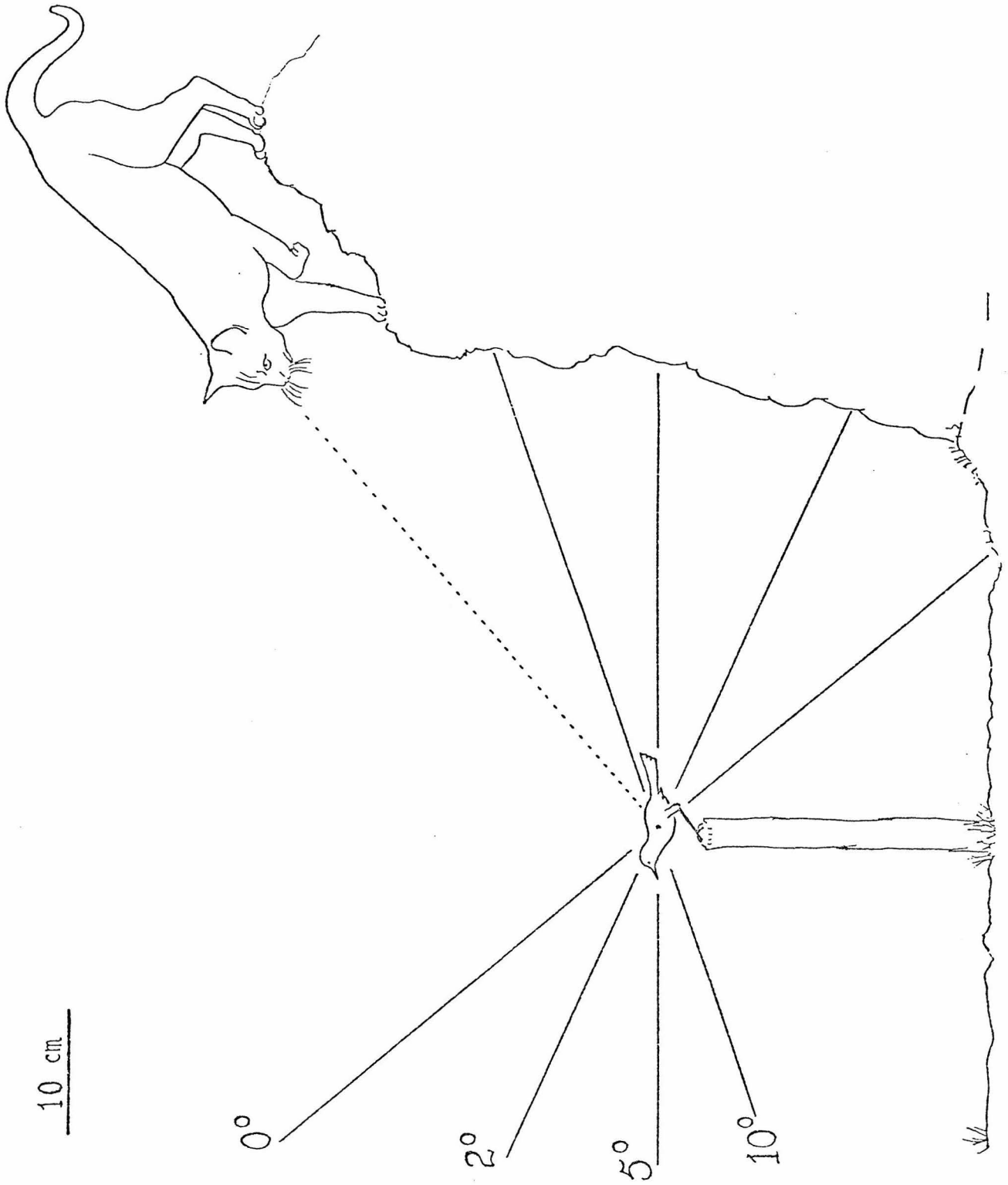


Figure 11

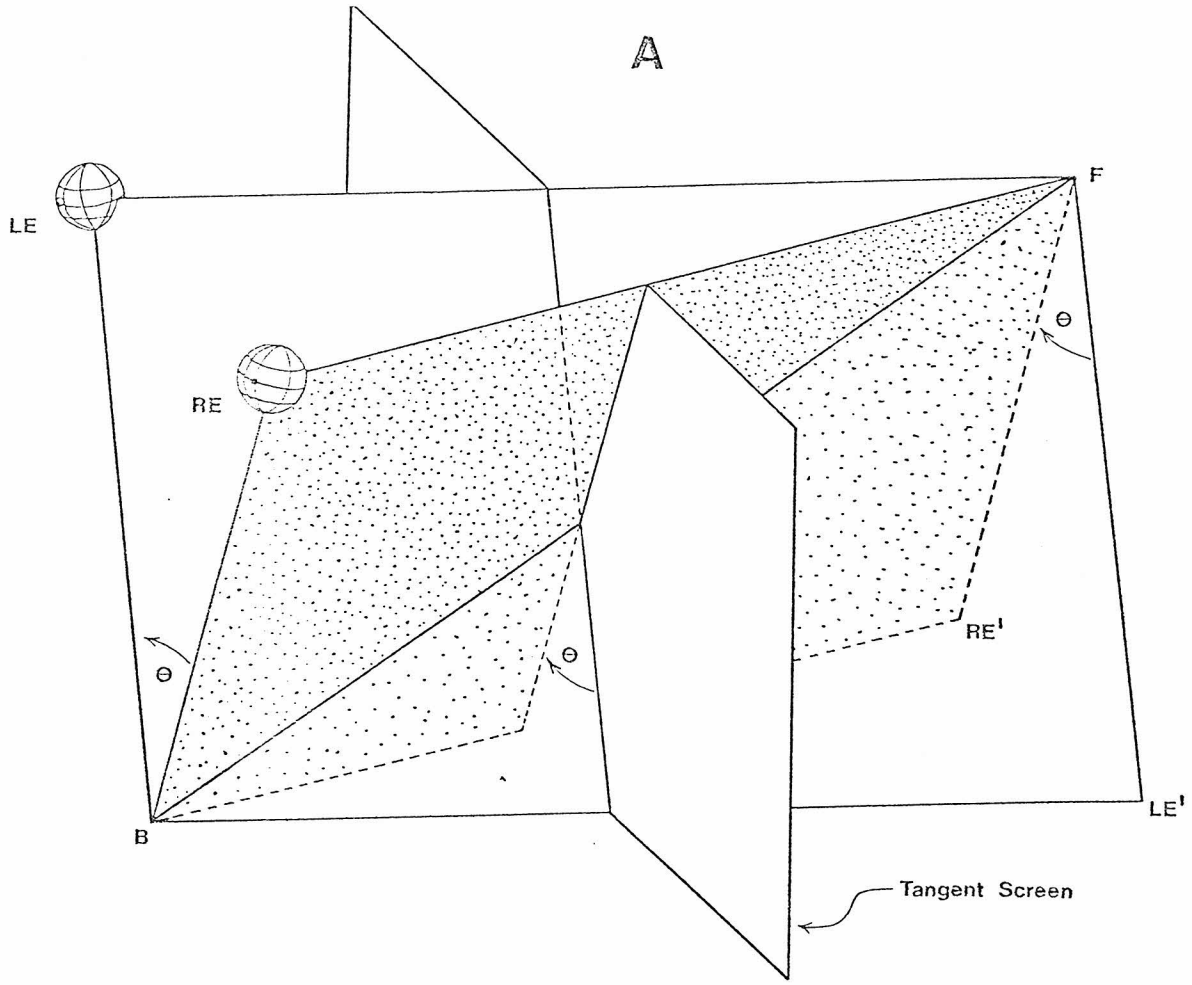
A
LE
F
RE
Θ
Θ
Θ
RE'
B
LE'
Tangent Screen

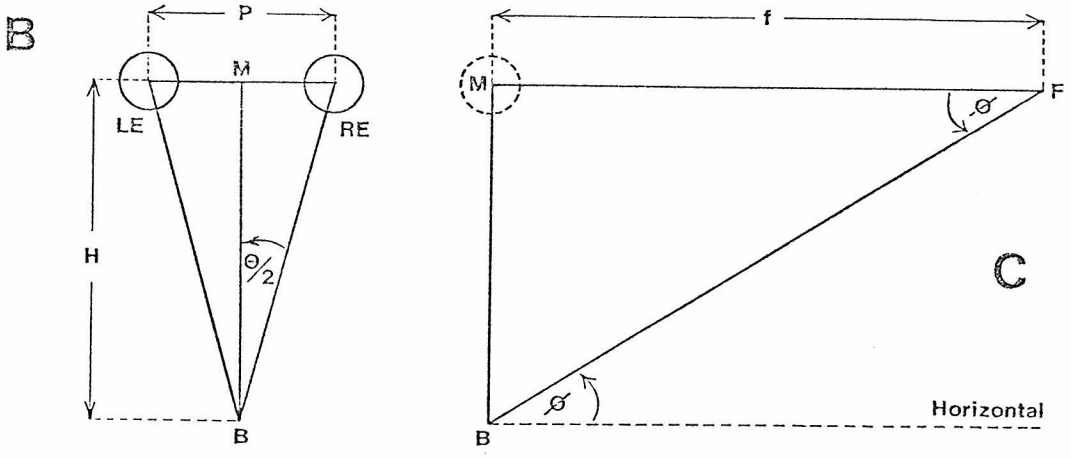
B
P
M
LE
RE
H
Θ/2
B
f
M
F
Ø
C
Ø
Horizontal
B

Figure 12